103

WIS-TCI-325 X

A Facsimile Report

SOT-62722R

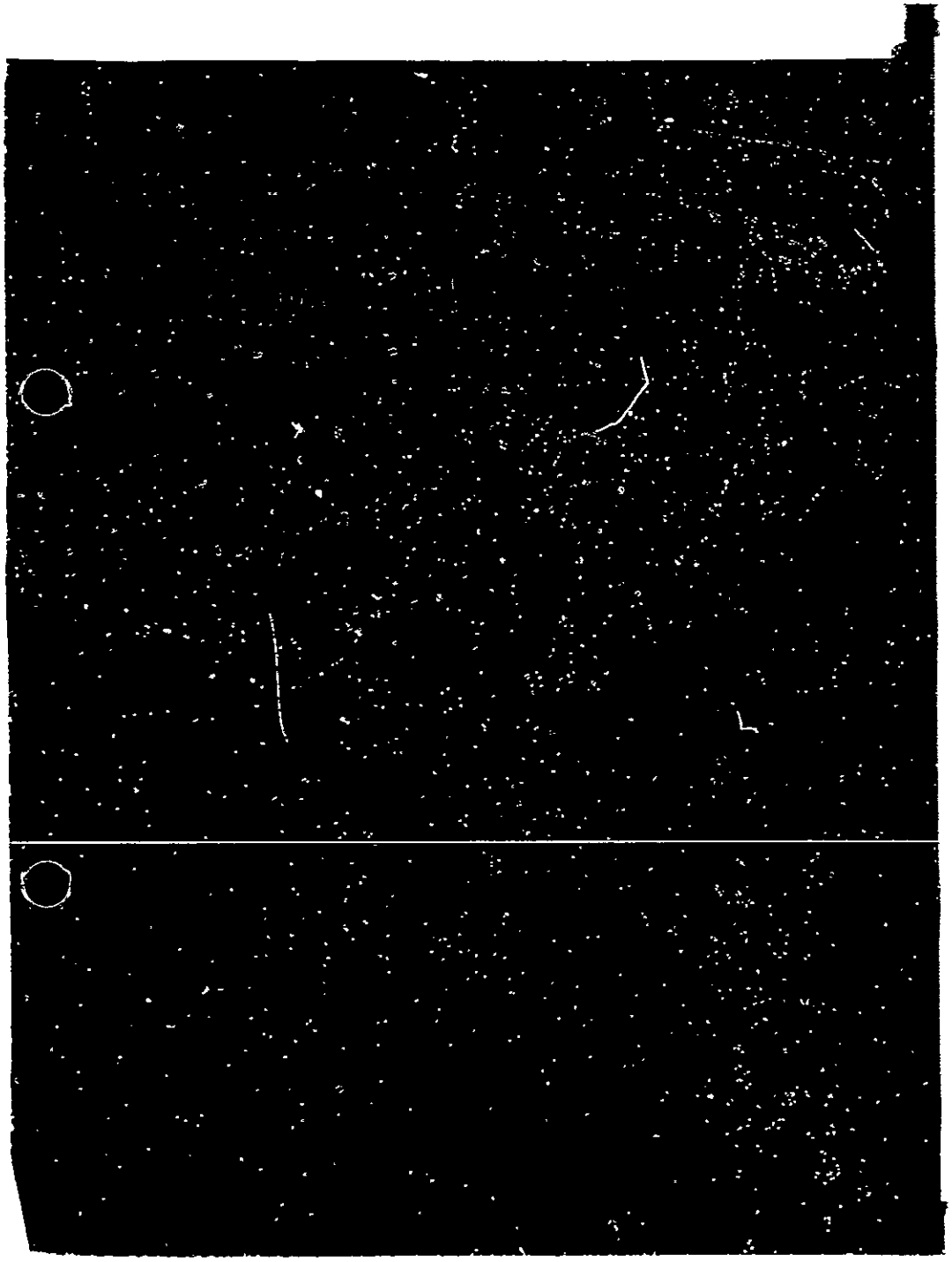

BLANK PAGE

CORRECTIONS TO TCI-325X

PAGE	LINE	COMMENT
I 1	9	particles'
II A.2	8	vectors
II B.2	5 up	$\vec{r}_o \approx$
II C.2	1	T&F
II C.2	3	$1 mm_{Hg}$ (torr)
II C.3	2 up	Graff
II E.2	3	Oven[e]
II E.4	3	maximize
II E.4	7	[e]With chrom-alumel thermocouple, 1 mv $\approx$ 25°C.
III A.1	11	absorption
III C.4	1	trajectory.
III C.6	6,10,2 up	V_{mp}, ΔV_{max}, V
III D.1	sketch	11.0193
III D.2	3 up	spatially
III E.1	5	failed,
III E.2	6 up	trajectories (see Eq. II A.12)
IV C.3	5	$V = \ln r_1 - \ldots$
IV C.4	3	cylindrical
IV C.6	4 up	(IV C.24) and (IV C.25)
IV E.7	7	(IV E.22).
IV E.10	6	(IV E.2)
IV F.2	2 up	focusing.
IV F.4	7	$\eta = 0$
IV F.5	1	discriminate

BLANK PAGE

PAGE	LINE	COMMENT
IV F.5	6 up	ca.
IV G.10	1	Fig. IV G.1
IV H.1	13	constants (see Fig. II A.1).
IV H.2	1 up	orifice
V A.1	3 up	ref. IV B.3.
V A.2	4 up	layer.
V A.11	3	out A-beam.
V A.11	10	ref.
V C.1	1 up	V C.2 - V C.7
V C.2	4 up	synchronously
V D.1	4	epoxied
V E.5		page V E.5, not IV E.5; also, erase GR on figure.
VI A.1	6 up	$H + H + M \longrightarrow$
VI C.1	5 up	R_e
VI C.2 - VI C.9		pages listed incorrectly

Molecular Beam Focusing of Diatomics in Selected States: Two New Methods

by

Theodore Gustav Waech

A thesis submitted in partial fulfillment of the requirements for the degree of

Doctor of Philosophy

(Chemistry)

NOTICE

PORTIONS OF THIS REPORT ARE ILLEGIBLE. It has been reproduced from the best available copy to permit the broadest possible availability.

University of Wisconsin
1968

Molecular Beam Focusing of Diatomics in Selected States: Two New Methods*

by

Theodore Gustav Waech

(Under the Supervision of Professor Richard B. Bernstein)

ABSTRACT

Two methods have been developed for the focusing and state selection of diatomic molecules in thermal molecular beams. The first utilizes a pair of four-pole electric fields, with an interposed crossed beam of microwaves, to select beams of chosen vibrational-rotational states. No mechanical velocity selector is needed. The second (requiring a selector) involves a ten-pole electric field which allows weak focusing and selection of rotational states of negative (or positive) Stark energy, including the "rotationless" state J,M = 0,0.

Also, calculations are presented on the scattering of thermal beams of atomic hydrogen by hydrogen atoms.

---

* Work supported by the National Aeronautics and Space Administration, Grant NsG-275-62; National Science Foundation, Grant GP-7409; U.S. Bureau of Naval Weapons, Applied Physics Laboratory Subcontract No. 181461 (Government Prime Contract NOw 62-0604-c; and U.S. Atomic Energy Commission, Division of Research, Contract AT(11-1)-1328.

ACKNOWLEDGMENTS

I wish to thank Professor R. B. Bernstein for his suggestions and his patience, and for his emphasis on teaching of research rather than only production of research.

Also appreciated is the work of Dr. K. H. Kramer, who expertly designed and built the major part of the apparatus used, and R. J. Beuhler, Jr., who made substantial improvements on the apparatus. R. W. Fenstermaker, R. W. Bickes, and other colleagues often gave helpful advice.

This work could not have been done without the services and skill of Leo Rogers and others in the chemistry machine shop.

The secretarial staff of the Theoretical Chemistry Institute were very helpful in typing and many other tasks.

The greatest "thankyou" must go to my parents and my wife, Donna, for their encouragement and help. Donna has made my last year of study here much more enjoyable.

TABLE OF CONTENTS

FIGURES

(not including those of the inserted publications)

TABLES

(not including those of inserted publications)

I INTRODUCTION

It is well known that beams of charged particles can be focused, accelerated, or moved about "easily" by the use of electric and magnetic fields. Such fields however, if they are inhomogeneous, can also somewhat influence the motion of neutral particles exhibiting a Stark or Zeeman effect. The particles "seek" a position of lowest potential energy which may be in either a high or low field. If the change in energy due to the field is of similar or greater magnitude than the particles translational energy, the motion can be affected appreciably.

This thesis discusses methods of using the Stark effect to select focused molecular beams of chosen rotational (or vibrational-rotational) states. Only methods applying to linear polar molecules (mainly diatomics) will be discussed in depth.

Actually, certain rotational states of diatomics have often been focused in the past with a four-pole field.[I.1] In fact, much molecular beam spectroscopy has been done using these states,[I.2] and their focusing will be discussed.

The thesis is divided into six main sections. Sections III B, IV B, and VI B are papers (already published or in press), and

- - - - -

I.1 See, for instance, reference III B 1 (in section III B).

I.2 See, for instance, reference III B 4b.

therefore contain their own figures and footnotes.[I.3,4] Those sections are independent of the rest of the text.

I.3 Pages, figures, footnotes, and tables are numbered according to their section; i.e., Fig. II B.1 is the first figure in section II B. The papers (designated sections III B, IV B, and VI B) do not (internally) include the section numbers.

I.4 Much of the work presented is not entirely the writer's own, but includes substantial contributions by the co-authors (as specified) of the published works. However, it is all included for the sake of completeness.

II. FOUR POLE FIELD FOCUSING

A. Theory[II A.1]

Let W be the energy of a heteronuclear diatomic molecule in an electric field E, assuming a $^1\Sigma$ electronic state,

$$W = W_o + W_2 + W_4 + \cdots \qquad \text{(II A.1)}$$

where W_o is the energy in the absence of a field, W_2 is the second order Stark energy (proportional to E^2), etc. For sufficiently low E, the higher order Stark energies are negligible compared to W_2. W_2 is well known to be[II A.2]

$$W_2 = \frac{\mu_o^2 E^2}{h^2/2I} f_2(J,M) \qquad \text{(II A.2)}$$

where μ_o = permanent dipole moment

I = moment of inertia of the molecule about its center of mass

$$f_2(J,M) = \frac{J(J+1) - 3M^2}{2J(J+1)(2J-1)(2J+3)}$$

$$= -\frac{1}{6} \quad \text{for } J,M = 0,0$$

J = rotational quantum number

M = orientation or magnetic quantum number. M can have

II A.1 See ref. III B.1 for more information.

II A.2 C. H. Townes and A. L. Schawlow, "Microwave Spectroscopy," (McGraw-Hill Book Co., Inc, New York, 1955), P. 250.

only values J, J - 1, . . . - J. M$\hbar$ is the component of the angular momentum in the direction of the electric field.

Neglecting W_2 and higher order Stark energies, the force ($\vec{F}$) on the dipole due to an inhomogeneous electric field is

$$\vec{F} = -\nabla W = \frac{-\mu_o^2}{\hbar^2/2I} f_2(J,M) \nabla E^2 =$$

$$-\frac{2\mu_o^2}{\hbar^2/2I} \cdot f_2(J,M)\left[E_x\left(\frac{\partial E_x}{\partial x}\hat{i} + \frac{\partial E_y}{\partial x}\hat{j}\right) + E_y\left(\frac{\partial E_x}{\partial y}\hat{i} + \frac{\partial E_y}{\partial y}\hat{j}\right)\right] \qquad \text{(II A.3)}$$

where $\hat{i}$ and $\hat{j}$ are unit vectors in the x and y directions respectively.

This is more often written

$$\vec{F} = -\nabla W = -\frac{\partial W}{\partial E}\nabla E \equiv \mu_{eff}\nabla E \qquad \text{(II A.4)}$$

where $\mu_{eff} = -\frac{2\mu_o^2 E}{\hbar^2/2I} f_2(J,M)$ (II A.5)

Note that μ_{eff} is proportional to E. Fig. 1 illustrates the linearity of μ_{eff} versus E for [illegible] E

[illegible] an inhomogeneous electric field (E = E(x,y)) can be built such that $\vec{F}$ is proportional to $-\vec{r}$ (for sufficiently small E) for

Fig. II A.1 $\langle\cos\theta\rangle = \frac{\mu_{eff}}{\mu_o}$ for a diatomic in an electric field E.

θ is the angle between $\vec{E}$ and the dipole moment. $Y = \frac{\mu_o E}{\hbar^2/2I}$. The dashed lines correspond to the low field limit where $\langle\cos\theta\rangle = 2\, f_2(J,M)\, Y$. The graph was made using calculations (of $\langle\cos\theta\rangle$ at integral values of Y) of K. H. Kramer using the continued fraction method of H. K. Hughes.[II A.3]

II A.3 H. K. Hughes, Phys. Rev. 72, 614 (1947).

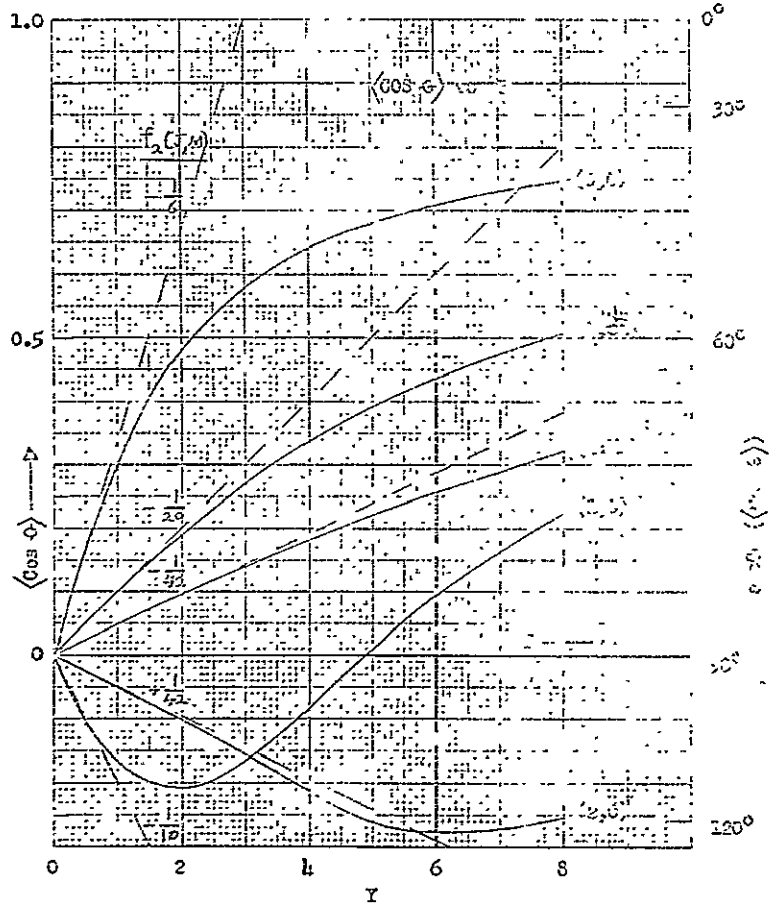

Fig. II A.1

a set of rotational states.[II A.4] This field is the four-pole field with a potential $V = \frac{V_o}{R^2}(y^2 - x^2)$ (II A.6)

where V_o is the absolute value of the voltage on any one of four hyperbolic electrodes as shown in the sketch.[II A.5]

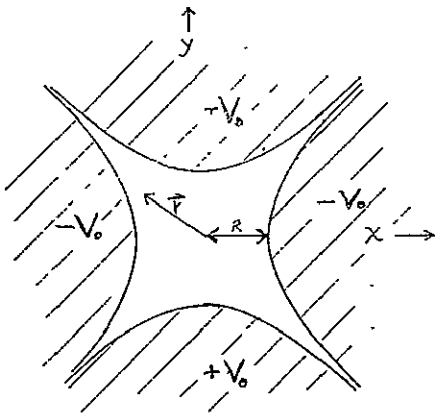

$$\vec{E} = -\nabla V = \frac{2V_o}{R^2}(x\hat{i} - y\hat{j}) \qquad \text{(II A.7)}$$

$$E = \frac{2V_o}{R^2}(x^2+y^2)^{1/2} = \frac{2V_o}{R^2}r \qquad \text{(II A.8)}$$

- - - - -

II A.4 See reference III B.1.

II A.5 The actual electrodes used are circular rods. See section V D.

Then from equation (II A.3) or (II A.4),

$$F = -\frac{\mu_o^2}{\hbar^2/2I} f_2(J,M) \frac{8V_o^2}{R^4} r(t) = m \frac{d^2 r(t)}{dt^2} \qquad \text{(II A.9)}$$

where m is the particle mass and t is time.

For positive $f_2(J,M)$ (as for J,M = 1,0; 2,0; etc.), there is a force toward r = 0. This is because such particles increase in potential energy in an electric field (see Eq. (II A.2)). Therefore they are repelled by the stronger field at large r (see Eq. (II A.8)). For negative $f_2(J,M)$ particles (e.g., those in the states J,M = 0,0; 1,1; 2,2; etc.), the force is directed outward toward large r. The solutions to Eq. (II A.9) are

$$f_2(J,M) > 0 : \quad r = r_o \cos 2\pi\nu t + \frac{\dot{r}_o}{2\pi\nu} \sin 2\pi\nu t \qquad \text{(II A.10)}$$

$$f_2(J,M) < 0 : \quad r = r_o \cosh 2\pi\nu t + \frac{\dot{r}_o}{2\pi\nu} \sinh 2\pi\nu t \qquad \text{(II A.11)}$$

where $$2\pi\nu = \frac{2V_o\mu_o}{R^2}\sqrt{\frac{2f_2(J,M)}{m\hbar^2/2I}} \qquad \text{(II A.12)}$$

$r_o = r$ at $t = 0$

$\dot{r}_o = \frac{dr}{dt}$ at $t = 0$

B. Experimental considerations

Consider the results of an experiment with a molecular beam (in a vacuum chamber) effusing into a four-pole field with $r_o = 0$ (see sketch). A particle for which $f_2(J,M) < 0$ is deflected with an exponential trajectory (Eq. (II A.11)). But for $f_2(J,M) > 0$, a sinusoidal trajectory brings the particle back to the $r_o = 0$ axis after a time

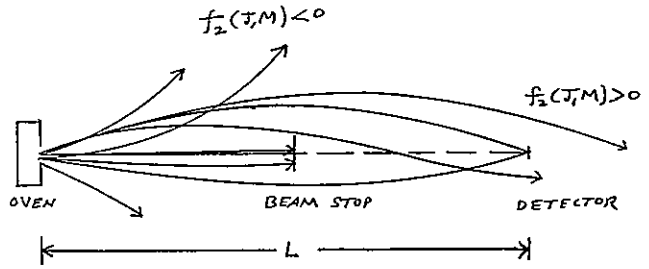

$$\frac{\tau}{2} = \frac{i}{2\nu} \qquad \text{(II B.1)}$$

during which it travels a distance

$$\frac{\lambda}{2} = \frac{v}{2\nu} \qquad \text{(II B.2)}$$

where λ is the "wavelength" of the trajectory and v is the velocity ($\frac{dz}{dt}$). If $\frac{\lambda}{2} = L$, the particle hits the detector; i.e., the detected focused beam consists of particles for which $L = \frac{V}{2\nu}$ or

$$\frac{V_o}{V} = \frac{\pi R^2}{2 M_o L} \sqrt{\frac{m \hbar^2 / 2I}{2 f_2(J,M)}} \qquad \text{(II B.3)}$$

Eq. (II B.3) is the condition for focusing with the four-pole field. The trajectories of these detected particles have an amplitude (A) of (using Eqs. (II A.10) and (II B.2))

$$A(r_o = 0) = \frac{L}{\pi} \left(\frac{dr}{dz}\right)_{t=0} \qquad \text{(II B.4)}$$

Note that at a given V_o, a certain velocity for each state is focused. Because of the wide velocity distribution normally found in a beam, a mechanical velocity selector (see section V B) is used. With V_o and v set, only one state is focused at a time as in the traced sketch (Fig. II B.1).[II B.1] The width of a peak is determined by the velocity selector resolution unless there are higher order Stark effects present, poor positioning of apparatus components, too high a background pressure, etc. Although a beam stop or "obstacle" is used to stop the direct beam (all states, $r_o \approx 0$) from hitting the detector, many particles are still forward scattered around the beam stop unless the pressure in the apparatus is

- - - - -

II B.1 H. G. Bennewitz, K. H. Kramer, W. Paul, and J. P. Toennies, Z. Physik 177, 84 (1964).

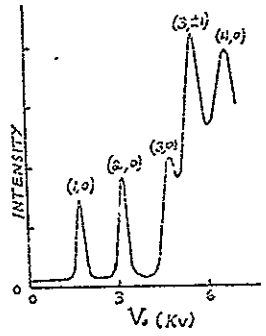

Fig. II B.1

Tracing of an excellent focusing curve of T&F obtained by Bennewitz et al.[II B.1]

very low. Also, at high V_o, there may be some "triple focusing" (see first sketch below).

Consider the case for which r_o is not necessarily zero. If $r_o \neq 0$, note from Eq. (II A.10) that the final r (at detector) is $-r_o$ if Eqs. (II B.1) - (II B.3) are satisfied. This suggests that for a velocity selected beam, the focused particles form an inverted image of the oven opening (which is usually a small circular hole or a thin slit) at the detector. Thus the four-pole field acts as a lens, as noted by several authors.

However the image is somewhat "fuzzy" for actual experiments. This is introduced by a non-zero velocity range, by background gas scattering, and by larger possible amplitudes[II B.2] which may give more high order Stark effects (see second sketch below).

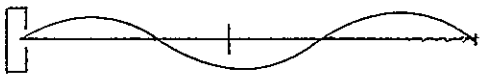

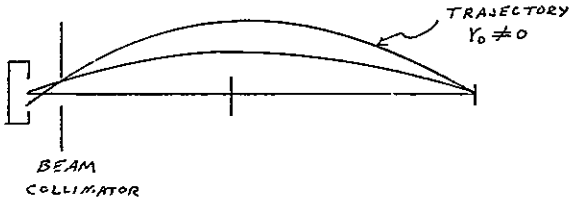

- - - -

II B.2 Assuming only a second order Stark effect:

$$A = \sqrt{r_o^2 + \left(\frac{L}{\pi}\left(\frac{dr}{dz}\right)_{t=0}\right)^2}$$

Various effects such as inhomogeneities in the field, possible "end effects," or perhaps oil or beam material on the field rods makes the field astigmatic. A small oven opening (and a small detector) is needed to form good images since it may be more accurately positioned (usually <u>off</u> the r = 0 axis) to give the least astigmatic effect (see sketch).

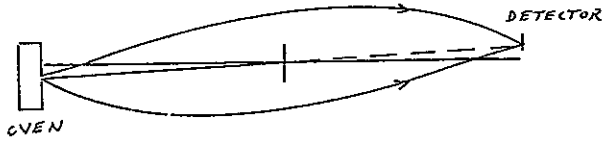

The inverted image may be magnified. This is because some field-free space along the beam axis is needed for equipment such as the velocity selector. Consider the case in which a velocity selector is positioned near the detector (see sketch below). The

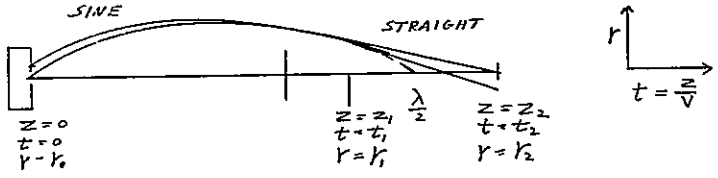

particles move in straight lines in this region. Then using Eq. (II A.10), at $t = t_2$

$$r_2 = r_1 + \dot{r}_1 (t_2 - t_1) =$$

$$r_0 \cos 2\pi\nu t_1 + \frac{\dot{r}_0}{2\pi\nu} \sin 2\pi\nu t_1 -$$

$$2\pi\nu r_0 (t_2 - t_1) \sin 2\pi\nu t_1 + \dot{r}_0 (t_2 - t_1) \cos 2\pi\nu t_1 \qquad \text{(II B.5)}$$

When ν is set so there is focusing at $t = t_2$, $r_2 = 0$ for $r_0 = 0$. Then

$$\frac{\dot{r}_0}{2\pi\nu} \sin 2\pi\nu t_1 + \dot{r}_0 (t_2 - t_1) \cos 2\pi\nu t_1 = 0 \qquad \text{(II B.6)}$$

or $$2\pi\nu (t_2 - t_1) = -\tan 2\pi\nu t_1 \qquad \text{(II B.7)}$$

for focusing with an initial sine trajectory and a straight trajectory near the detector.[II B.3] At $t = t_2$

$$r_2 = r_0 (\cos 2\pi\nu t_1 - 2\pi\nu (t_2 - t_1) \sin 2\pi\nu t_1) \qquad \text{(II B.8)}$$

$$= r_0 \left(\frac{1}{\cos 2\pi\nu t_1} \right)$$

The expression in parentheses is the magnification which is always greater than one in absolute value for this case.

- - - - -

II B.3 $\frac{\lambda}{2}$ can be determined from ν.

For the straight portion of the trajectory put first, one can show in analogous fashion (see sketch) that the focusing condition

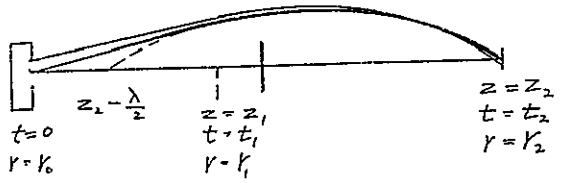

is[II B.4]

$$\frac{t_1}{2\pi\nu} = -\tan 2\pi\nu (t_2 - t_1) \qquad \text{(II B.9)}$$

and the magnification equation is[II B.5]

$$r_2 = r_0 \cos 2\pi\nu (t_2 - t_1) \qquad \text{(II B.10)}$$

where the magnification is always less than one in absolute value.

- - - - -

II B.4 Eq. (II B.9) is the "same" as (II B.7) if one identifies $t_2 - t_1$ in (II B.9) with t_1 in (II B.7), etc.

II B.5 The magnifications are reciprocals of one another if $t_2 - t_1$ in (II B.10) is the same as t_1 in (II B.8), etc.

It is obvious that the detector should not be much larger than the focused image. If it is, one will detect a larger fraction of the particles that are scattered around the beam stop, but no more focused signal. Also, the per cent of any given state focused ("direct beam"[II B.6] is considered the 100% base) will be less since the detected direct beam will be large. A large detector may partially detect another state while the desired one is properly focused. Of course, if the detector or oven opening is too small, the signal will be too small to detect easily.

Fig. II B.2 illustrates the geometry used to obtain the focusing curve of Fig. III B.1. In addition, section II E gives data for four-pole focusing runs made with various geometries by the writer.

- - - - -

II B.6 "Direct beam" is the signal obtained with no beam stop and with $V_o = 0$.

Fig. II B.2 Illustration of "fine" geometry.

This was needed to four-pole focus with good resolution. Possible trajectories with and without voltage on the fields are shown. The scale of dimensions along the beam axis is, of course, much compressed relative to the scale perpendicular to the axis, for clarity.

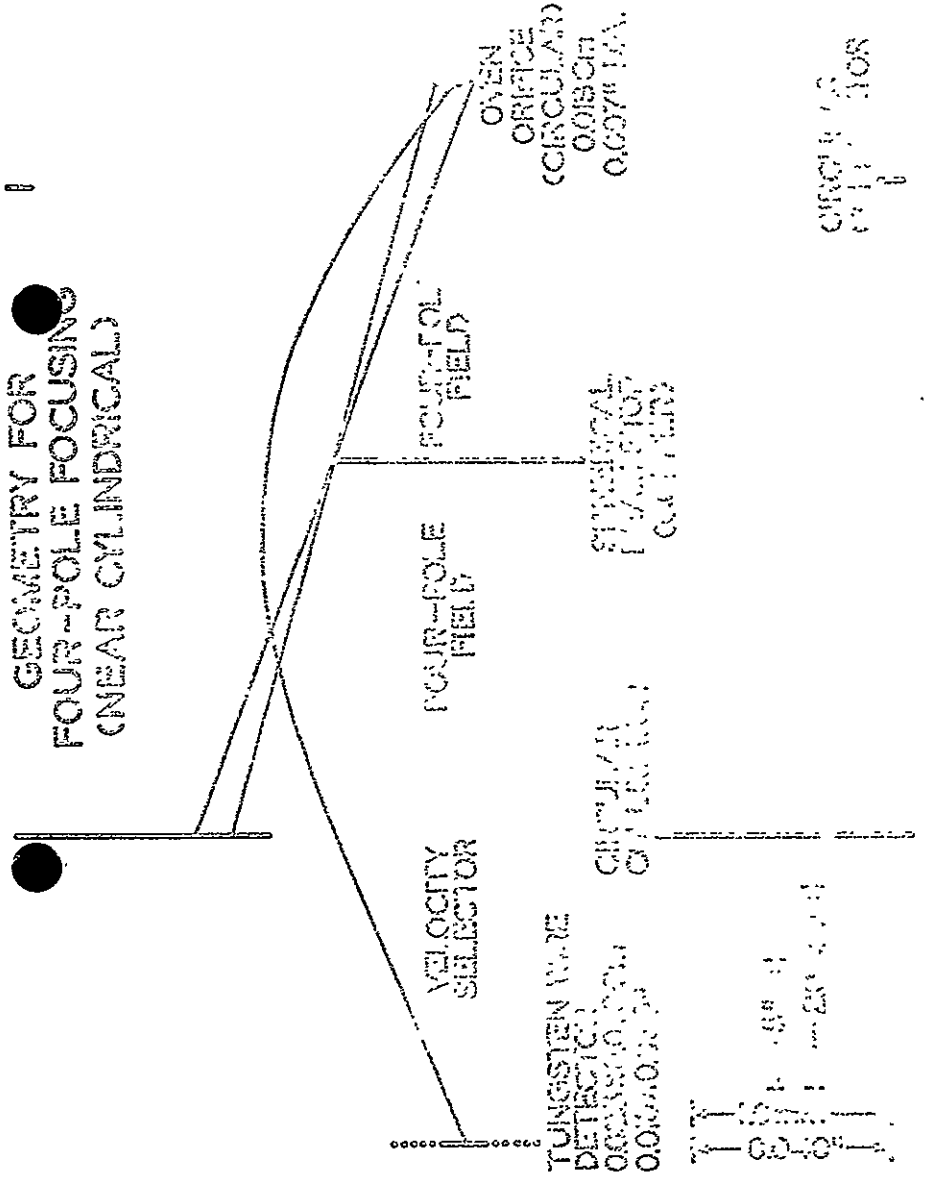

Fig. II B.2

C. Choice of Focusable Molecules

Most of the diatomic molecules which are likely possibilities for focusing are listed in Table II.1 (following). The values of M (molecular weight), μ_0, B_e and ω_e for the alkali halides are taken from a report by Herm and Herschbach.[II C.1] The value of $\frac{\sqrt{mk^2/2I}}{\mu_0}$ was calculated to be the same as $\frac{\sqrt{19.66 \cdot MB(cm^{-1})}}{\mu_0 \text{ (daltons)}}$ in units of volt $\frac{\text{sec}}{\text{cm}^2}$.

The table is intended to help decide which molecules to focus. Note that the cesium and rubidium halides are the most easily detected with a Langmuir-Taylor detector. The TlF, in experience at this laboratory, decomposed at appreciable rates at temperatures above about 320°C. Putting the material in a glass vial in the oven helped reduce the decomposition problem, however.

At the most probable velocity, the "angle of aperture" (ϕ), from an oven, of a molecular beam over which a four-pole field (for a given rotational state) can focus, is proportional to $\sqrt{\frac{B}{T}}$.[II C 2] (T is the oven temperature.) The amount of the given state focused should then be proportional to this squared (for $K_0 \approx 0$) times the fraction of the beam in the given state. Since the probability of a low rotational state (i.e., of given J and M) is (for $B \ll kT$) about B/kT, one might conclude that a "figure of merit" for a four-pole focused diatomic could be $(\frac{B}{T_p})^2$, where T_p is the oven temperature needed to get a given reasonable vapor

- - - - -

II C.1 R. R. Herm and D. R. Herschbach, UCRL Report 16039 (University of California Radiation Laboratory, Berkley, July, 1965).

II C.2 See ref. III B.1.

Table II C.1 PROPERTIES OF ALKALI HALIDES AND Tl F

Molecule	Molecular Weight M (gms/mole)	Dipole Moment μ_0 (Debye)	Rotational Constant B_e (cm^{-1})	Vibrational frequency ω_e (cm^{-1})	$\sqrt{m\hbar^2/2I}/\mu_0$ (volt sec/coul)	T for 1 mm pressure[b] (°C)
Li^6F	25.94	6.6	1.5087	906.2	5.2	1047
Li^7Cl^{35}	42.40	7.12	0.7065	667	4.19	783
Li^7Br^{79}	86.86	6.19	0.5554	576	6.11	748
Li^7I^{127}	133.85	6.64	0.4432	501	6.32	723
NaF	41.99	8.37	0.4369	(463)	2.78_7	1077
$NaCl^{35}$	58.45	8.5	0.2181	366	2.2_9	865
$NaBr^{79}$	102.91	9.4	0.1513	302	2.2_9	806
NaI^{127}	149.90	(9.3)[a]	0.1178	258	2.4_6	767
$K^{39}F$	58.10	7.33	0.2799	400	2.99_6	885
$K^{39}Cl^{35}$	74.56	10.48	0.1286	281	1.609	821
$K^{39}Br^{79}$	119.02	10.41	0.0812	213	1.626	795
$K^{39}I^{127}$	166.01	11.1	0.0609	(173)	1.56	745

(continued on the next page)

Table II C.1 (Continued)

Molecule	Molecular Weight	Dipole Moment	Rotational Constant	Vibrational frequency	$\sqrt{m\hbar^2/2I}/\mu_0$	T for 1mm pressure[b]
$Rb^{85}F$	104.48	8.80	0.2107	390	2.904	921
$Rb^{85}Cl^{35}$	120.94	10.6	0.0876	225	1.67	792
$Rb^{85}Br^{79}$	165.40	10.5	0.0475	(166)	1.45	781
$Rb^{85}I^{127}$	212.39	(10.8)	0.0328	(128)	1.33	748
CsF	151.91	7.88	0.1844	352[c]	3.66	712
$CsCl^{35}$	168.37	10.5	0.0721	209	1.81	744
$CsBr^{79}$	212.83	10.7	0.0361	(139)	1.41	748
CsI^{127}	259.82	12.1	0.0236	(101)	1.11	733
$Tl^{205}F$	223.4	4.23[d]	0.2223[d]	475[e]	9.08	-

[a] Values in parenthesis are theoretical estimates.

[b] Handbook of Chemistry and Physics (Ed. 42) (The Chemical Rubber Publishing Co., Cleveland, 1961).

[c] See ref. III B.8b.

[d] G. Graff, W. Paul, and Ch. Schlier, Z. Physik 153, 38 (1958).

[e] Howell, H. G., Proc. Roy. Soc. (London) 160, 242 (1937).

pressure. This number is meaningful if the beam intensity at the most probable velocity is proportional to oven pressure, and if one can obtain the necessary experimental conditions (T, velocity, V_o, field assembly size, etc.)

D. Appendix 1 Calculation of V_o/v for a typical case.

From section II, one notes that for the four-pole field,

$$\frac{V_o}{v} = \frac{\pi R^2}{2\mu_o L}\sqrt{\frac{m\hbar^2/2I}{2 f_2(J,M)}}$$

For the state J,M = 1,0; $f_2(1,0) = \frac{1}{10}$ (see Fig. II A.1). For CsF,

$$\frac{\sqrt{m\hbar^2/2I}}{\mu_o} = 3.66 \ \frac{\text{volt sec}}{\text{cm}^2}$$

from Table II.1. For the apparatus used in this work,

R = 0.413 cm

L = 107 cm

Then

$$\frac{V_o}{v} = 0.0205 \ \frac{\text{volt sec}}{\text{cm}} = \frac{1}{502} \ \frac{\text{Kv. sec}}{\text{m.}}$$

The fact that $\frac{\lambda}{2} \approx \frac{L}{1.05}$ for a focused beam in the given apparatus suggests that $\frac{V_o}{v}$ is actually higher by 5%. Usually high order Stark effects will raise $\frac{V_o}{v}$ also (50% or more for coarse geometry).

E. Appendix 2. Four-pole focusing data.

Table II E.1 illustrates the results of preliminary four-pole focusing runs. The apparatus pressure was typically 5×10^{-7} torr except in the oven chamber where it was normally higher. All of the runs other than 6 and 7 were done using CsF. The space left between the field assemblies was there because of the work of section III of this thesis.

Table II·E.1 Four-Pole Focusing Data

Run No.	% (1,0) focused	Resolution (Valley / (1,0) peak)	(1,0) peak S/N	Oven T (mv)	Oven Slit (0.001")	Detector Length (0.001")
1	.25	~ 1	6	20 7	6 x 250	200
2[c]	~ .3	.55	30	21.28	"	"
3[c]	~ 1.	.67	40	20.28	6 x 250(?)	"
4[c]	$.4_6$	.54	30	20-25	3 x 250	"
5[c]	.34-.14	.51	40	20.65	10 x 250	"
6[cd]	?	.53	15	12.7(?)	10 x 250	"
7[cd]	.3	.38	10	12(?)	"	"
8	-	-	-	~18	10 x 50	80
9	1.2_8	.65	15	~23.4	10 x 50	"
10	3.1	.79	30	~20.6	10 x 30	50
11		LITTLE DATA				
12	5.5-8.5	.72	50	~22.5	10 x 30	50
13	2.25	.04	100	~29.2	7 ⊙	30
14	~ 1.	.19	50	30.0	"	"
15[b]	?	.065	50	~30.5	"	"
16	1.5	.14	70	24.57	10	"
17	~1-3	.18	>100	25.98	"	"

Table II E.1 (Continued)

COLLIMATOR		BEAM STOP		SELECTOR		Space Between Fields
Size (0.001")	Position	Size[a] (0.001")	Position	End	Speed (m/sec)	
170 x 120	near vel. sel.	60	center	oven	386	~ 2"
"	"	"	"	"	371	"
"	"	"	"	"	270	~ 0
"	"	30	vel. sel.	"	370(?)	~ 2
200 ⊙	center	60	center	oven	325(?)	"
"	"	30	"	"	~220	"
>200 ○	"	"	"	"	~200	"
120 x 180	vel. sel.	"	vel. sel.	det	not on	~ 0
"	"	"	"	"	~270	"
190 ⊙	"	50 ⊘	center	"	225	"
		LITTLE DATA				
100 ⊙	vel. sel.	50 ⊙	center	det	~270	~0
77 ⊙	"	"	"	"	396	"
"	"	"	"	oven	~368	~ 4"
"	"	"	"	"	34_2	"
"	"	"	"	"	414	"
"	"	"	"	"	396(?)	"

Table II E.1: (Continued)

a Beam stop is wire unless it is indicated to be spherical by ⊙.

b There was almost no effort to maximize the signal or resolution with the velocity selector on.

c Older fields.

d T1F beam.

III. SELECTION OF VIBRATIONAL-ROTATIONAL STATES

A. Introduction

The paper which comprises section III B concerns a method of producing and detecting beams of specified vibration-rotational states.[III A.1,2] The method combines focusing (with, say, four-pole fields) of a chosen J,M state with microwaves which cause transitions to states which are defocused (see Fig. III A.1A).

If one varies the microwave frequency (ν),[III A.3] one observes decreases in signal at frequencies corresponding to transitions $|\nu\ J\ M> \rightarrow |\nu\ J'M'>$ (see Fig. III A.1B). One can remain tuned to any given absorption line and modulate the microwaves (and therefore the detected beam intensity) at a convenient, low frequency of, say, 25 Hz (see Fig. III A.1C). A phase sensitive (or lock-in) detector will detect only the AC, in-phase, component of the signal; in this instance, only the $|010>$ molecules are detected.

Note also that the focusing field acts as a velocity selector (see Eq. (II B.3)), so a mechanical selector is not needed.[III A.4] Other J,M states will strike the detector then (and add to the

- - - - -

III A.1 T. G. Waech and R. B. Bernstein, Chem. Phys. Lett. 2, 0000 (1968) in press.

III A.2 The original method was an adaptation of the molecular beam electric resonance (MBER) technique, in collaboration with Dr. S. S. Bernstein. Suggestions by R. W. Fenstermaker and R. J. Beuhler helped the writer in the experimental development of the method.

III A.3 Not to be confused with the ν of Eqs. (II A.10) - (II A.11).

III A.4 See ref. III B 2.

BLANK PAGE

Fig. III A.1 Basic considerations of the MBER method.

Microwaves cause transitions to defocused states (A) and decrease the focused beam intensity for certain microwave frequencies (B). This decrease is modulated (C).

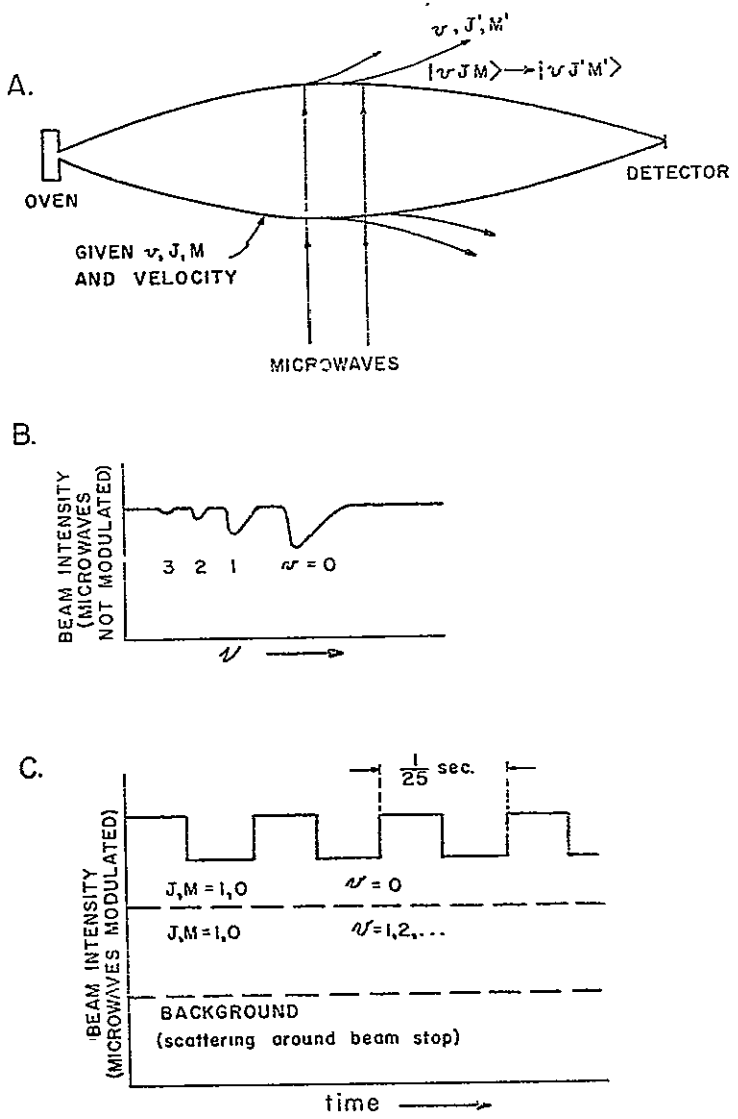

Fig. III A.1

"statistical" noise), but, not being modulated, they will not be lock-in detected.

The following communication concerns the technique and its use. The geometry used is given in Fig. III A.2. The apparatus is described more fully in section V. It should be pointed out here that the signal-to-noise has by no means been optimized. Higher oven temperatures (a "laval"-type oven might be used) and less collimation would lead to more signal. A larger beam stop might give less contributions to the noise due to other J,M states and background scattering, as well as better velocity selection (see appendix, section III C).

The communication is followed by two appendices which give more information on frequency and velocity considerations. A third appendix describes calculations which were carried out in an effort to understand the fate of the $|\nu' 00>$ particles formed in the experiment.

BLANK PAGE

Fig. III A.2 Illustration of coarse geometry.

This was used to produce a large signal-to-noise ratio for one vibrational-rotational state. Note the use of an oven slit, a long detector, and a long beam stop.

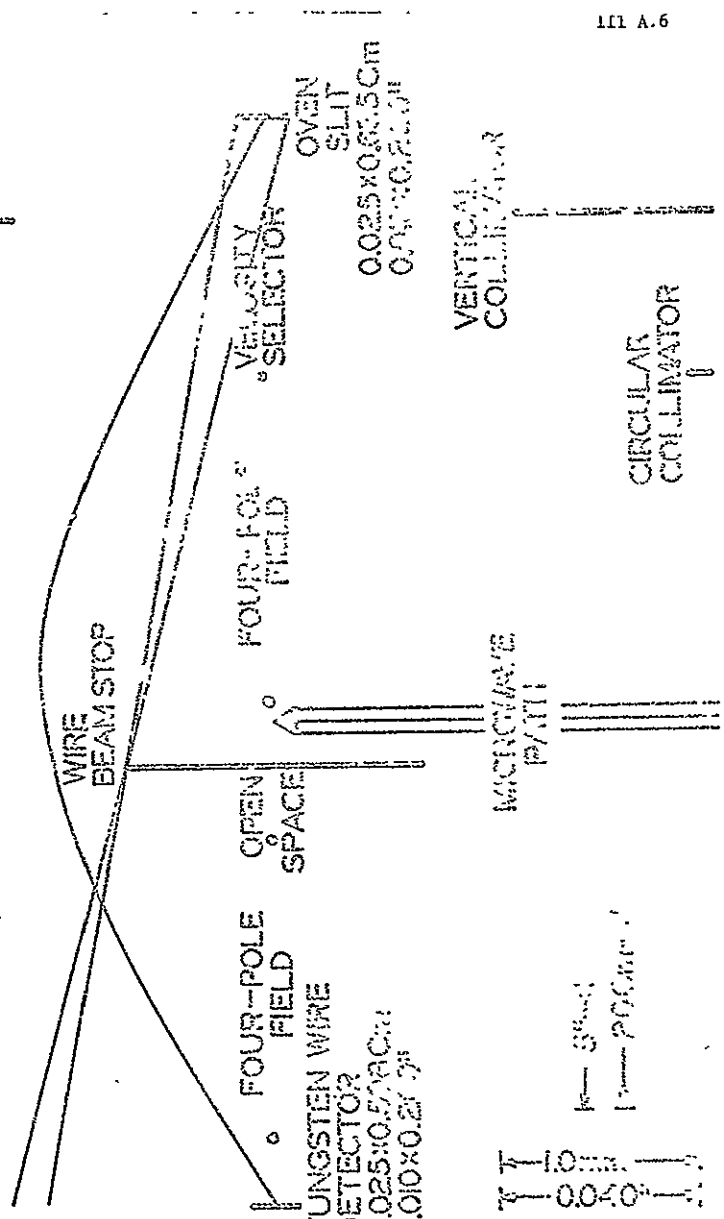

B. "Production of Focused Beams of Polar Diatomic Molecules in Selected Vibrational-Rotational States," by T. G. Waech and R. B. Bernstein, Chem. Phys. Letters 2, 0000 (1968), to be published.

(See journal article for this section)

C. Appendix 1. Velocity considerations.

1. Determination of the selected velocity.

With no mechanical velocity selector, the four-pole field focuses a different velocity for each state at one V_o. A mechanical velocity selector can be used; or microwave modulation, as previously described, eliminates this problem by "isolating" a beam signal of the desired state (see Fig. III C.1).

The velocity can be determined by eq. (II B.3) unless high order Stark effects are important in the focusing. However, one may still approximate the velocity if assumptions are made concerning effective values of certain quantities for a total focused beam. Somewhat tenuous arguments must be used. An example is given here considering the beam of Fig. III B.2. With the mechanical velocity selector on, at high oven temperature, one finds $\frac{V_o}{v} = \frac{1}{285} \frac{\text{Kv sec}}{\text{m.}}$. But for the geometry used, $\frac{V_o^{(2)}}{v} = \frac{1}{483} \frac{\text{Kv sec}}{\text{m.}}$ where $V_o^{(2)} = V_o$ assuming a second order effect.

$$\frac{V_o^{(2)}}{V_o} = \frac{285}{483} = \frac{V_o^{(2)}}{1.65\ Kv} \qquad \text{(III C.1)}$$

$$V_o^{(2)} = 0.97\ Kv \qquad \text{(III C.2)}$$

That is, the 1.65 Kv acted the same as .97 Kv would if only a second order Stark effect were present.

Assume that one can take effective or average values of μ_{eff}, $\langle \cos \theta \rangle$, the force constant, and Y for the detected beam even though

Fig. III C.1. Intensity of $|010>$ signal versus V_o.

A chart recording from the first trial of the method (with mechanical velocity selector on) illustrates the "isolation" of the $|010>$ (or $|000>$) signal. The recording was taken with very poor focusing resolution between the (1,0) and (2,0) states, yet the (2,0) peak is not observed with modulated microwaves. The observed intensity distribution could be somewhat dependent on the microwave frequency.

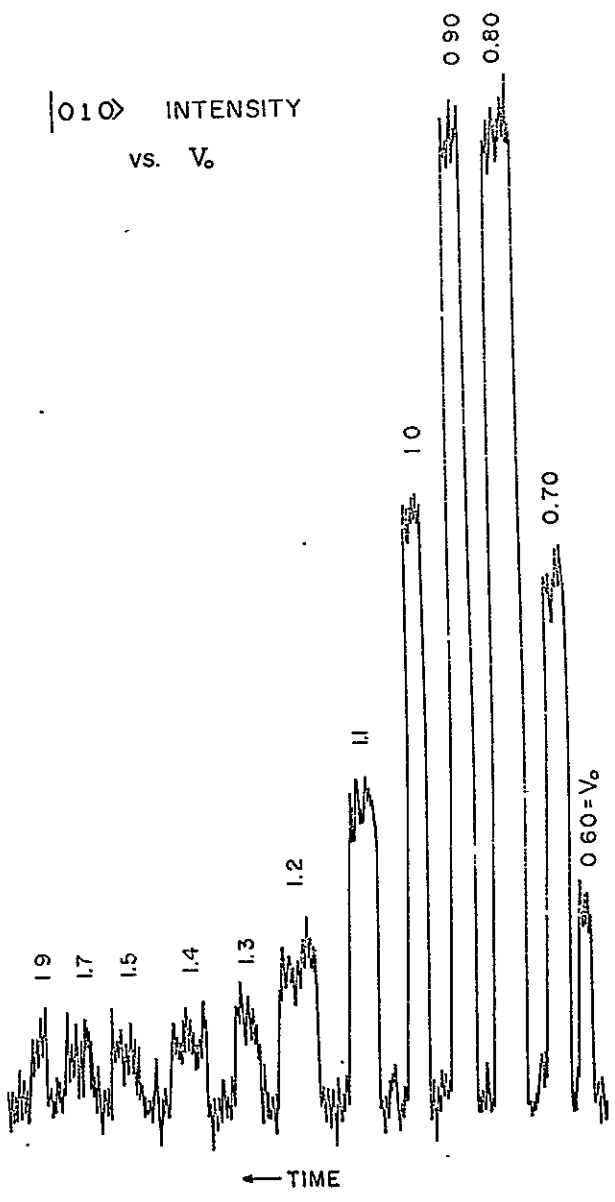

Fig. III C.1

they vary differently over each trajectory (The averaging is not indicated for each variable). Using Eq. (II A.4)

$$\frac{\mu_{eff}^{(2)}\ .97\ Kv}{\mu_{eff}^{(2)}\ 1.65\ Kv} = \frac{\mu_{eff}\ 1.65\ Kv}{\mu_{eff}^{(2)}\ 1.65\ Kv} = \frac{\text{Force constant } 1.65\ Kv}{\text{Force constant}^{(2)}\ 1.65\ Kv} =$$

$$\left(\frac{0.97}{1.65}\right)^2 = 0.346 \qquad \text{(III C.3)}$$

Since $\langle \cos\theta \rangle = \frac{\mu_{eff}}{\mu_o}$.

$$0.346 = \frac{\langle \cos\theta \rangle_{1.65}}{\langle \cos\theta \rangle^{(2)}} = \frac{\langle \cos\theta \rangle_{1.65}}{-2 f_2(1,0) Y_{1.65}} = \frac{\langle \cos\theta \rangle_{1.65}}{-.2 Y_{1.65}}$$

$$\langle \cos\theta \rangle_{1.65} = -0.0692 Y_{1.65} \qquad \text{(III C.4)}$$

Then from Fig II A.1 or the sketch, Y = 2.7 at 1.65 Kv effectively.

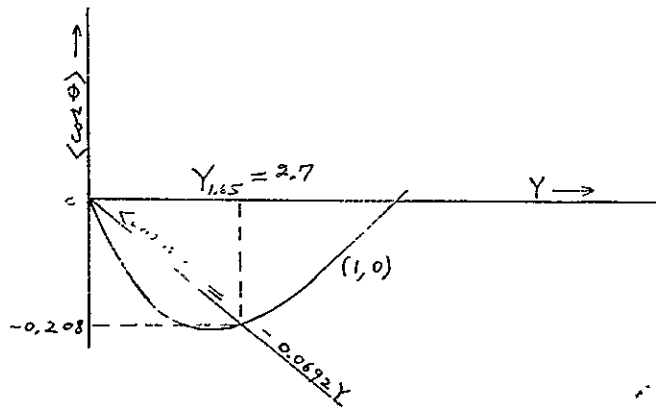

Y at a given position in the field is proportional to E which depends on V_o. Then at 1.2 Kv one might expect Y (effectively) to be

$$Y_{1.2} = \frac{1.2\ Kv}{1.65\ Kv} \times 2.7 = 1.97 \qquad \text{(III C.5)}$$

Now we may return to Eq. III C.3 for 1.2 Kv where data without mechanical velocity selection were obtained.

$$\frac{\langle \cos\theta \rangle_{1.2}}{\langle \cos\theta \rangle_{1.2}^{(2)}} = \frac{\langle \cos\theta \rangle_{1.2}}{-2 f_2(1,0) Y_{1.2}} = \frac{-.208}{-.394} =$$

$$\left(\frac{V_o^{(2)}/V}{V_o/V}\right)^2 = \left(\frac{1/485}{V_o/V}\right)^2 \qquad \text{(III C.6)}$$

$$\frac{V_o}{V} = \frac{1}{352}\ \frac{Kv\ sec}{cm} \qquad \text{(III C.7)}$$

$$V = 352\ \frac{cm}{sec\ Kv.} \times 1.2\ Kv = 422\ \frac{m}{sec} \qquad \text{(III C.8)}$$

Note that this value of $\frac{V_o}{V}$ is between the second order result and that at 1.65 Kv, as it must be.

Although this "calculation" is only very approximate, it agrees well with a second calculation based on the fact that the experiments

at 1.2 Kv were carried out at the velocity at which there was a maximum in the intensity. For a maxwellian velocity-selected (by the field) beam, the most probable velocity is

$$V_{mp} = 2\sqrt{\frac{RT}{M}} \qquad \text{(III C.9)}$$

(R = gas constant)

where m = molecular weight. This yields $V_{mp} = 426 \frac{m}{sec}$ which agrees well with the approximate value of Eq. III C.8.

2. Velocity resolution

Some information is easily derived concerning the maximum velocity range (ΔV_{max}) that one detects using the four-pole focusing fields at constant V_o. This range depends strongly on the minimum allowed amplitude of the trajectory.

Consider Fig. III C.2. Assume all the angles labeled ϕ_{min} are equal. This is a good approximation if $A_{min} \gg S_o, S_p$. For small ϕ_{min},

$$\phi_{min} \doteq \tan\phi_{min} = \frac{4S_o}{\Delta\lambda_o} = \frac{4S_D}{\Delta\lambda_D} \qquad \text{(III C.10)}$$

$$\Delta\lambda = \Delta\lambda_o + \Delta\lambda_D = \frac{4(S_o + S_D)}{\phi_{min}} \qquad \text{(III C.11)}$$

For constant V_o and J,M state, $V \propto \lambda$ so that

$$\frac{\Delta V_{max}}{V} = \frac{\Delta\lambda}{\lambda} = \frac{4(S_o + S_D)}{\phi_{min}\lambda} \qquad \text{(III C.12)}$$

One can calculate ϕ in terms of A for small ϕ (see inset, Fig. III C.2).

$$r = A\sin\frac{2\pi z}{\lambda} \qquad \text{(III C.13)}$$

$$\left(\frac{dr}{dz}\right)_{z=0} = \frac{2\pi}{\lambda}A = \tan\phi \approx \phi \qquad \text{(III C.14)}$$

$$\phi \approx \frac{2\pi A}{\lambda} \qquad \text{(III C.15)}$$

$$\frac{\Delta V}{V} = \frac{2(S_o + S_D)}{\pi A} \qquad \text{(III C.16)}$$

or for A_{min},

$$\frac{\Delta V_{max}}{V} = \frac{2(S_o + S_D)}{\pi A_{min}} \qquad \text{(III C.17)}$$

For the four-pole focusing of Figs. II B.2 and III B 1, it is found that

$$\frac{\Delta V_{max}}{V} = 0.46 \qquad \text{(III C.18)}$$

For the apparently more coarse focusing of Figs. III A.2 and III B.2, one finds

$$\frac{\Delta V_{max}}{V} = 0.21 \qquad \text{(III C.19)}$$

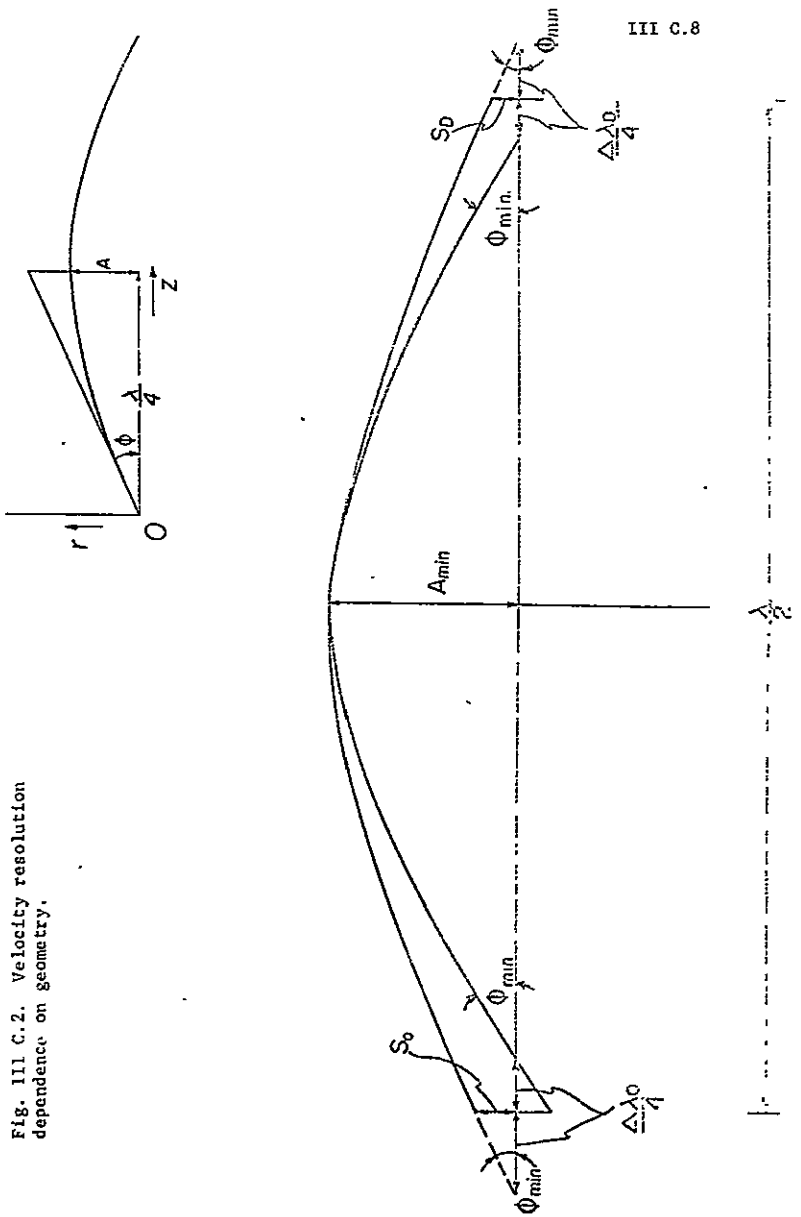

Fig. III C.2. Velocity resolution dependence on geometry.

This resolution may be compared with that of the mechanical velocity selector, FWHM = 13.7 %; $\therefore \quad \frac{\Delta V_{max}}{V} \approx 0.27$.

D. Appendix 2. Frequency information

Although new knowledge of the CsF rotational spectrum was not obtained in the present work, spectral measurements (frequencies) were made to verify the assignment of peaks. It was found for one set of conditions that at the expected frequency for the transition $|010> \rightarrow |000>$, the modulated beam intensity was one third of the maximum intensity of the $|010>$ peak (see sketch). Measurements of

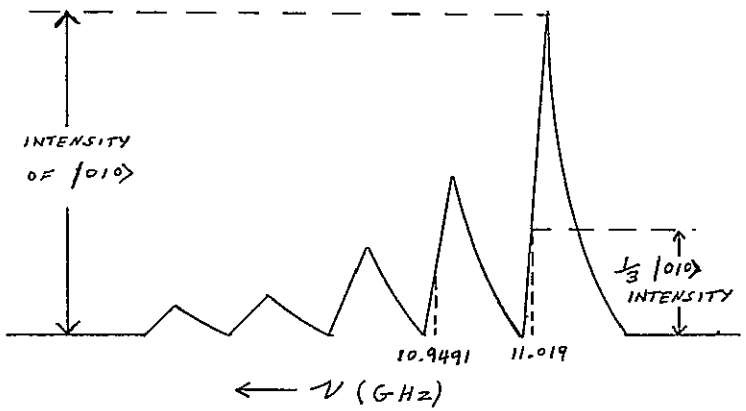

frequency at analogous intensities for other peaks gave the results in Table III D.1 below.

The shift with electric field of the transition frequencies measured in the experiment ($|\nu 10> \rightarrow |\nu 00>$) can be calculated for small fields. Using Eq. (II A.2),[III D.1]

$$h\Delta\nu = \Delta W_2 = \frac{\mu_0^2 E^2}{\hbar^2/2I}\left[f_2(1,0) - f_2(0,0)\right] \qquad \text{(III D.1)}$$

Table III D.2 FREQUENCY MEASUREMENTS

	$\lvert\nu 10> \rightarrow \lvert\nu 00>$ frequency (GHz)	α (MHz)
0	11.0193[a]	$35._1$
1	10.9491	$35._0$
2	10.8791	
accepted value of α_e		35.247[a]

[a] See reference III B.8b. The given transition frequency (for $J = 1 \rightarrow 0$) is $2B_e - \alpha_e$ where $B_e = 5.527265$ GHz.

$$h\Delta\nu = \frac{8}{15}\frac{(\mu_0 E)^2}{\hbar^2/2I} = \frac{8}{15}\mu_0 E Y \qquad \text{(III D.2)}$$

For CsF,

$$\Delta\nu(KHz) = 1.229\, E\left(\frac{Kv}{cm}\right)^2 \qquad \text{(III D.3)}$$

From this, it can be seen that to get a line width of, say, 12 MHz E can vary from zero to only about 0.1 $\frac{Kv}{cm}$ (see Fig. III D.1). For this reason the transition could not be carried out near the axis of a focusing four-pole field, where the field strength is strongly spacially dependent.

- - - - -

III D.1 Here ν is the microwave frequency, and $\Delta\nu$ is the change of the absorption frequency with electric field.

Fig. III D.1 A low resolution microwave scan.

A tracing of chart records at low resolution illustrates the broadening due to the Stark effect. Possible peak shapes (dashed) suggest that the broadening of a given ν peak "contaminates" mainly peaks of lower ν than itself

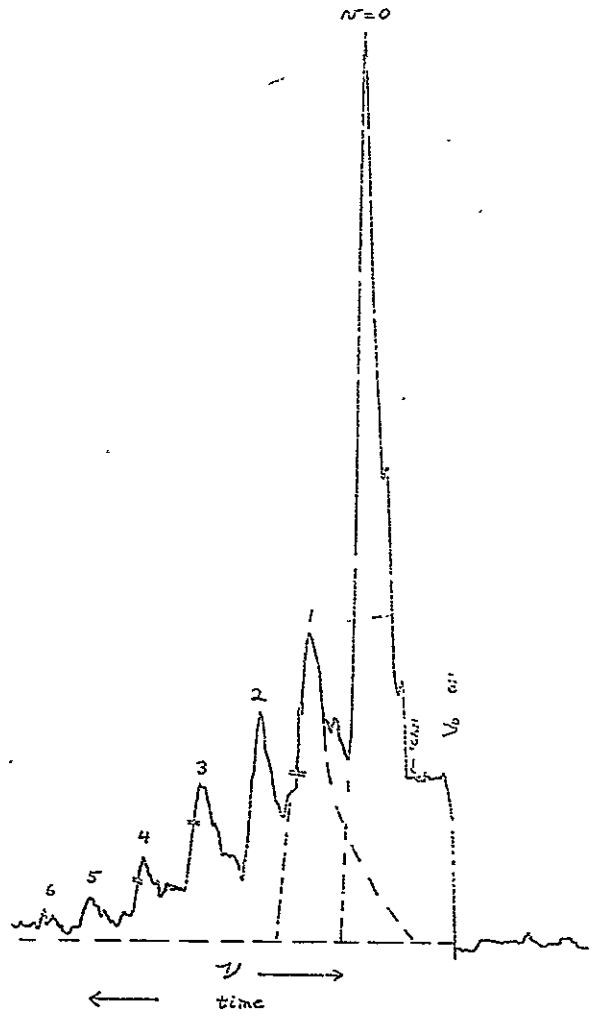

Fig. III D.1

E. Appendix 3. Attempt at focusing of J,M = 0,0 state.

Originally it was desired to focus the induced $|\nu 00\rangle$ state in the preceding work. This peak was expected at a V_o between those of the (1,0) and (2,0) peaks (using a mechanical velocity selector). However the attempt failed i.e., no significant intensity of $|\nu 00\rangle$ was detected. The difficulty is believed to be due to a magnification of the image which makes it diffuse and undetectable with a small detector.

Presented here are formulas for these magnification effects. These might be useful if the method were to be reinvestigated under better conditions, such as with a larger detector. The same methods were used as for the magnification calculation in section II B. Second order Stark effects are assumed so that the induced state follows an exponential (EXP) path in the field (see Fig. III E.1). The values $\mathcal{V}_1$ and $\mathcal{V}_0$ pertain to the 1,0 and 0,0 trajectories respectively (although $\mathcal{V}_1$ could be for any state focusable by the four-pole field, etc.). Magnifications for the present apparatus are presented. Here it is assumed that the voltages (V_o) on the two four-pole field assemblies are equal (then, $\mathcal{V}_0 = 1.285\,\mathcal{V}_1$). A path length of $\sim$107 cm is assumed with straight sections (ST) of $\sim$20 cm.

BLANK PAGE

Fig. III E.1. Trajectory types.

The magnifications for particles in the (1,0) state (A, B, and C) and for particles starting as (1,0) particles and becoming (0,0) particles (D - G), can be calculated

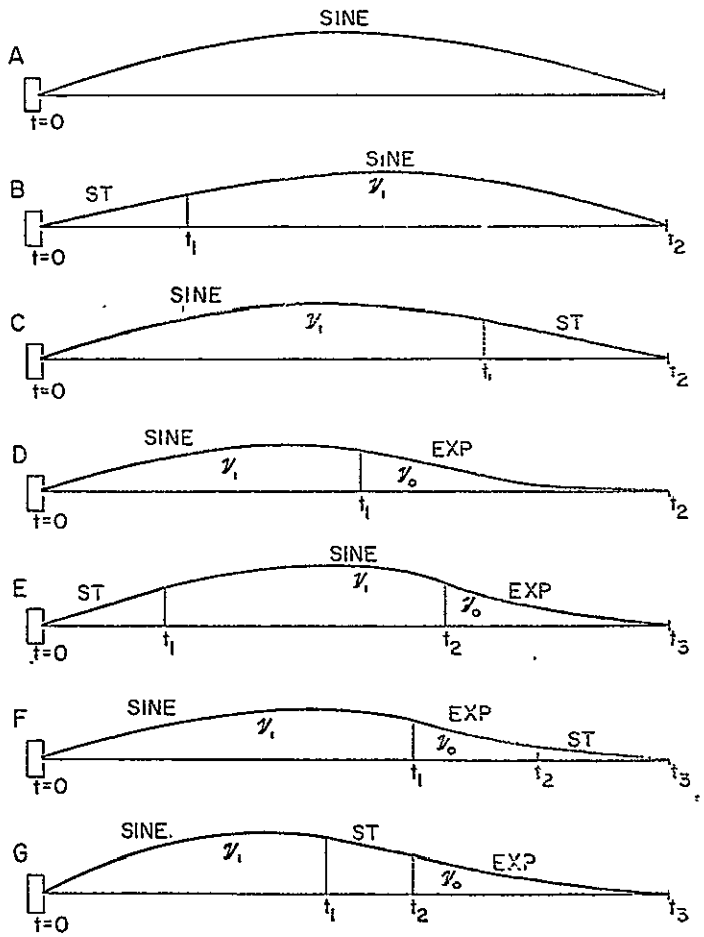

Fig. III E.1

Table III E.1: MAGNIFICATION EQUATIONS

Case	Focusing Condition
a	$2\pi \nu_1 = \frac{\pi v}{L}$
b	$\tan 2\pi \nu_1 (t_2 - t_1) = -2\pi \nu_1 t_1$
c	$\tan 2\pi \nu_1 t_1 = -2\pi \nu_1 (t_2 - t_1)$
d	$\tanh 2\pi \nu_0 (t_2 - t_1) = \frac{\nu_0}{\nu_1} \tan 2\pi \nu_1 t_1$
e	$-2\pi \nu_0 t_1 = \frac{\nu_0}{\nu_1} \tan 2\pi \nu_1 (t_2 - t_1)$ $-2\pi \nu_1 t_1 \tan 2\pi \nu_1 (t_2 - t_1) \times$ $\tanh 2\pi \nu_0 (t_3 - t_2) +$ $\tanh 2\pi \nu_0 (t_3 - t_2)$
f	$-2\pi \nu_1 (t_3 - t_1) = \tan 2\pi \nu_1 t_1$ $+ \frac{\nu_1}{\nu_0} \tanh 2\pi \nu_0 (t_2 - t_1) +$ $2\pi \nu_0 (t_3 - t_2) \tan 2\pi \nu_1 t_1 \times$
g	$\tanh 2\pi \nu_0 (t_2 - t_1)$ $-2\pi \nu_0 (t_2 - t_1) = \frac{\nu_0}{\nu_1} \tan 2\pi \nu_1 t_1$ $+ \tanh 2\pi \nu_0 (t_3 - t_2)$

Table III E.1: (Continued)

Case	Magnification	Magnification (Present Apparatus) $\nu_0 = 1.285\,\nu_1$	
a	-1	-1	J,M = 1,0
b	$\cos 2\pi \nu_1 (t_2 - t_1)$	- .8	
c	$(\cos 2\pi \nu_1 t_1)^{-1}$	-1.3	
d	$\cos 2\pi \nu_1 t_1 \cosh 2\pi \nu_0 (t_2 - t_1)$ $-\frac{\nu_1}{\nu_0} \sin 2\pi \nu_1 t_1 \sinh 2\pi \nu_0 (t_2 - t_1)$	-10	J,M = 0,0
e	$\cos 2\pi \nu_1 (t_2 - t_1) \cosh 2\pi \nu_0 (t_3 - t_2)$ $-\frac{\nu_1}{\nu_0} \sin 2\pi \nu_1 (t_2 - t_1) \sinh 2\pi \nu_0 (t_3 - t_2)$	-6	
f	$\cos 2\pi \nu_1 t_1 \cosh 2\pi \nu_0 (t_2 - t_1)$ $-\frac{\nu_1}{\nu_0} \sin 2\pi \nu_1 t_1 \sinh 2\pi \nu_0 (t_2 - t_1)$ $+ (t_3 - t_2) 2\pi \nu_0 \cosh 2\pi \nu_1 t_1 \times$ $\sinh 2\pi \nu_0 (t_2 - t_1)$ $-(t_3 - t_2) 2\pi \nu_1 \sin 2\pi \nu_1 t_1 \times$ $\cosh 2\pi \nu_0 (t_2 - t_1)$	-21	
g	$\cos 2\pi \nu_1 t_1 \cosh 2\pi \nu_0 (t_3 - t_2)$ $-2\pi \nu_1 (t_2 - t_1) \sin 2\pi \nu_1 t_1 \times$ $\cosh 2\pi \nu_0 (t_3 - t_2)$ $-\frac{\nu_1}{\nu_0} \sin 2\pi \nu_1 t_1 \times$ $\sinh 2\pi \nu_0 (t_3 - t_2)$	-11	

IV. TWO- AND TEN-POLE FOCUSING

A. Introduction

It is well known that the four-pole field, previously discussed, does not have the capability of focusing diatomics of positive Stark energy (negative $f_2(J,M)$). The following paper (section IV B) discusses fields which can do so, although only weakly.[IV A.1] The focusing geometry used is shown in Fig. IV A.1.

Additional information concerning these fields is given in the appendices of section IV.

IV A.1 This focusing work was begun by Dr. K. H. Kramer using a two-pole field. After considerable experimentation, it became clear that this type of field geometry was not entirely satisfactory. He then designed an improved field, the ten-pole field. The writer made a number of calculations concerning the field, came to the conclusion that it could indeed focus and separate states of positive Stark energy, built it, experimented with it for many geometries and conditions, and showed that it functioned as designed.

BLANK PAGE

Fig. IV A.1. Ten-pole field focusing geometry.

A slit geometry for the detector and beam stop is necessary to detect the resolved (0,0) and (1,1) states of CsF with the ten-pole field.

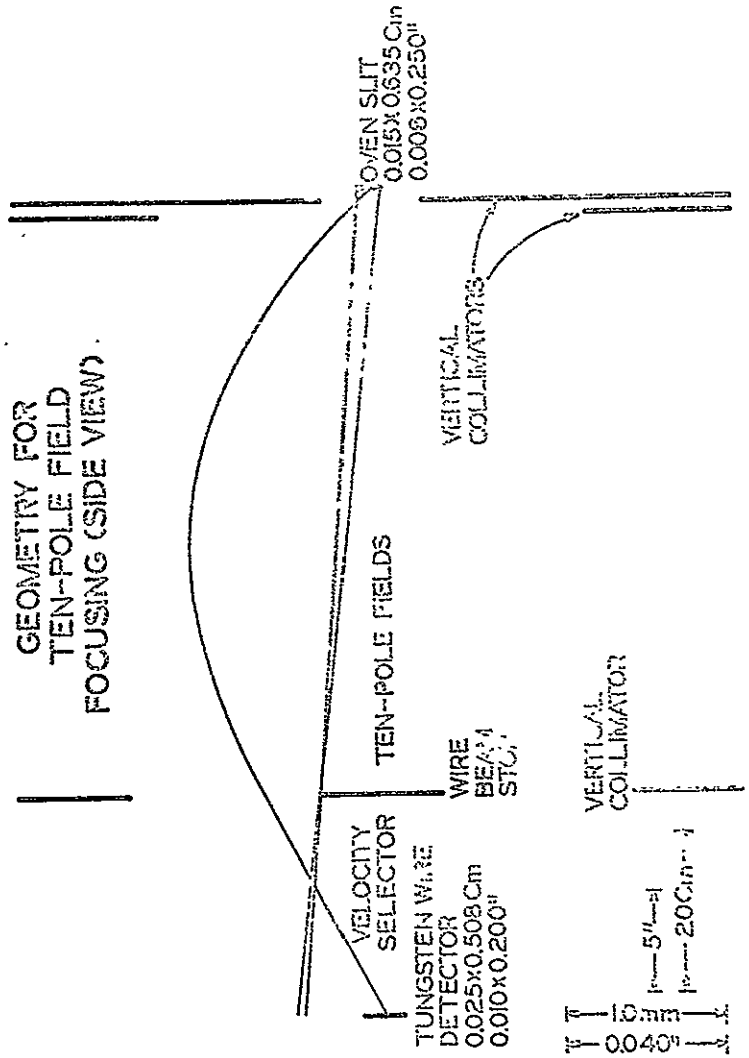

Fig. IV A.1

B. "Selection and Focusing of Polar Diatomics in States of Positive Induced Electric Dipole Moment Using a Ten-Pole Field," by T. G. Waech, K. H. Kramer, and R. B. Bernstein, J. Chem. Phys. 48, 3978 (1968).

(See journal article for this section.)

C. Appendix 1. Focusing of Polar Diatomic Molecules with a two-pole field*

1. Electrostatics

Consider an infinitely long, straight, infinitesimally thin filament with a certain charge per unit length. In such a case, the Laplace equation, $\nabla^2 V = 0$, reduces to

$$r^2 \frac{\partial^2 V}{\partial r^2} + r \frac{\partial V}{\partial r} = 0 \qquad \text{(IV C.1)}$$

where V is the electrostatic potential due to the filament at a distance r from the filament. Then

$$V = A \ln r + \text{constant} \qquad \text{(IV C.2)}$$

Now consider two parallel filaments (perpendicular to Fig. IV C.1) at the points O and Q with positive and negative charges respectively. Let the charges be equal in magnitude. Then

$$V = A \ln r_1 - A \ln r_2 = \frac{A}{2} \ln \frac{r_1^2}{r_2^2} \qquad \text{(IV C.3)}$$

The equipotential curves are

$$\frac{r_1^2}{r_2^2} \equiv m^2 = \frac{(x-2a)^2 + y'^2}{x^2 + y'^2} \qquad \text{(IV C.4)}$$

---

* Based mainly on work of K. H. Kramer and R. B. Bernstein; also H. Friedmann, Z. Phys. 161, 74 (1961).

Fig. IV C.1. Two-pole field diagram.

Possible two-pole field rods (and equipotential lines) are given by the solid or dashed circles whose construction is illustrated.

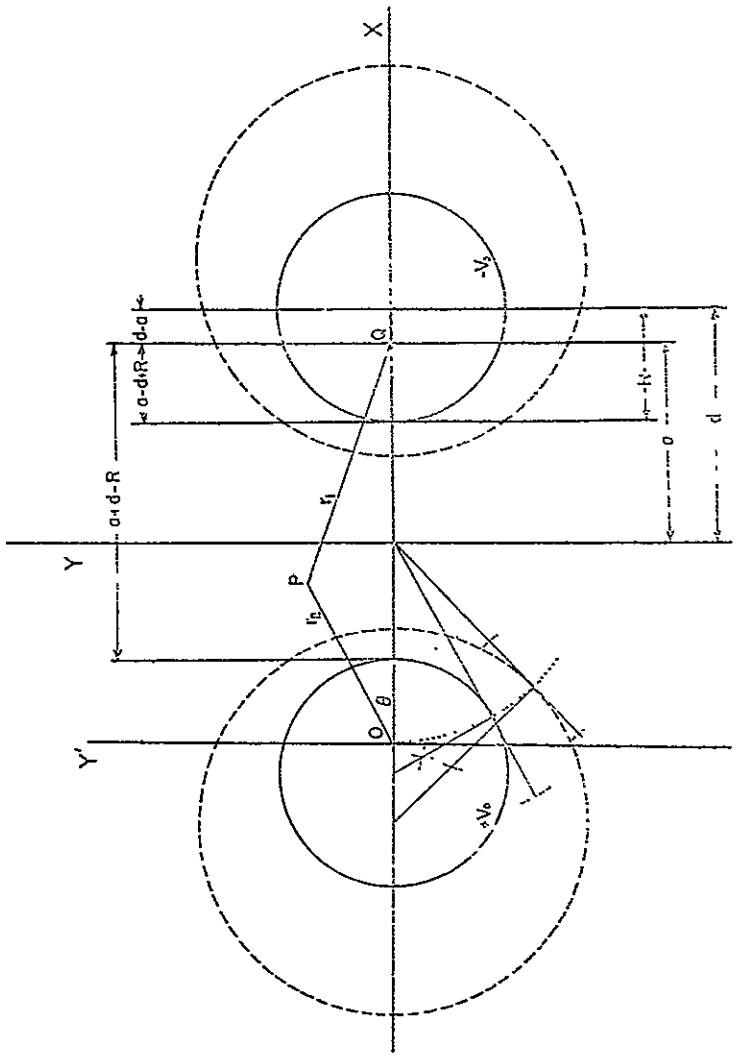

Fig. IV C.1

$$\left(x + \frac{2a}{m^2-1}\right)^2 + y'^2 = \left(\frac{2ma}{m^2-1}\right)^2 \qquad \text{(IV C.5)}$$

Note that the equipotentials are circles.

If one substitutes cylindrical bars or poles coinciding with two of the equipotential surfaces of equal radius for the filaments and lets the poles have the corresponding voltages ($\pm V_o$) the field outside the poles is unchanged. This is because the boundary conditions are equivalent.

We will now find the constant A. Let R = radius of the poles, m' = m corresponding to the surface of one of the poles.[IV C.1]

$$R = \frac{2m'a}{(m'^2-1)} \qquad \text{(IV C.6)}$$

$$d = \left|a + \frac{2a}{m'^2-1}\right| = \left|\frac{m'^2+1}{m'^2-1}a\right| \qquad \text{(IV C.7)}$$

$$d^2 - R^2 = a^2$$

$$a^2 - d^2 + R^2 = 0 =$$

$$(2ad^2 - 4ad^2) + (2adR - 2adR) + 2a^3 + 2aR^2 =$$

$$(d+a)(a^2 + d^2 + R^2 - 2ad - 2dR + 2aR) -$$

$$(d+a)(a^2 + d^2 + R^2 + 2ad - 2dR - 2aR) \qquad \text{(IV C.9)}$$

$$\frac{d+a}{d-a} = \left(\frac{a+d-R}{a-d+R}\right)^2 \qquad \text{(IV C.10)}$$

IV C.1 Not to be confused with the mass m.

$$-V_o = A \ln\left(\frac{a-d+R}{a+d-R}\right) = -\frac{A}{2}\ln\left(\frac{d+a}{d-a}\right) \qquad \text{(IV C.11)}$$

Here $-V_o$ is the potential on the pole on the right side of Fig. IV C.1.

$$A = \frac{2V_o}{\ln\left(\frac{d+a}{d-a}\right)} = \frac{2V_o}{\ln\left(\frac{d+\sqrt{d^2-R^2}}{d-\sqrt{d^2-R^2}}\right)} \qquad \text{(IV C.12)}$$

We will now derive expressions useful for the discussion on focusing.

Let $\xi = \frac{x}{a}$, $\eta = \frac{y}{a}$ (IV C.13)

$$V = \frac{A}{2}\ln\left(\frac{\xi^2+\eta^2-2\xi+1}{\xi^2+\eta^2+2\xi+1}\right) \qquad \text{(IV C.14)}$$

The components of the electric field ($\vec{E}$) are

$$E_x = -\frac{\partial V}{\partial x} = -\frac{1}{a}\frac{\partial V}{\partial \xi} = \frac{2A}{a}\,\frac{1-\xi^2+\eta^2}{1-2\xi^2+2\eta^2+\xi^4+2\xi^2\eta^2+\eta^4} \qquad \text{(IV C.15)}$$

$$E_y = -\frac{\partial V}{\partial y} = -\frac{1}{a}\frac{\partial V}{\partial \eta} = \frac{4A}{a}\,\frac{\xi\eta}{1-2\xi^2+2\eta^2+\xi^4+2\xi^2\eta^2+\eta^4} \qquad \text{(IV C.16)}$$

$$E = \sqrt{E_x^2+E_y^2} = \frac{2A}{a}\left[1-2\xi^2+2\eta^2+\xi^4+2\xi^2\eta^2+\eta^4\right]^{-\frac{1}{2}} \qquad \text{(IV C.17)}$$

$$\frac{\partial \xi}{\partial x} = \frac{1}{a}\frac{\partial E}{\partial \xi} \qquad \text{(IV C.18)}$$

$$\frac{\partial E}{\partial y} = \frac{1}{a}\frac{\partial E}{\partial \eta} \qquad \text{(IV C.19)}$$

$$\frac{\partial E}{\partial x} = \frac{4A\xi}{a^2}\left[1 - 2\xi^2 + 2\eta^2 + \xi^4 + 2\xi^2\eta^2 + \eta^4\right]^{-3/2} \left[1 - \xi^2 - \eta^2\right] \qquad \text{(IV C.20)}$$

$$\frac{\partial E}{\partial y} = \frac{-4A\eta}{a^2}\left[1 - 2\xi^2 + 2\eta^2 + \xi^4 + 2\xi^2\eta^2 + \eta^4\right]^{-3/2} \left[1 + \xi^2 + \eta^2\right] \qquad \text{(IV C.21)}$$

For small ξ and η (x and y small compared to a)

$$\frac{\partial E}{\partial x} \approx \frac{4A}{a^2}\xi\left(1 + 2\xi^2 - 4\eta^2\right) \qquad \text{(IV C.22)}$$

$$\frac{\partial E}{\partial y} \approx \frac{-4A}{a^2}\eta\left(1 + 4\xi^2 - 2\eta^2\right) \qquad \text{(IV C.23)}$$

where higher order terms have been neglected.

$$E\frac{\partial E}{\partial x} = \frac{8A^2\xi}{a^3}\left[\frac{1 - \xi^2 - \eta^2}{\left[1 - 2\xi^2 + 2\eta^2 + \xi^4 + 2\xi^2\eta^2 + \eta^4\right]^2}\right] \qquad \text{(IV C.24)}$$

$$E\frac{\partial E}{\partial y} = \frac{-8A^2\eta}{a^3}\left[\frac{1 + \xi^2 + \eta^2}{\left[1 - 2\xi^2 + 2\eta^2 + \xi^4 + 2\xi^2\eta^2 + \eta^4\right]^2}\right] \qquad \text{(IV C.25)}$$

For small ξ and η, (IVC24) and (IVC25) reduce to

$$E\frac{\partial E}{\partial x} \approx \frac{8A^2\xi}{a^3}\left[1 + 3\xi^2 - 5\eta^2\right] \qquad \text{(IV C.26)}$$

$$E\frac{\partial E}{\partial y} \approx \frac{-8A^2\eta}{a^3}\left[1 + 5\xi^2 - 3\eta^2\right] \qquad \text{(IV C.27)}$$

where higher order terms have been neglected.

2. Focusing

We wish to find the path of a polar diatomic molecule in a two-pole field. Using the methods of section II, the force (F) is

$$\vec{F} = -\nabla w = \frac{-\mu_0^2}{\hbar^2/2I} f_2(J,M)\,\nabla E^2 \qquad \text{(IV C.28)}$$

$$F_x = \frac{-2\mu_0^2}{\hbar^2/2I} f_2(J,M) E\frac{\partial E}{\partial x} = m\frac{d^2x}{dt^2} \qquad \text{(IV C.29)}$$

$$F_y = \frac{-2\mu_0^2}{\hbar^2/2I} f_2(J,M) E\frac{\partial E}{\partial y} = m\frac{d^2y}{dt^2} \qquad \text{(IV C.30)}$$

where m is the mass of the particle. $E\frac{\partial E}{\partial x}$ and $E\frac{\partial E}{\partial y}$ are given in (IV C.24) and (IV C.25). For small x and y compared to a

$$E\frac{\partial E}{\partial x} \approx \frac{8A^2\xi}{a^3} = \frac{8A^2x}{a^4} \qquad \text{(IV C.31)}$$

$$E\frac{\partial E}{\partial y} \approx \frac{-8A^2\eta}{a^3} = \frac{-8A^2y}{a^4} \qquad \text{(IV C.32)}$$

Contour maps showing level curves of the bracketed parts of Eqs. (IV C.24) and (IV C.25), which are assumed to be of value one in Eqs. (IV C.31) and (IV C.32), are shown in Figs. IV C.2 and IV C.3 respectively.

One can solve Eqs. (IV C.29) and (IV C.30) using (IV C.31) and (IV C.32)

Case 1 $f_2(J,M) < 0$ (e.g. states (0,0), (1,1), (2,2), . . .)

$$x = x_0 \cosh 2\pi\nu t + \frac{\dot{x}_0}{2\pi\nu}\sinh 2\pi\nu t \qquad \text{(IV C.33)}$$

Fig. IV C.2. Level curves of $\frac{F_x}{k_{J,M} a \xi}$ (two-pole field).

The figure shows that for negative $k_{J,M}$ the force is near harmonic only near the origin.

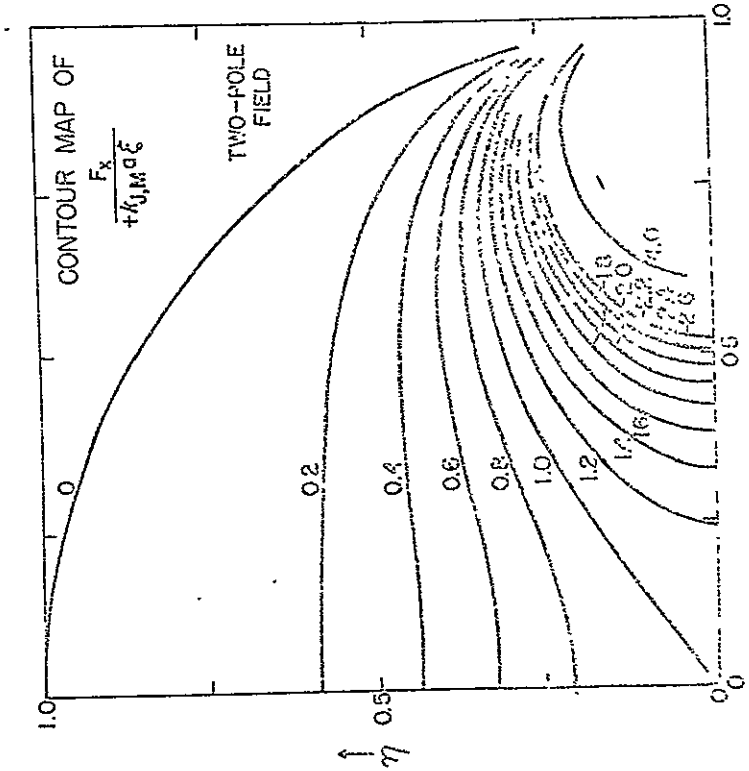

Fig. IV C.2

Fig. IV C.3. Level curves of $\frac{F_y}{-k_{J,M}{}^a \eta}$ (two-pole field).

For a harmonic force this quantity would be independent of ξ and η.

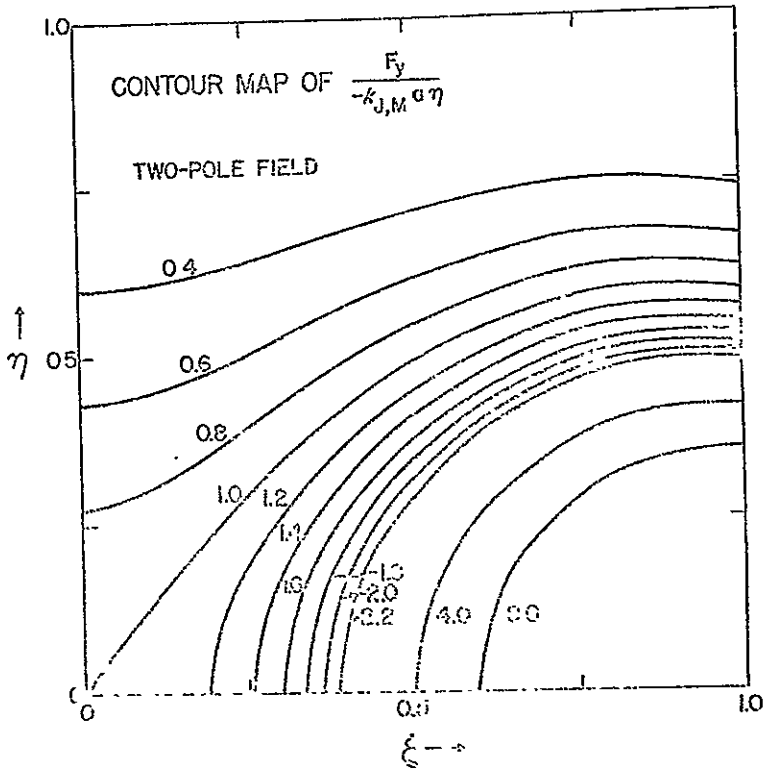

Fig. IV C.3

$$y = y_0 \cos 2\pi\nu t + \frac{\dot{y}_0}{2\pi\nu} \sin 2\pi\nu t \qquad \text{(IV C.34)}$$

where x_0, y_0, $\dot{x}_0$, $\dot{y}_0$ are the conditions when a particle enters the field at t = 0.

$$\nu = \frac{2A\mu_0}{\pi a^2 L}\sqrt{\frac{2I|f_2(J,M)|}{m}} \qquad \text{(IV C.35)}$$

The solutions are exponential in the X direction, but periodic in the Y direction. If the detector and oven have large X dimensions as compared to their y dimensions ($y_0 \approx 0$), it should be possible to focus states with negative $f_2(J,M)$ (see Fig. IV B.1).

Case 2. $f_2(J,M) < 0$ Then

$$x = x_0 \cos 2\pi\nu t + \frac{\dot{x}_0}{2\pi\nu} \sin 2\pi\nu t \qquad \text{(IV C.36)}$$

$$y = y_0 \cosh 2\pi\nu t + \frac{\dot{y}_0}{2\pi\nu} \sinh 2\pi\nu t \qquad \text{(IV C.37)}$$

In case 2 the oven and detector should have large y dimensions.

Note that ν, corresponding to the frequency of oscillation of the molecule along one axis is

$$\nu = \frac{v}{2L} \qquad \text{(IV C 38)}$$

BLANK PAGE

for focusing, where $\mathcal{V}$ and L are the same as defined in section II.

Using (IV C.35)

$$\mathcal{V} = \frac{V}{2L} = \frac{4V_o \mu_e}{a^2 \pi \ln\left(\frac{d+a}{d-a}\right)\hbar} \sqrt{\frac{2I\,|f_2(J,M)|}{m}} \qquad \text{(IV C.39)}$$

For focusing, then IV C.2

$$\frac{V_o}{V} = \frac{\pi a^2 \ln\left(\frac{d+a}{d-a}\right)}{8\mu_e L} \sqrt{\frac{m\hbar^2/2I}{|f_2(J,M)|}} \qquad \text{(IV C.40)}$$

IV C.2 $\frac{V_o}{V}$ may be calculated from (IV C.40) and Table II C.1, or one may use the equation

$$\frac{V_o}{V} = 0.879\,\delta\rho\,|f_2(J,M)|^{-\frac{1}{2}}$$

where

$$\delta = \frac{a^2}{L}\ln\left(\frac{d+a}{d-a}\right)$$

with a, d, and L in cm.

$$\rho = \frac{1}{\mu_o}\left(\frac{M}{I}\right)^{1/2}$$

μ_e = dipole moment (debyes)
M = molecular weight (amu)
I = moment of inertia (amu Å^2)

Note that δ, ρ, and $f_2(J,M)$ depend respectively upon apparatus, molecule, and rotational state.

D. Appendix 2. Ten-pole field focusing--electrostatics and force laws.

Let a potential be written in the form of a power series in two dimensions including up to fifth order terms only.

$$V = a_0 + a_1\xi + a_2\eta + a_3\xi^3 + a_4\xi\eta + a_5\eta^2 + a_6\xi^3 + a_7\xi^2\eta + a_8\xi\eta^2 + a_9\eta^3 + a_{10}\xi^4 + a_{11}\xi^3\eta + a_{12}\xi^2\eta^2 + a_{13}\xi\eta^3 + a_{14}\eta^4 + a_{15}\xi^5 + a_{16}\xi^4\eta + a_{17}\xi^3\eta^2 + a_{18}\xi^2\eta^3 + a_{19}\xi\eta^4 + a_{20}\eta^5 \qquad \text{(IV D.1)}$$

where $\xi = \frac{x}{a}$, $\eta = \frac{y}{a}$ are reduced coordinates, and a is a constant which determines the physical size of the field. Some terms must be zero if we impose the symmetry of the two-pole field.

$$V(0,\eta) = 0, \therefore a_0 = a_2 = a_5 = a_9 = a_{14} = a_{20} = 0$$

$$V(\xi,\eta) = V(\xi,-\eta); \therefore a_4 = a_7 = a_{11} = a_{13} = a_{16} = a_{18} = 0$$

$$V(\xi,\eta) = -V(-\xi,\eta); \therefore a_3 = a_{10} = a_{12} = 0 \qquad \text{(IV D.2)}$$

Then

$$V = a_1\xi + a_6\xi^3 + a_8\xi\eta^2 + a_{15}\xi^5 + a_{17}\xi^3\eta^2 + a_{19}\xi\eta^4 \qquad \text{(IV D.3a)}$$

$$E_\xi = aE_x = -a_1 - 3a_6\xi^2 - a_8\eta^2 - 5a_{15}\xi^4 - 3a_{17}\xi^2\eta^2 - a_{19}\eta^4 \qquad \text{(IV D.4a)}$$

$$E_\eta = aE_y = -2a_8\xi\eta - 2a_{17}\xi^3\eta - 4a_{19}\xi\eta^3$$

$$\frac{\partial E_\xi}{\partial \xi} = a^2 \frac{\partial E_x}{\partial x} = -6a_6\xi - 20a_{15}\xi^3 - 6a_{17}\xi\eta^2$$

$$\frac{\partial E_\xi}{\partial \eta} = a^2 \frac{\partial E_x}{\partial y} = -2a_8\eta - 6a_{17}\xi^2\eta - 4a_{19}\eta^3 \qquad \text{(IV D.5a)}$$

$$\frac{\partial E_\eta}{\partial \xi} = a^2 \frac{\partial E_y}{\partial x} = -2a_8\eta - 6a_{17}\xi^2\eta - 4a_{19}\eta^3$$

$$\frac{\partial E_\eta}{\partial \eta} = a^2 \frac{\partial E_y}{\partial y} = -2a_8\xi - 2a_{17}\xi^3 - 12a_{19}\xi\eta^2$$

In the absence of a changing magnetic field, one of Maxwell's equations is $\nabla \times E = 0$ (here $\frac{\partial E_x}{\partial y} - \frac{\partial E_y}{\partial x} = 0$), which is already satisfied. In a region of zero charge density and constant dielectric constant, another of Maxwell's equations is $\nabla \cdot E = 0$ or

$$\frac{\partial E_\xi}{\partial \xi} + \frac{\partial E_\eta}{\partial \eta} = 0 \qquad \text{(IV D.6)}$$

Then

$$(6a_6 + 2a_8)\xi + (20a_{15} + 2a_{17})\xi^3 + (6a_{17} + 12a_{19})\xi\eta^2 = 0 \qquad \text{(IV D.7)}$$

for all ξ, η.

$$a_8 = -3a_6$$
$$a_{17} = -10a_{15}$$
$$a_{19} = 5a_{15} \qquad \text{(IV D.8)}$$

If Eqs. (IV D.4a), (IV D.5a), and (IV D.8) are substituted into Eq. (II A.3), and only terms of third order or less in ξ and η are included, one finds

$$F_\xi = m\ddot{\xi} \propto a_6\xi\left[1 + \left(\frac{10}{3}\frac{a_{15}}{a_6} + 3\frac{a_6}{a_1}\right)\xi^2 - \left(10\frac{a_{15}}{a_6} - 3\frac{a_6}{a_1}\right)\eta^2\right] \qquad \text{(IV D.9)}$$

$$F_\eta = m\ddot{\eta} \propto a_6\eta\left[1 + \left(10\frac{a_{15}}{a_6} - 3\frac{a_6}{a_1}\right)\xi^2 - \left(\frac{10}{3}\frac{a_{15}}{a_6} + 3\frac{a_6}{a_1}\right)\eta^2\right] \qquad \text{(IV D.10)}$$

To get rid of the main ξ term in the η force equation and vice versa, one may let

$$10\frac{a_{15}}{a_6} = 3\frac{a_6}{a_1} \qquad \text{(IV D.11)}$$

$$\text{Let } \alpha = \frac{a_6}{a_1} \qquad \text{(IV D.12)}$$

$$F_\xi \propto \alpha\xi\left[1 + 4\alpha\xi^2\right] \qquad \text{(IV D.13)}$$

$$F_\eta \propto \alpha\eta\left[1 - 4\alpha\eta^2\right] \qquad \text{(IV D.14)}$$

for small ξ and η.

Using (IV D.8), (IV D.11), and (IV D.3a), one finds

$$V = a_1\left[\xi + \alpha\xi^3 - 3\alpha\xi\eta^2 + \tfrac{3}{10}\alpha^2\xi^5 - 3\alpha^2\xi^3\eta^2 + \tfrac{3}{2}\alpha^2\xi\eta^4\right] \quad \text{(IV D.3b)}$$

where $a_1 \propto V_o$ where V_o is the potential on the poles of the field [IV D 1]

Using Eq. (IV D.3b) one can find the exact force law in the field.

$$E_\xi = a_1\left[-1 - 3\alpha\xi^2 + 3\alpha\eta^2 - \tfrac{3}{2}\alpha^2\xi^4 + 9\alpha^2\xi^2\eta^2 - \tfrac{3}{2}\alpha^2\eta^4\right]$$

$$E_\eta = a_1\left[6\alpha\xi\eta + 6\alpha^2\xi^3\eta - 6\alpha^2\xi\eta^3\right] \quad \text{(IV D.4b)}$$

from which we may find E:

$$E^2 = a^{-2}a_1^2\left[1 + 6\alpha\xi^2 - 6\alpha\eta^2 + 12\alpha^2\xi^4 + 12\alpha^2\eta^4 + 9\alpha^3\xi^6 + 9\alpha^3\xi^4\eta^2 - 9\alpha^3\xi^2\eta^4 - 9\alpha^3\eta^6 + \tfrac{9}{4}\alpha^4\xi^8 + 9\alpha^4\xi^6\eta^2 + \tfrac{27}{2}\alpha^4\xi^4\eta^4 + 9\alpha^4\xi^2\eta^6 + \tfrac{9}{4}\alpha^4\eta^8\right] \quad \text{(IV D.15)}$$

IV D.1 It is convenient if $a_1 = V_o$, but not necessary. If instead one let $a_1 = \frac{1}{2}V_o$, this would correspond to displacing the field poles out from the center and changing their shape. Except for particles which may strike the poles, the trajectories and E are the same for a given a_1.

Note that (IV D.3b) and (IV D.15) describe a capacitor for $\alpha = 0$.

$$\frac{\partial E_\xi}{\partial \xi} = a_1\left[-6\alpha\xi - 6\alpha^2\xi^3 + 18\alpha^2\xi\eta^2\right]$$

$$\frac{\partial E_\eta}{\partial \eta} = -\frac{\partial E_\xi}{\partial \xi}$$

$$\frac{\partial E_\xi}{\partial \eta} = a_1\left[6\alpha\eta + 18\alpha^2\xi^2\eta - 6\alpha^2\eta^3\right] \quad \text{(IV D.5b)}$$

$$\frac{\partial E_\eta}{\partial \xi} = \frac{\partial E_\xi}{\partial \eta}$$

$$\vec{F} = m a\ddot{\xi}\hat{\imath} + m a\ddot{\eta}\hat{\jmath} \quad \text{(IV D.16)}$$

where m = particle mass.

$$\ddot{\xi}\hat{\imath} + \ddot{\eta}\hat{\jmath} = \frac{-2\mu_o^2 f_2(J,M)}{(\hbar^2/2I)\,a^4 m}\left[\left(E_\xi\frac{\partial E_\xi}{\partial \xi} + E_\eta\frac{\partial E_\eta}{\partial \xi}\right)\hat{\imath} + \left(E_\xi\frac{\partial E_\xi}{\partial \eta} + E_\eta\frac{\partial E_\eta}{\partial \eta}\right)\hat{\jmath}\right] \quad \text{(IV D.17)}$$

from (II A.3). If we let

$$K = \frac{-12\mu_o^2 f_2(J,M)\,a_1^2\alpha}{(\hbar^2/2I)\,m\,a^4} = \frac{k_{J,M}}{m} \quad \text{(IV D.18)}$$

then

$$\ddot{\xi} = K\xi\left[1 + \tfrac{1}{2}\left(8\alpha\xi^2 + 9\alpha^2\xi^4 + 6\alpha^2\xi^2\eta^2 - 3\alpha^2\eta^4 + 3\alpha^3\xi^6 + 9\alpha^3\xi^4\eta^2 + 9\alpha^3\xi^2\eta^4 + 3\alpha^3\eta^6\right)\right] \quad \text{(IV D.19)}$$

$$\ddot{\eta} = -K\eta\left[1 + \tfrac{1}{2}\left(-8\alpha\eta^2 - 3\alpha^2\xi^4 + 6\alpha^2\xi^2\eta^2 + 9\alpha^2\eta^4 - 3\alpha^3\xi^6 - 9\alpha^3\xi^4\eta^2 - 9\alpha^3\xi^2\eta^4 - 3\alpha^3\eta^6\right)\right] \quad \text{(IV D.20)}$$

The bracketed parts of Eqs. (IV D.19) and (IV D.20) are shown in Figs. IV D.1 and IV D.2.

Note that since $K \propto \alpha$, each of the two equations above goes into the other as $\alpha \rightarrow -\alpha$, $\eta \rightarrow \xi$, $\xi \rightarrow \eta$. This suggests that one can build two different fields with identical focusing properties by rotating one field on its axis with respect to the other by 90° and changing the sign of α (see Fig. IV D.3 and Fig. IV D.4).

Just as for the ten-pole field, to first order

$$\ddot{\xi} = K\xi \qquad \text{(IV D.21)}$$

$$\ddot{\eta} = -K\eta \qquad \text{(IV D.22)}$$

For positive K ($f_2(J,M) < 0$)

$$\eta = \eta_0 \cos\sqrt{K}t + \frac{\dot{\eta}_0}{\sqrt{K}} \sin\sqrt{K}t \qquad \text{(IV D.23)}$$

$$\xi = \xi_0 \cosh\sqrt{K}t + \frac{\dot{\xi}_0}{\sqrt{K}} \sinh\sqrt{K}t \qquad \text{(IV D.24)}$$

For $\eta_0 = 0$, $\eta = \frac{\dot{\eta}_0}{\sqrt{K}} \sin\sqrt{K}t$ (IV D.25)

For focusing, $\sqrt{K} = \frac{\pi V}{L}$ (IV D.26)

Fig. IV D.1 Level curves of $\frac{\ddot{\xi}}{K\xi}$ (or $\frac{F_x}{k_{J,M}ax}$) for $\alpha = +1/3$.

Note on comparison with Fig. IV C.2 that the ten-pole field curves indicate a more nearly harmonic force in x-direction over a wide range of ξ and η.

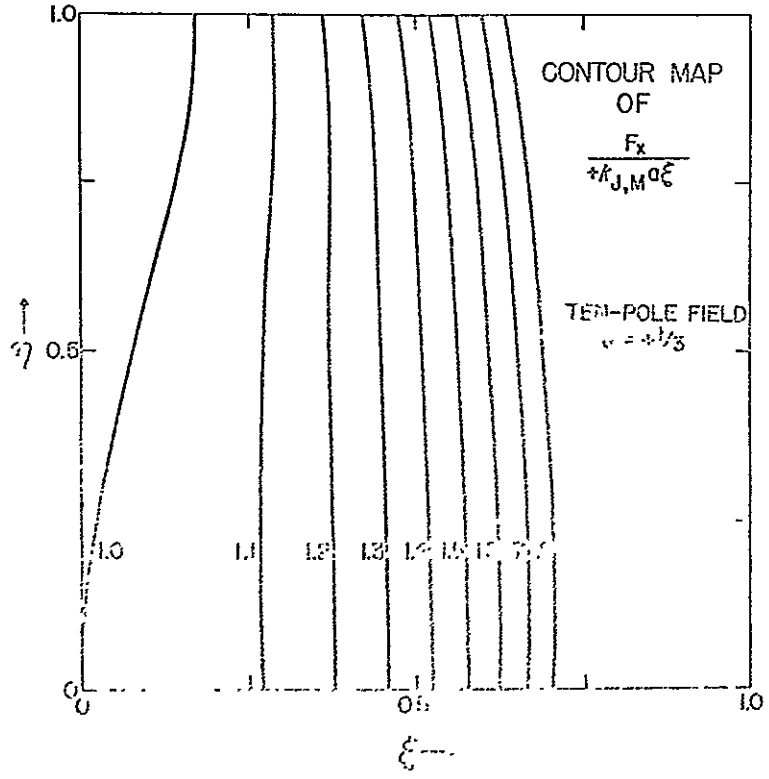

Fig. IV D.1

Fig. IV D.2. Level curves of $\frac{\ddot{\eta}}{K\eta}$ (or $\frac{-F_y}{k_{J,M}\, a_y}$) for $\alpha = +\frac{1}{3}$. The force in the y (or η) direction is nearly harmonic for η not too large. Compare with Fig. IV C.3.

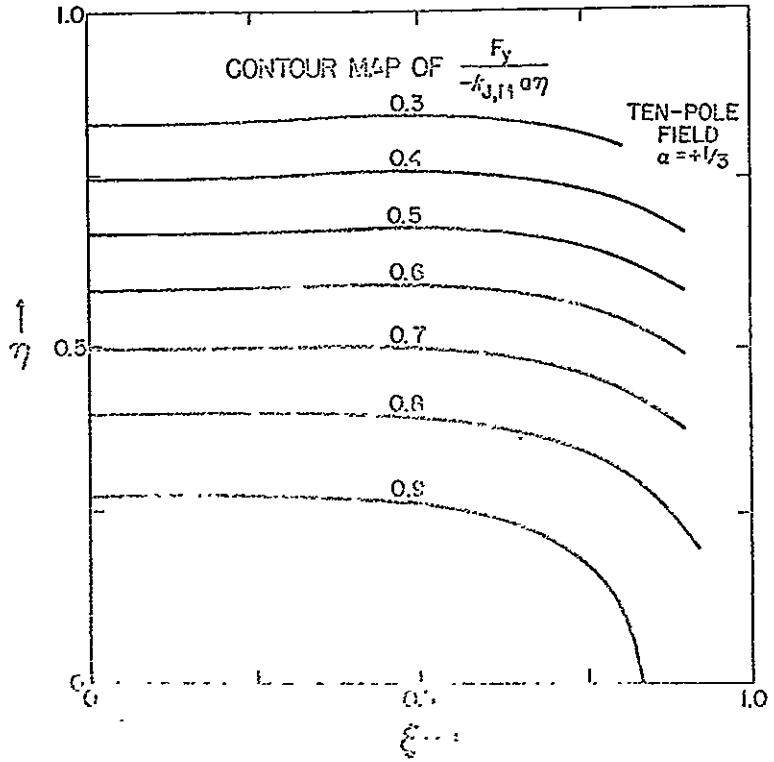

Fig. IV D.2

Fig. IV D.3 Ten-pole equipotential lines (α = + 1/3).

The numbers next to each curve indicate $\frac{V}{a_1}$, where V is the potential (in the experiment $a_1 = V_o$). A V = 0 line is shown near η = 1. This suggests that one might replace this ten-pole field with a two-pole field and two grounded planes.

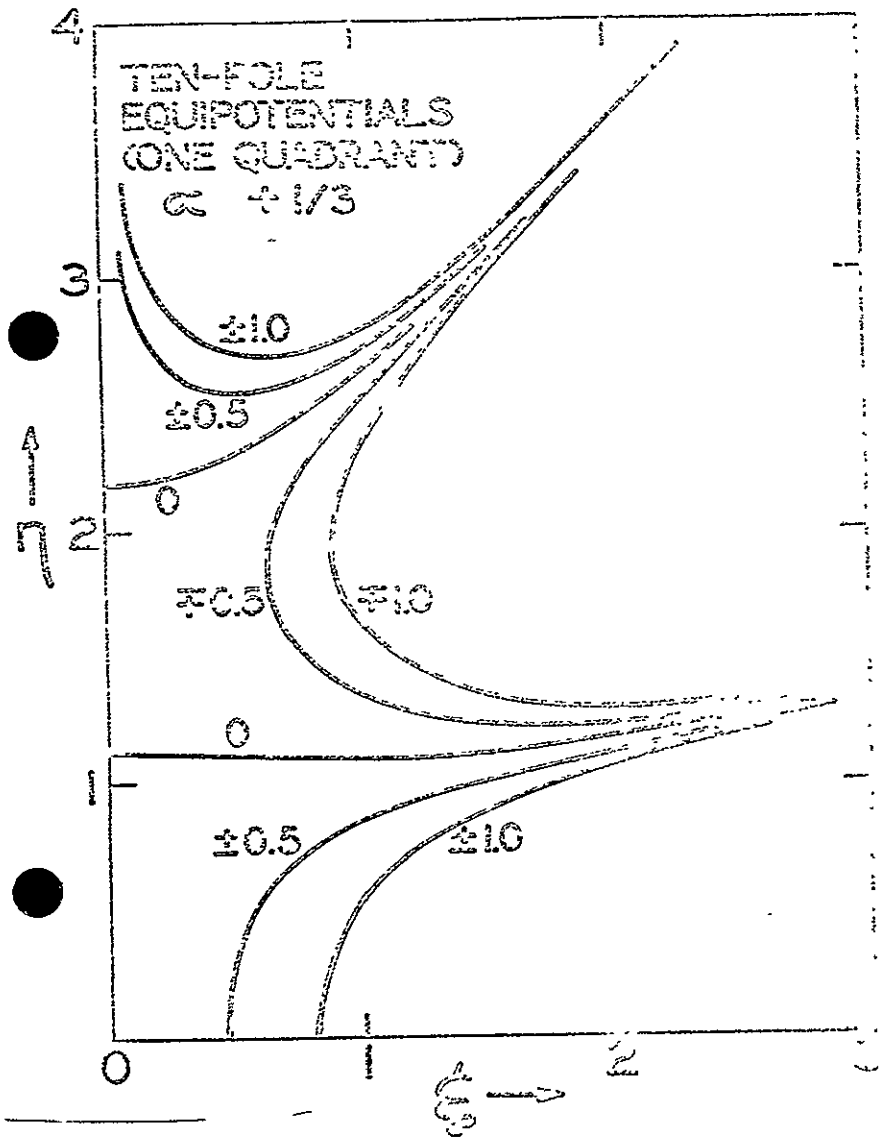

Fig. IV D.3

Fig. IV D.4. Ten-pole equipotential lines for $\alpha = -1/3$.

Cf. Fig. IV D.3.

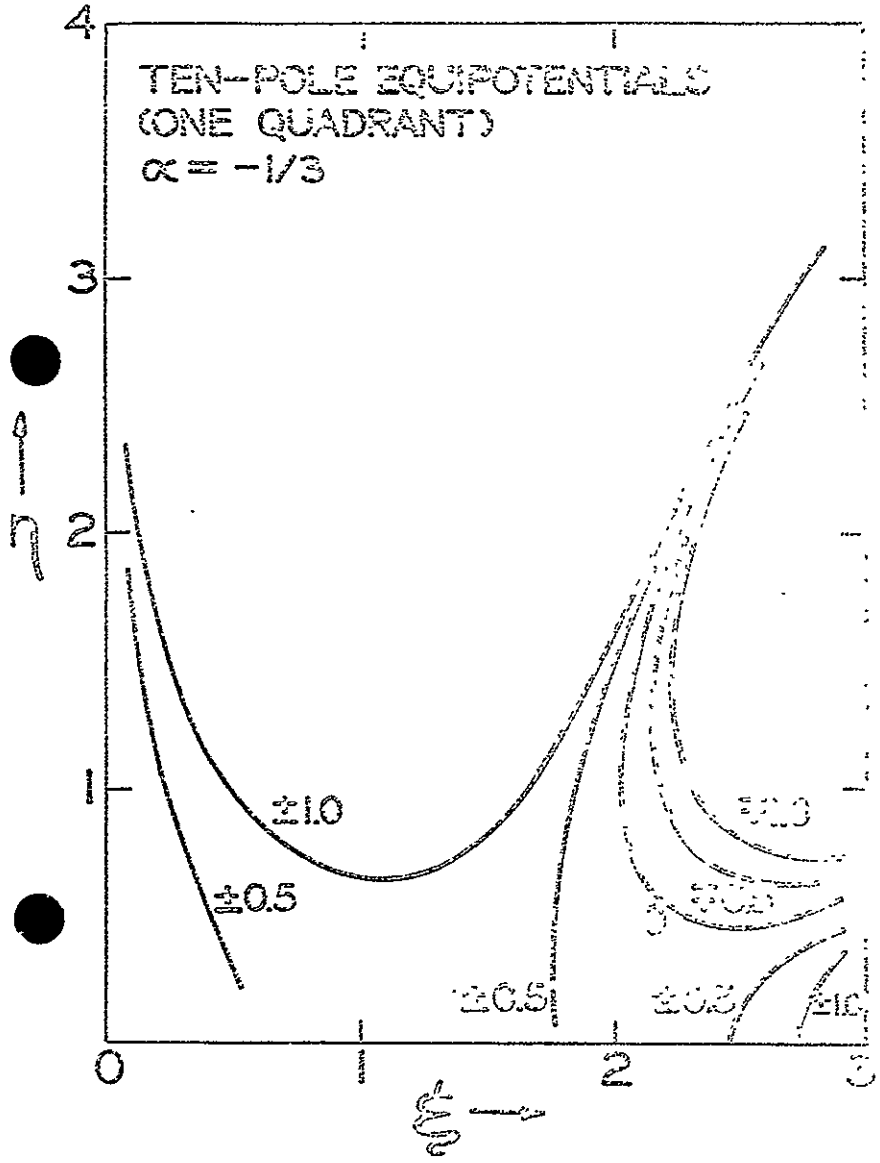

Fig. IV.D.4

Then, for the ten-pole field (with $a_1 = V_o$)

$$\frac{V_o}{V} = \frac{\pi a^2 \alpha^{-\frac{1}{2}}}{d\,\mu_o} \sqrt{\frac{m\,\hbar^2/2I}{12\,|f_2(J,M)|}} \qquad \text{(IV D.27)}$$

for focusing of a given state where the voltage on any field electrode is $\pm V_o$.

E. Appendix 3. Second approximation in ten-pole field focusing.

1. Trajectories (η coordinate for $f_2(J,M) < 0$)

If one neglects terms above third order in η and ξ, the equations of motion for a heteronuclear diatomic molecule ($^1\Sigma$ state) in a ten-pole field are (see Eqs. (IV D.19) and (IV D.20)):

$$\ddot{\xi} = K\xi(1+4\alpha\xi^2) \qquad \text{(IV E.1)}$$

$$\ddot{\eta} = -K\eta(1-4\alpha\eta^2) \qquad \text{(IV E.2)}$$

where α depends only on the shape of the fields and K depends on the apparatus, the molecule, and the quantum state (J,M).

Two important facts should be noted from these equations:[IV E.1]

a) The ξ and η motions are independent of each other in this approximation.

b) Trajectories with turning points in either coordinate (e.g., $\frac{d\eta}{dt} = 0$ at a turning point for η are symmetric in that coordinate about the turning points. To see this, note that there is no force along the z axis of the field. Then v is independent of t and of z.

$$\frac{1}{dt} = \frac{v}{dz} \qquad \text{(IV E.3)}$$

IV E.1 The corresponding equations for the two-pole field are:
$\ddot{\xi} = +K'(1+5\xi^2-3\eta^2)$
$\ddot{\eta} = -K'(1+3\xi^2-5\eta^2)$.

BLANK PAGE

$$\frac{d^2\eta}{dt^2} = V^2 \frac{d^2\eta}{dz^2} = -K\eta(1-4\alpha\eta^2) \quad \text{(IV E.4)}$$

Let $z = z_o$ at a turning point (assuming one exists). Note that the last equation is the same for differential changes in the + z or - z directions as are the conditions at $z = z_o$

$$V\left(\frac{d\eta}{dt}\right)_{z_o} = \left(\frac{d\eta}{dz}\right)_{z_o} = \left(\frac{d\eta}{d(-z)}\right)_{z_o} = 0 \quad \text{(IV E.5)}$$

Therefore the trajectories in the + z and - z directions are identical,[IV E 2] i.e., symmetric and about z_o

From this point on in this section, the main concern will be the η equation of motion for positive K and α and $4\alpha\eta^2 < 1$. From (IV E.1) one finds

$$\frac{d\dot{\eta}^2}{dt} = 2\ddot{\eta}\dot{\eta} = -2K\eta(1-4\alpha\eta^2)\dot{\eta} \quad \text{(IV E.6)}$$

$$\dot{\eta}^2 = -2K\int_{\eta_o}^{\eta}(\eta - 4\alpha\eta^3)d\eta + \dot{\eta}_o^2 =$$

$$-2K\left[\tfrac{1}{2}\eta^2 - \alpha\eta^4\right]_{\eta_o}^{\eta} + \dot{\eta}_o^2 =$$

$$-K\left[\eta^2 - \eta_o^2 - 2\alpha(\eta^4 - \eta_o^4)\right] + \dot{\eta}_o^2 \quad \text{(IV E.7)}$$

IV E.2 It is not necessary that $(\frac{d\xi}{dz})_{z_o} = (\frac{d\xi}{d(-z)})_{z_o}$ since the ξ and η motions are independent.

where

$$\dot{\eta}_o \equiv \left(\frac{d\eta}{dt}\right)_{t=0} \quad \text{(IV E.8)}$$

$$dt = \frac{d\eta}{\sqrt{\dot{\eta}_o^2 - K(\eta^2 - \eta_o^2) + 2K\alpha(\eta^4 - \eta_o^4)}} \quad \text{(IV E.9)}$$

$$\text{Let } D' \equiv \frac{\dot{\eta}_o^2}{K} + \eta_o^2 - 2\alpha\eta_o^4 \quad \text{(IV E.10)}$$

$$\text{Then } t = \int_o^t dt = \int_{\eta_o}^{\eta} \frac{d\eta}{\sqrt{K}\sqrt{D' - \eta^2 + 2\alpha\eta^4}} \quad \text{(IV E.11)}$$

Eq. (IV E.11) may be recognized as an elliptic integral. It may be put into a standard form by substitutions so tables may be used.

$$D' - \eta^2 + 2\alpha\eta^4 = D'\left(1 - \frac{\eta^2}{D'} + \frac{2\alpha}{D'}\eta^4\right) \equiv$$

$$D'(1 - g^2\eta^2)(1 - h^2\eta^2) =$$

$$D'\left[1 - (g^2 + h^2)\eta^2 + g^2h^2\eta^4\right] \quad \text{(IV E.12)}$$

$$\text{Then } g^2 + h^2 = 1/D' \quad \text{(IV E.13)}$$

$$g^2h^2 = \frac{2\alpha}{D'} \quad \text{(IV E.14)}$$

$$g^2 = \frac{2\alpha}{D' h^2} \qquad \text{(IV E.15)}$$

$$h^4 - \frac{h^2}{D'} + \frac{2\alpha}{D'} \qquad \text{(IV E.16)}$$

The last equation must also hold for h replaced by g.

$$h^2 = \tfrac{1}{2}\left(\frac{1}{D'} + \sqrt{\frac{1}{D'^2} - 4\,\frac{2\alpha}{D'}}\right) = \frac{1}{2D'}\left(1+\sqrt{1-8\alpha D'}\right) \qquad \text{(IV E.17)}$$

$$g^2 = \tfrac{1}{2}\left(\frac{1}{D'} + \sqrt{\frac{1}{D'^2} - 4\,\frac{2\alpha}{D'}}\right) = \frac{1}{2D'}\left(1-\sqrt{1-8\alpha D'}\right) \qquad \text{(IV E.18)}$$

Let $h\eta \equiv T$ (IV E.19)

$$dT = h\,d\eta \qquad \text{(IV E.20)}$$

Let $\frac{g}{h} \equiv k \leq 1$ (IV E.21)

$$k = \sqrt{\frac{1-\sqrt{1-8\alpha D'}}{1+\sqrt{1-8\alpha D'}}} \qquad \text{(IV E.22)}$$

Substituting (IV E.19) and (IV E.21) in (IV E.12), one finds

$$D' - \eta^2 + 2\alpha\eta^4 \equiv D'(1-k^2T^2)(1-T^2) \qquad \text{(IV E.23)}$$

Using (IV E.20) and (IV E.23) in (IV E.11):

$$t = \frac{1}{\sqrt{KD'}\,h}\int_{T_0}^{T} \frac{\alpha T}{\sqrt{(1-k^2T^2)(1-T^2)}} \qquad \text{(IV E.24)}$$

Let $T \equiv \sin\phi \leq 1$ (IV E.25)

$$t = \frac{1}{\dot\eta_0 h}\int_{\phi_0}^{\phi} \frac{d\phi}{\sqrt{1-k^2\sin\phi}} =$$

$$\frac{1}{\dot\eta_0 h}\left(F(k,\phi) - F(k,\phi_0)\right) =$$

$$\left(\frac{2}{K\left(1+\sqrt{1-8\alpha D'}\right)}\right)^{1/2}\left(F(k,\phi) - F(k,\phi_0)\right) \qquad \text{(IV E.26)}$$

where F = elliptic integral of first kind.

$$K \equiv F\left(k, \tfrac{\pi}{2}\right) = K(k) \qquad \text{(IV E.27)}$$

It is known that $F(k, m\pi) = 2mK(k)$ (IV E.28)

where m = integer or half integer so that if one integrates over π in (IV E.26), one finds $\frac{1}{2}\tau = \frac{2K(k)}{\dot\eta_0 h}$ where $\tau =$ (IV E.29) period of motion, since T, (and therefore η) goes through a maximum and η comes to $-\eta_0$ over the time $\frac{1}{2}\tau$. Since T = 1 at its maximum,

$$\eta_{max} = \frac{1}{h} = \sqrt{\frac{2D'}{1+\sqrt{1-8\alpha D'}}} = \sqrt{\frac{1-\sqrt{1-8\alpha D'}}{4\alpha}} \qquad \text{(IV E.30)}$$

One can also derive this result by noting that $\dot\eta = 0$ at $\eta = \eta_{max}$ in (IV E.10).

This discussion after this point will be confined to the special case for which $\eta_0 = 0$ (i.e., infinitesimal slit width).

$D \equiv D'(\eta_0 = 0) = \frac{\dot\eta_0^2}{K}$

The distance the particle travels before returning to $\eta = 0$ is $\frac{\lambda}{2}$.

$$\frac{\lambda}{2} = \frac{v\tau}{2} = \frac{2vK}{\dot{\eta}_0 h} \qquad \text{(IV E.31)}$$

where v is the velocity in the z direction.

According to (IV E.1), the trajectories should be sinusoidal for low α or negligible η^2. As $\alpha \to 0$ (with K constant), we can see from (IV E.22) that $k \to 0$ and from (IV E.17) that

$$h \to \frac{1}{\sqrt{D}} \qquad \text{(IV E.32)}$$

From (IV E.30) $\eta_{max} \to \sqrt{D} = \frac{\dot{\eta}_0}{\sqrt{K}}$ (IV E.33)

From IV E.3 (IV E.26): $t \to \frac{1}{\sqrt{K}} \int_0^{\phi} \alpha \, d\phi' =$ (IV E.34)

$$\frac{1}{\sqrt{K}} \arcsin T \qquad \text{(IV E.35)}$$

$$\eta = \frac{1}{h} \sin\sqrt{K}\, t = \sqrt{D} \sin\sqrt{K}\, t \qquad \text{(IV E.36)}$$

From (IV E.34): $\frac{1}{2}\tau \to \frac{\pi}{\sqrt{K}}$ (IV E.37)

- - - - -

IV E.3 Note that (IV E.32) and (IV E.33) correspond (as they must), for suitable redefinition of K and a, to the first order solution to the two-pole field.

Then IV E.4 $\frac{\lambda}{2} = \frac{v\tau}{2} \to \frac{\pi v}{\sqrt{K}}$ (IV E.38)

Let us define $\Lambda = \frac{\lambda}{\lambda(\alpha=0)} = \frac{\tau}{\tau(\alpha=0)}$ (IV E.39)

Then, using (IV E.30) and (IV E.38)

$$\Lambda = \frac{\frac{2vK}{\dot{\eta}_0 h}}{\pi v / \sqrt{K}} = \frac{2\sqrt{K}\,K}{\pi \dot{\eta}_0 h} \qquad \text{(IV E.40)}$$

Using (IV E.17):

$$\Lambda = \sqrt{\frac{2}{1+\sqrt{1-8\alpha D}}}\;\frac{2K(k)}{\pi} \qquad \text{(IV E.41)}$$

Note that $k = k(\alpha D)$ from (IV E 22), Then

$$\Lambda = \Lambda(\alpha D) \qquad \text{(IV E.42)}$$

which is an important result. If $\alpha^2 D = \frac{1}{8}$, then $k = 1$ (see (IV E.22)),

$$\therefore \quad K(k) \to \infty \qquad \text{(IV E.43)}$$

and

$$\Lambda \to \infty \qquad \text{(IV E.44)}$$

The solutions are plotted in Fig. IV E 1.

- - - - -

IV E.4 This result also follows from (IV E.30) since $K(k=0) = \frac{\pi}{2}$

Fig. IV E.1. Λ -1 versus $\sqrt{8\alpha D}$.

The graph is correct for the second approximation for η trajectories if $k_{J,H}$ positive, α positive, $\eta_o = 0$, or for ξ if $k_{J,M}$ negative, α negative, $\xi_o = 0$.

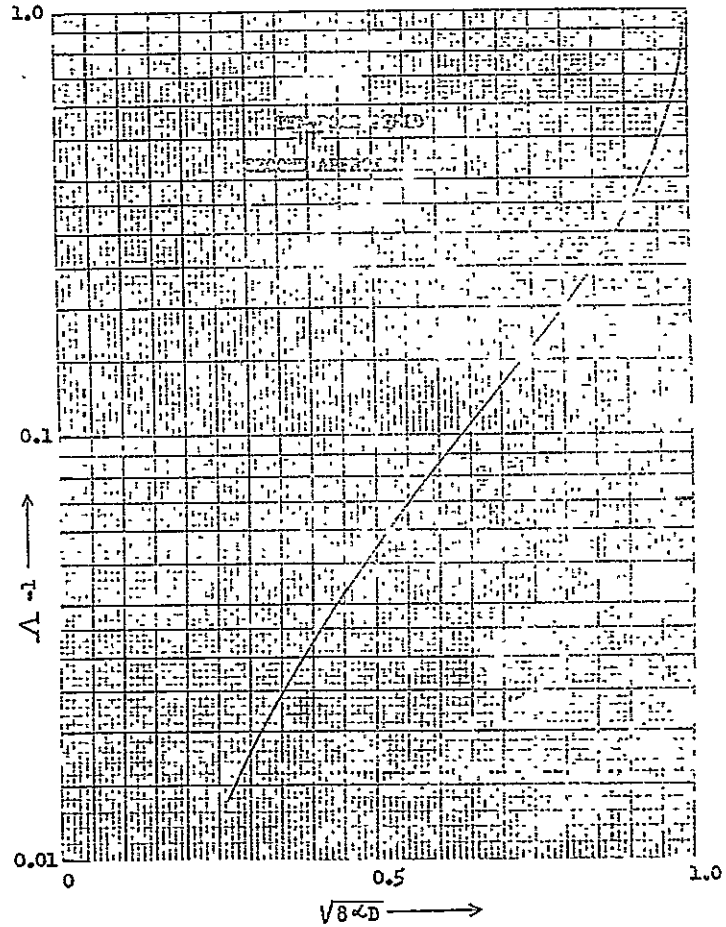

Fig. IV E.1

Solutions for $\alpha D > \frac{1}{8}$ are not given here.

Note that for $\alpha D = \frac{1}{8}$ (IV E.45)

$$D = \frac{1}{8\alpha} \quad \text{(IV E.46)}$$

From (IV E.30) $\eta_{MAX} = \sqrt{2}\, D = \sqrt{1/4\alpha}$ (IV E.47)

or $4\alpha \eta_{MAX}^2 = 1$ (IV E.48)

Compare this result with (IV E.1). The corresponding $\dot{\eta}_0$ can be taken from (IV E. 46) $\dot{\eta}_{0MAX} = \sqrt{K/8\alpha}$ = maximum $\dot{\eta}_0$ (IV E.49)

above which particles are accelerated away from the η = 0 plane.

A sketch of the trajectories for the second approximation may help in understanding some of preceding.

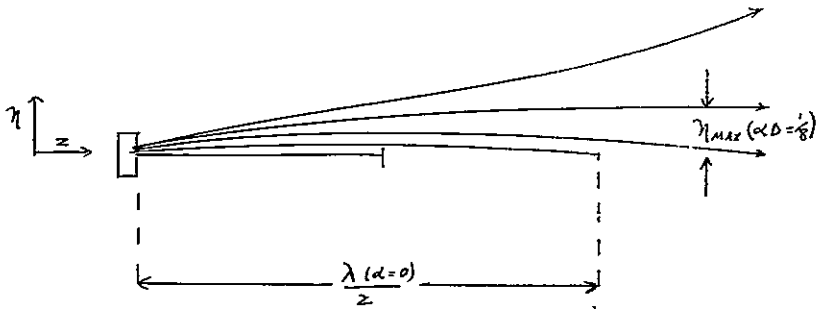

Trajectories are for one state and velocity. In addition, Fig. IV E.2 shows trajectories for both first and second order approximations.

3. Trajectories (ξ coordinate for $f_2(J,M) > 0$)

The ξ solution for negative K is very similar to that for with positive K. Note that Eq. (IV E.2) $\longrightarrow$ (IV E.1) if one makes the following substitutions.

$$\alpha \longrightarrow -\alpha$$

$$\eta, \dot{\eta}, \ddot{\eta} \longrightarrow \xi, \dot{\xi}, \ddot{\xi}$$

$$K(+) \longrightarrow -K(-) \quad \text{(i.e., K is now negative)}$$

$$D \longrightarrow \frac{\dot{\xi}_0^2}{-K} \quad \text{(a positive value)} \quad \text{(IV E.50)}$$

$$D' \longrightarrow \frac{\dot{\xi}_0}{-K} + \xi_0^2 + 2\alpha\xi_0^4 \quad \text{(IV E.51)}$$

Equations (IV E.3) to (IV E.14) hold with these substitutions. g and h will be redefined to keep g real. The new equivalent to Eq. (IV E.15) is: $D' - \xi^2 - 2\alpha\xi^4 = D'\left(1 - \frac{\xi^2}{D'} - \frac{2\alpha}{D'}\xi^4\right) =$

$$D'(1+g^2\xi^2)(1-h^2\xi^2) =$$

$$D'\left(1 + (g^2 - h^2)\xi^2 - g^2h^2\xi^4\right) \quad \text{(IV E.52)}$$

Fig. IV E.2 Ten-pole field trajectories.

A sine wave and a second order trajectory are shown for the same $\dot{\eta}_0$ (with D = 0.1875, $\alpha = +\frac{1}{3}$). If K (or V_0) is raised (D = 0.154), the trajectory shows focusing for a smaller λ or τ. Note that $\dot{\eta}_0 t$ is proportional to z here.

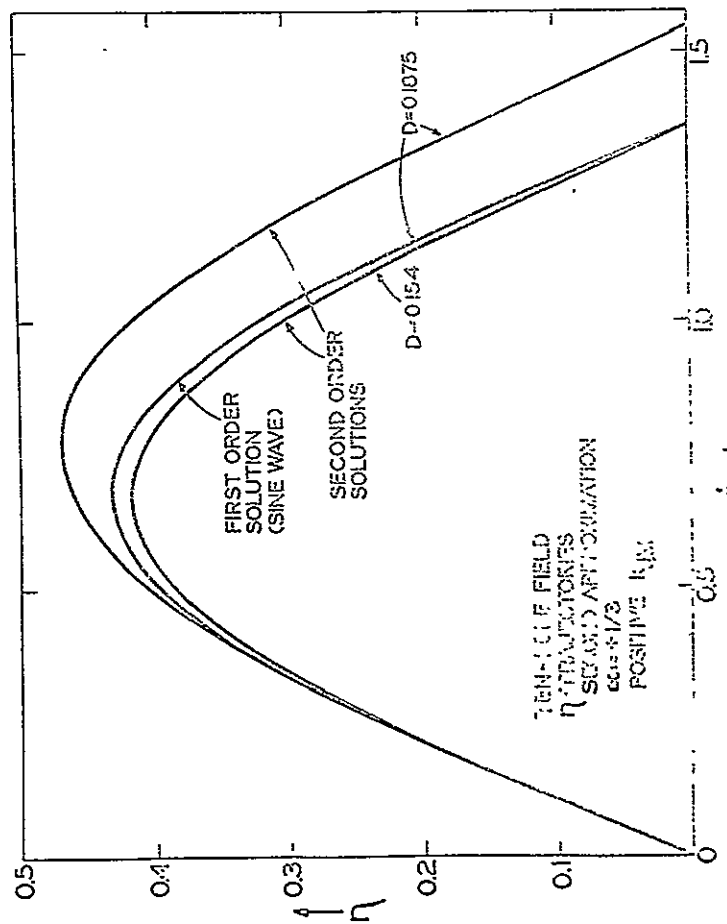

Fig. IV E.2

$$g^2 - h^2 = -\frac{1}{D'} \qquad \text{(IV E.53)}$$

$$g^2 h^2 = \frac{2\alpha}{D'} \qquad \text{(IV E.54)}$$

$$g^2 = \frac{2\alpha}{D' h^2} \qquad \text{(IV E.55)}$$

Substitute Eq. (IV E.55) in (IV E.53).

$$h^4 - \frac{h^2}{D'} - \frac{2\alpha}{D'} = 0 \qquad \text{(IV E.56)}$$

$$h^2 = \frac{1}{2}\left(\frac{1}{D'} \pm \sqrt{\left(\frac{1}{D'}\right)^2 + \frac{8\alpha}{D'}}\right) = \frac{1}{2D'}\left(1 \pm \sqrt{1+8\alpha D'}\right) \qquad \text{(IV E.57)}$$

Similarly $$h^2 = \frac{2\alpha}{D' g^2} \qquad \text{(IV E.58)}$$

$$g^4 + \frac{g^2}{D'} - \frac{2\alpha}{D'} = 0 \qquad \text{(IV E.59)}$$

$$g^2 = \frac{1}{2}\left(-\frac{1}{D'} \pm \sqrt{\left(\frac{1}{D'}\right)^2 + \frac{8\alpha}{D'}}\right) = \frac{1}{2D'}\left(-1 \pm \sqrt{1+8\alpha D'}\right) \qquad \text{(IV E.60)}$$

Eqs. (IV E.53) and (IV E.54) are satisfied if we use only the plus signs or only the minus signs in (IV E.58) and (IV E.60). The plus signs will be used so g and h are real.

$$g \equiv \sqrt{\frac{1}{2D'}\left(-1 + \sqrt{1+8\alpha D'}\right)} \qquad \text{(IV E.61)}$$

$$h \equiv \sqrt{\frac{1}{2D'}\left(1 + \sqrt{1+8\alpha D'}\right)} \qquad \text{(IV E.62)}$$

$$c \equiv \frac{g}{h} = \sqrt{\frac{-1+\sqrt{1+8\alpha D'}}{1+\sqrt{1+8\alpha D'}}} < 1 \qquad \text{(IV E.63)}$$

Let $$h\xi = T \qquad \text{(IV E.64)}$$

$$h\,d\xi = dT \qquad \text{(IV E.65)}$$

Substitute (IV E.63) and (IV E.64) in (IV E.52).

$$D'(1+g^2\xi^2)(1-h^2\xi^2) =$$

$$D'(1+c^2T^2)(1-T^2) \qquad \text{(IV E.66)}$$

The ξ integral equivalent to (IV E.27) is

$$t = \frac{1}{\sqrt{-KD'}\,h}\int_{T_0}^{T} \frac{dT}{\sqrt{(1+c^2T^2)(1-T^2)}} \qquad \text{(IV E.67)}$$

Let cos ϕ = T (IV E.68)

$$k^2 = \frac{c^2}{1+c^2} =$$

$$\frac{1}{2}\left(1 - \frac{1}{\sqrt{1+8\alpha D'}}\right) \qquad \text{(IV E.69)}$$

Then (IV E.67) becomes

$$t = \frac{1}{\sqrt{-KD'}\,h} \int_{\phi_0}^{\phi} \frac{(-d\phi)}{\sqrt{1+c^2\cos^2\phi}} =$$

$$\frac{1}{\sqrt{-KD'}\,h} \int_{\phi_0}^{\phi} \frac{(-d\phi)}{\sqrt{1+c^2-c^2\sin^2\phi}} =$$

$$\frac{1}{\sqrt{-KD'}\,h\sqrt{1+c^2}} \int_{\phi_0}^{\phi} \frac{(-d\phi)}{\sqrt{1-\frac{c^2}{1+c^2}\sin^2\phi}}$$

$$\frac{1}{\sqrt{-KD'}\,h\sqrt{1+c^2}} \int_{\phi_0}^{\phi} \frac{(-d\phi)}{\sqrt{1-k^2\sin^2\phi}}$$

$$\frac{-1}{\sqrt{-KD'}\,h\sqrt{1+c^2}} \left(F(k,\phi) - F(k,\phi_0) \right) \qquad \text{(IV E.70)}$$

Using (IV E.62), (IV E.63), and the last part of (IV E.51), one finds

$$t = \frac{F(k,\phi_0) - F(k,\phi)}{\sqrt{-K}\sqrt{1+8\alpha D'}} \qquad \text{(IV E.71)}$$

$$\phi(\xi = 0) = \pm \frac{\pi}{2} \qquad \text{(IV E.72)}$$

Using Eq. (IV E.28), one finds

$$\frac{1}{2}\gamma = \frac{2K(k)}{\sqrt{-K}\sqrt{1+8\alpha D'}} \qquad \text{(IV E.73)}$$

Since T = 1 at the maximum ξ for each trajectory,

$$\xi_{MAX} = \frac{1}{h} = \sqrt{\frac{2D'}{1+\sqrt{1+8\alpha D'}}} \qquad \text{(IV E.74)}$$

$$\frac{\lambda}{2} = \frac{1}{2} v \gamma = \frac{2v\,K(k)}{\sqrt{-K}\sqrt{1+8\alpha D'}} \qquad \text{(IV E.75)}$$

For $\alpha \to 0$ with K kept constant, or for negligible ξ^2 compared to 1, one finds that $k \to 0$ (IV E.76)

from Eq. (IV E.69). Then from Eq. (IV E.71), for $\xi_0 = 0$,

$$t \longrightarrow \frac{\frac{\pi}{2} - \phi}{\sqrt{-K}} = \frac{\frac{\pi}{2} - \arccos \frac{\xi}{\sqrt{D}}}{\sqrt{-K}} \qquad \text{(IV E.77)}$$

since $$K(0) = \frac{\pi}{2} \qquad \text{(IV E.78)}$$

$$F(0,\phi) = \phi \qquad \text{(IV E.79)}$$

and

$$h \longrightarrow \frac{1}{\sqrt{D}} \qquad \text{(IV E.80)}$$

$$\xi \longrightarrow \sqrt{D}\cos\left(-\sqrt{-K}\,t + \frac{\pi}{2}\right) = \sqrt{D}\sin\sqrt{-K}\,t \qquad \text{(IV E.81)}$$

Using Eq. (IV E.39), (IV E.75), and the equation

$$\frac{\lambda}{2} = \frac{1}{2} v \tau \rightarrow \frac{v\pi}{\sqrt{K}} \qquad \text{(IV E.82)}$$

one finds

$$\Lambda = \frac{2K(k)}{\pi\sqrt{1+8\alpha D}} \qquad \text{(IV E.83)}$$

Since k is a function only of αD (see (IV E.69)), for $\eta_0 = 0$,

$$\Lambda = \Lambda(\alpha D) \qquad \text{(IV E.84)}$$

F. Appendix 4. Alternate gradient focusing using two two- (or ten-)pole fields.

A rather general analysis of alternate gradient focusing of beams of polar molecules has been presented by Wharton et al.[IV F.1] The following treatment is confined to the consideration of one arrangement, which was thought worthy of experimental investigation.

The configuration is shown in the sketch. Consider the result of

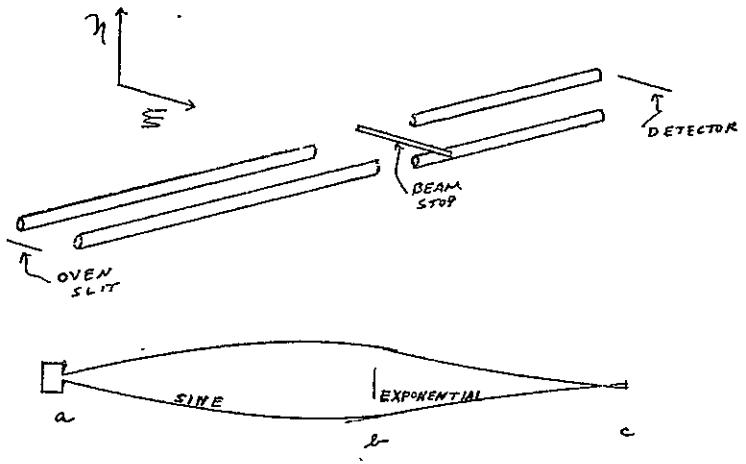

an experiment with a second two- (or ten-)pole field rotated 90° with respect to the first for a diatomic with negative $f_2(J,M)$. To first order, from a to b:

$$\frac{d^2\eta}{dt^2} = -K\eta \qquad \text{(IV F.1)}$$

$$\eta = \frac{\dot{\eta}_0}{\sqrt{K}} \sin\sqrt{K}\, t \qquad \text{(IV F.2)}$$

IV F.1 See reference IV B.9. Also see A. Septier (Ed.), "Focusing of Charged Particles," (Academic Press, New York, 1967), Vol. I, p. 368.

$$\dot{\eta} = \dot{\eta}_o \cos \sqrt{K}\, t \qquad \text{(IV F.3)}$$

From b to c:

$$\frac{d^2\eta}{dt^2} = K\eta \qquad \text{(IV F.4)}$$

$$\eta = \eta_b \cosh \sqrt{K}\,(t-t_b) + \frac{\dot{\eta}_b}{\sqrt{K}} \sinh \sqrt{K}\,(t-t_b)$$

$$= \frac{\dot{\eta}_o}{\sqrt{K}} \sin \sqrt{K}\, t_b \cosh \sqrt{K}\,(t-t_b) + \frac{\dot{\eta}_o}{\sqrt{K}} \cos \sqrt{K}\, t_b \sinh \sqrt{K}\,(t-t_b) \qquad \text{(IV.F.5)}$$

Set $\eta = o$ at $t = t_c$; then

$$\tan \sqrt{K}\, t_b = -\tanh \sqrt{K}(t_c - t_b) \qquad \text{(IV F.6)}$$

Note that this condition for focusing holds independent of $\dot{\eta}_o$. If one knew t_b and t_c, one could find $\sqrt{K}$ (and thereby the necessary voltage V_o). Assume $t_b = \frac{1}{2} t_c$ and $\tanh \sqrt{K}\, t_b \doteq 1$ since $\sqrt{K}\, t_b > \frac{\pi}{2}$ to have $\frac{d\eta}{dt} < o$ between the two fields and since $\tanh \frac{\pi}{2} > 0.90$. Then $\tan \sqrt{K}\, \frac{t_c}{2} \doteq -1$ (IV F.7)

$$\sqrt{K}\, \frac{t_c}{2} \doteq \frac{3}{4}\pi \qquad \text{rather than the } \frac{\pi}{2} \qquad \text{(IV F.8)}$$

for sine wave focusing).

$$\lambda = v\tau = 2v\, t_c \qquad \text{(IV F.9)}$$

$$\sqrt{K} \doteq \frac{3}{2}\frac{\pi}{t_c} = 3\pi \frac{v}{\lambda} \qquad \text{(IV.F.10)}$$

For the normal configuration (both fields "parallel")

$$\sqrt{K} = 2\pi \frac{v}{\lambda} \qquad \text{(IV F.11)}$$

Since $\sqrt{K} \propto V_o$,

$$V_{o\ \text{alt.}} = {}^3/_2 \quad V_{o\ \text{normal}} \qquad \text{(IV F.12)}$$

$$\left(\frac{d\eta}{dt}\right)_c = \dot{\eta}_o \sin \sqrt{K}\, t_b \sinh \sqrt{K}\,(t_c - t_b) +$$

$$\dot{\eta}_o \cos \sqrt{K}\, t_b \cosh \sqrt{K}\,(t_c - t_b) =$$

$$\dot{\eta}_o \left(\sin \tfrac{3}{4}\pi \sinh \tfrac{3}{4}\pi + \cos \tfrac{3}{4}\pi \cosh \tfrac{3}{4}\pi\right) \approx 0 \qquad \text{(IV F.13)}$$

The slope of the trajectories at the detector is nearly zero.

It is also possible that the positive f_2 (J, M) states will be focused in the same plane (see sketch).

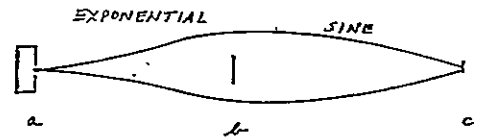

a to b: $$\frac{d^2\eta}{dt^2} = K\eta \qquad \text{(IV F.14)}$$

$$\eta = \frac{\dot{\eta}_o}{\sqrt{K}} \sinh \sqrt{K}\, t \qquad \text{(IV F.15)}$$

$$\dot{\eta} = \dot{\eta}_o \cosh \sqrt{K}\, t \qquad \text{(IV F.16)}$$

b to c: $$\frac{d^2\eta}{dt^2} = -K\eta \qquad \text{(IV F.17)}$$

$$\eta = \frac{\dot{\eta}_o}{\sqrt{K}} \cosh \sqrt{K}\, t_b \sin \sqrt{K}(t-t_b) + \frac{\dot{\eta}_o}{\sqrt{K}} \sinh \sqrt{K}\, t_b \cos \sqrt{K}(t-t_b) \qquad \text{(IV F.18)}$$

Set $\eta = 0$ at $t = t_c$

$$\tan \sqrt{K}\,(t_c - t_b) = -\tanh \sqrt{K}\, t_b \qquad \text{(IV F.19)}$$

If $t_b = \frac{1}{2} t_c$

$$\tan \sqrt{K}\, \frac{t_c}{2} = -\tanh \sqrt{K}\, t_b \text{ as before,} \qquad \text{(IV F.20)}$$

so that one expects $$V_{o\ \text{alt.}} = \frac{3}{2} V_{o\ \text{normal}} \qquad \text{(IV F.21)}$$

Note that $$\dot{\eta}_c = \dot{\eta}_o \cosh \sqrt{K}\, t_b \cos \sqrt{K}\, t_b - \dot{\eta}_o \sinh \sqrt{K}\, t_b \sin \sqrt{K}\, t_b \approx$$

$$\frac{-1}{\sqrt{2}} \dot{\eta}_o \left(\cosh \tfrac{3}{4}\pi + \sinh \tfrac{3}{4}\pi\right) \approx 7.5\, \dot{\eta}_o \neq 0 \qquad \text{(IV F.22)}$$

This would indicate that one might discriminate against positive $f_2(J,M)$ states by allowing only trajectories of low slope to hit the detector (see sketch).

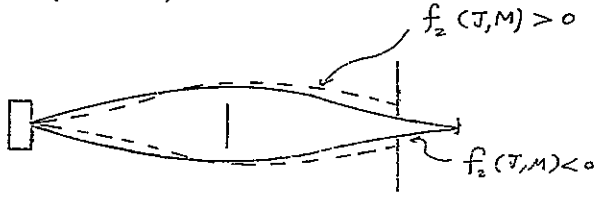

The above analysis led to the decision that it was worthwhile to attempt alternate gradient focusing of the negative $f_2(J,M)$ states with ten-pole fields. The experiments indicated that the percent focused (i.e. focusing yield) was only about as much as usually found (ca 0.1%) in the normal ten-pole focusing; moreover, it was not possible to obtain as good a resolution. The problem may have been that of a magnification of the image at the detector, as discussed in section III E. However, the results were inconclusive as insufficient effort was spent in testing the method with the ten-pole fields.

G. Appendix 5. Description of computer program for intensity distribution.

A computer program (in Fortran IV) has been written to simulate the trajectories of particles in a two- or ten-pole field. A sample is given here for focusing particles of negative $F_2(J,M)$. The integration of the differential equations is carried out using the trapezoidal rule. The program 'follows' particles with given ξ_o, $\dot{\xi}_o$, η_o, $\dot{\eta}_o$ and velocity, each with an initial V_o. This is repeated with V_o changed until the particle strikes the 'detector' (XZ- or YZ - plane) close to the detector. A final trajectory for each of the given initial conditions rejects particles which hit the beam stop, a field rod, etc.

A weighting factor is used to calculate the contribution of each particle to the intensity. This is because for given initial conditions, the particle will hit the detector for a range of V_o, ΔV_o.

$$\Delta V_o \doteq \left(\frac{\partial V_o}{\partial L}\right)_{Focus} \Delta L \qquad \text{(IV G.1)}$$

where V_o and $\left(\frac{\partial V_o}{\partial L}\right)_{Focus}$ are the values for a trajectory which leads to the detector. For such a trajectory and a circular cylindrical (wire) detector, $\Delta L = \frac{2r}{\sin\phi}$ (IV G.2)

where r is the wire radius and ϕ is the angle between the trajectory and the Z axis at the detector (see sketch on the following page).

BLANK PAGE

The value of ΔV_0 (or of $\Delta V^*/f_2(J,M)$) serves as a weighting factor. Finally, the relative intensity within given ranges of $\Delta V^*/f_2(J,M)$ is tabulated.

By trial and error, initial combinations of values of the starting parameters (e.g., the range of ξ_e for given ξ_0 over which particles might strike the detector) were chosen.

The sample program follows. Results are shown in Fig. IV G.1.

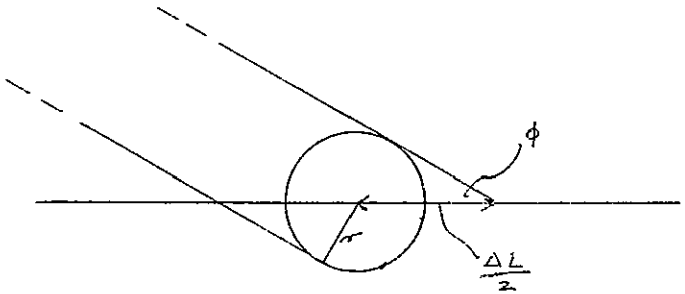


```
1
2
3
4
5
6
7
8
9
10
11
12
13
14
15
16
17
18
19
20
21
22
23
24
25
26
27
28
29
30
```

```
      43 HXI3(J1)=J.
         TOTI=0.0
         TP=2.J828/JT
         NT=TP
         BST=.3850202*TP
         DT5=.5*DT
         IVD=4
C        VARY VELOCITY
         DO 15 IV=88,112,IVD
         PIV=IV
C        FOR 13.5 PERCENT VELOCITY SELECTOR
C        HP VS. IV IS TRIANGLE OF AREA ONE
C        182.25=13.5**2
         HV(IV)=(13.5-ABSF(PIV-100.))/182.25*IVD
         PIV=PIV/100.
         ASS=JST/PIV/360.
C        VARY ETA ANGLE
         DO 15 I1=200,1100,25
         FLPI=I1*PIV
C        VARY XI AT T=0
         DO 15 J1=5,5,5
         J=J1-1
         J1000=J*(13000/IV)*10
         J1000=J1000+900000*(J*IV)**3/1000000/12544
         J.000=J1000+I1*J/2
         J1000=J1000+(I1/100*J)**2/2
C        FOR /X.*AX/ F.0,   XII+XIJ1 IS B.TWEEN -.07 AND +.07 FOR IV NEAR 100
C        FOR 1ST ORDER EQUATIONS OVER COMPLETE TRAJECTORY
         FLO=-900-J1000
C        VARY XI ANGLE
         DO 15 XI=100,2200,300
```

IV G.4

```
         V=PIV*(1.+0.0004*I1+.00002*(I1/100)**4)
         FC=V*V*1179421.
         IEND=0
         N=1
C        INCLUDE NEGATIVE XID1
         K=XI+FLO
         FLPK=K *PIV
         ETA1=0.
  102    ETAD1=FLPI *.001
         E  A1=ETAD1*SQRK
         ETAD2=ETAD1
         XII=0.1*J
         XID1=       FLPK*.0001
         XID1=XID1*SQRK
         X.12=XII*XII
         X.14=XII2*XII2
         X.16=XII4*XII2
         XID01=(2.48*X*X*XII2-9.5X2*XII**3.*X**XII0)/2.
         XID2=FC*XII*XID01ADT+XID1
         XI2=XI1+(XID1+XID2)*DT5
         N=2
         E  A2=ETAD1*DT  +ETA1
      3  N=N+1
C        FOUR DIFFERENTIAL EQUATIONS MAY BE COUPLED
         X 2=XI2**2
         X.24=X12.*X12
         X.26 X124*X22
         ETA4=ETA2*ETA2
         ETA6=.TA2*ETA4.
         X.28=X12*X26
```

IV G.5

```
      XIETA4=ETA22*XIETA2
      XIETA2=XI22*XIETA
      ETADD2=-FC*ETA2
      XIDD2=FC*XI2
      ETADD2=ETADD2*(2.-D*ETA22-E*XI24*D*XIETA2+C*ETA24-F*XI26-G*XIETA4
     1-G*XIET24-F*ETA26)/2.
      XIDD2=XIDD2*(2.+D*XI22*C*XI24+D*XIETA2-E*ETA24+F*XI26+G*XIETA2
     1+G*XIET24+F*ETA26)/2.
      ETAD3=ETAD1+2.*DT*ETADD2
      XID3=XID1+2.*DT*XIDD2
C     FORM ETA3=NEW ETA2
      ETA2=ETA2+DT5*(ETADD2+ETADD3)
      XI2=XI2+DT5*(XIDD2+XID3)
      ETAD1=ETADD2
      XID1=XIDD2
      ETAD2=ETADD3
      XID2=XIDD3
      IF (ABSF(XI2)-2.00)1,1,4
    1 IF (ETA2-1.5)2,5,5
    5 PRINT 6
    6 FORMAT ( 9H ETA HIGH)
      PRINT 10, ETA2 ,XI2,I1,K, J, IV, N,V
      GO TO 15
    2 IF (ETA2)103,103,45
   45 IF (N-ABS) 3,46, 3
C     REMEMBER 5 PERCENT WHEN COMPARING WITH EXPERIMENT
  149 IF (5(AD2-1.E-100) 149,200,200
  200 PRINT 201
  201 FORMAT (11H ETAD2 IS +)
      GO TO 15
```

IV G.6

```
  149 IF (IEND-1) 150,110,110
  110 IF (ETA2-.1158) 47,47,111
  111 IF (ETA2-.4825) 150,47,47
   47 PRINT 48, AMBDA,XI2,I1,K, J, IV, N,V
   48 FORMAT (2E16.8, I5, I7, I3, 2I5, E16.8,14H HIT BEAM STOP)
      GO TO 15
  150 DELTAT=-ETA2/ETAD2
      FLPN=N*DT+DELTAT
      XI2=XI2+XID2*DELTAT
      GO TO 6
  103 FLPN=N *DT
      XI2= XI2- ETA2/ETAD2*XID2
    6 AMBDA=FLPN/1.0414
      AMBDA=AMBDA*PIV*360.
   17 PRINT 10, AMBDA,XI2,I1,K, J, IV, N,V
   10 FORMAT (2E16.8, I5, I7, I3, 2I5, E16.8)
      V2=V1
      V1=V
      AMBDA2=AMBDA1
      AMBDA1=AMBDA
      DIFF=AMBDA-1.
      IF (N-2) 101,105,105
  101 V=V+DIFF/1.25/V/AMBDA
      GO TO 95
  105 DELDV=(AMBDA1-AMBDA2)/(V1-V2)
      V=V-DIFF/DELDV
  106 IF (IEND-1)51,100,100
   51 IF (ABSF(DIFF)-.05)52,52,101
  151 IF (N-5) 50,50,52
   52 IEND=1
   53 PCAV=V*1179421.
```

IV G.7

```
153               M=M+1
154               GO TO 102
155            100 IF (ABSF(XI2)-.77)104,104,4
156              4 PRINT  7, AMBDA,XI2,I1,K, J, IV, N,V
157              7 FORMAT (2E16.8, I5, I7, I3, 2I5, E16.8,3H XI HIGH)
158               GO TO 15
159            104 ETAA=ETA2*.00529
160               SIN=-ETAA/.27939
161               PRINT 11, AMBDA,XI2,I1,K, J, IV, N, V, M, DLDV, SIN
162             11 FORMAT (2E16.8, I5, I7, I3, 2I5, E16.8, I5, 2E16.8)
163               LAMBDA=V*100.+.5
164               MXI=XI2*10.+10.5
165               HP(IV)=HV(IV)/DLDV/SIN
166               H(LAMBDA)=H(LAMBDA)+HP(IV)
167               HXI(MXI)=HXI(MXI)+HP(IV)
168               HXIO(J1)=HXIO(J1)+HP(IV)
169            15 CONTINUE
170               PRINT 29
171            29 FORMAT (// 25H LAMBDA*100              H)
172               DO 23 LAMBDA=80,200,1
173               PRINT 24, LAMBDA, H(LAMBDA)
174            24 FORMAT (I10, E15.8)
175            23 TOTI=TOTI+H(LAMBDA)
176               PRINT 9, TOTI
177             9 FORMAT (///6H TOTI= E15.8)
178               PRINT 30
179            30 FORMAT (//25H INTENSITY Vs. FINAL XI  )
180               PRINT 22
181            22 FORMAT (/22H        LXI          HXI )
182               DO 27 MXI=2,19
```



```
183               LXI=MXI-10
184            27 PRINT 24,LXI,HXI(MXI)
185               PRINT 44
186            44 FORMAT (25H INTENSITY Vs. INITIAL XI )
187               PRINT 41
188            41 FORMAT(/22H        J          HXIO )
189               DO 40 J1=1,9
190               J=J1-1
191            40 PRINT 24, J,HXIO(J1)
192            16 STOP
193               END
194               END
195                  FINIS
196         'EXECUTE.
```

Fig. VI G.1. The expected intensity distribution versus V_o for ten-pole focused peaks.

To the first approximation the peaks should appear at $V^*/f_2(J,M) = 1.05$. The "noise" is due to the poor statistics associated with the relatively few trajectories.

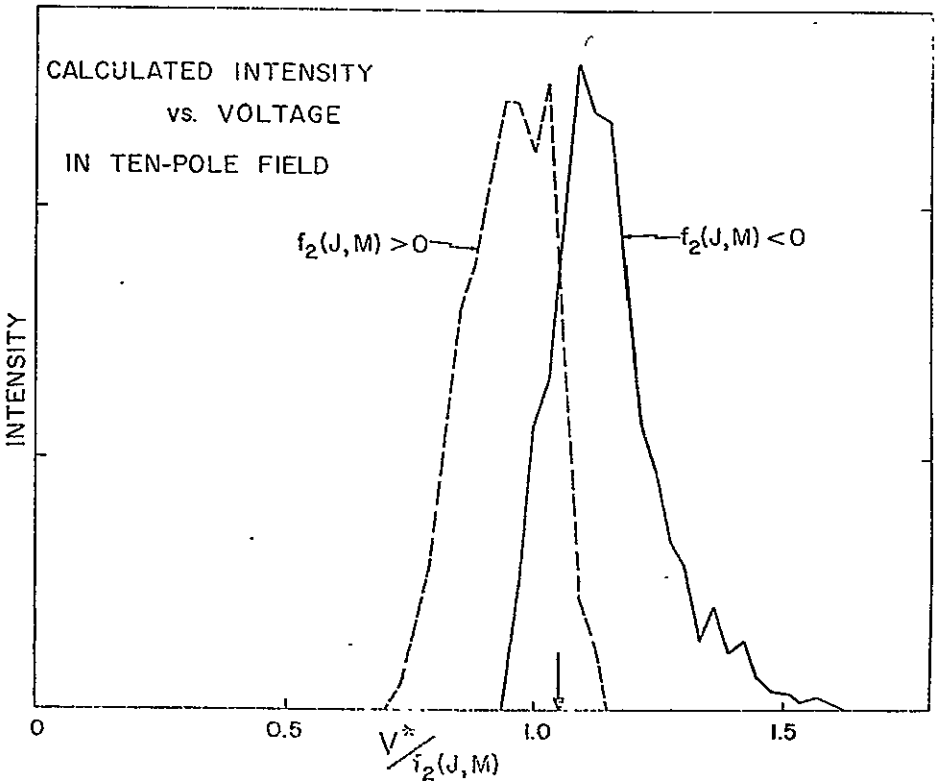

Fig. G.1

H. Appendix 6. Other possible applications of two- or ten-pole fields

The preceding sections demonstrate focusing of particles with second order Stark effects with the two- and ten-pole fields. However, it has not been mentioned that they should also focus particles with a first order Stark effect (such as symmetric top molecules). In such a case, $\vec{F} \propto -\nabla W \propto \pm \nabla E$. From Eqs. (IV C.20) and (IV C.21) (or using (IV D.15) for the ten-pole field) one can see that, to first order, such particles should be focused in the same manner as linear molecules.

This also suggests that one might similarly focus linear molecules using a section of the μ_{eff} curve (say for J,M = 0,0, from Y = 3 to 5) where $\mu_{eff} \propto C_1 + C_2 E$ and $W - W_o \propto C_1 E + C_2 E^2$ where C_1 and C_2 are constants.

Fields with potentials similar to, but not the same as that of Eq. IV D.3b might be designed to give good focusing for the experiments suggested here.

Table IV H.1 gives a comparison of electrostatic focusing techniques for polar molecules.

Table IV H.1 ELECTROSTATIC FOCUSING FIELDS FOR POLAR MOLECULES[a]

Field	Four-pole	Six-pole[b]	Two-pole	Ten-pole
Focuses:	Polar linear molecules in $^1\Sigma$ electronic states. Also asymmetric tops. Also NH_3.	Symmetric top molecules heteronuclear linear molecules in $^1\Sigma$ states (such as NO).	Same as for four- and six-pole fields.	
in states:	of positive Stark energy.	of positive Stark energy.	of positive or negative Stark energy.	
Approximate intensity[c] focused:	0.1 - 10 % of direct beam (for each state for diatomics)	up to several times the direct beam (states not separated for symmetric top).	small (Poor resolution)	small ~0.1 % (Resolution adequate)
Approximate trajectory r, ξ, η = 0 at t = 0, Z = 0	$r = \frac{V\phi}{2\pi\nu} \sin 2\pi\nu \frac{z}{v}$ where $2\pi\nu = \frac{2V_o\mu_o}{R^2}\sqrt{\frac{2J_x(J,M)}{m\hbar^2/2\pi}}$	$r = \frac{V\phi}{2\pi\nu} \sin 2\pi\nu \frac{z}{v}$ where $2\pi\nu = 2\pi\sqrt{\frac{6\mu_o V_o \langle\cos\theta\rangle}{m^3 r_o^3}}$	$\eta = \eta_o \cos 2\pi\nu \frac{z}{v} + \frac{\dot{\eta}_o}{2\pi\nu} \sin 2\pi\nu \frac{z}{v}$ see Eqs. (IV C.33-35), (IV D.23-27).	

[a] See reference II B.1.

[b] See reference IV B.3.

[c] The percent focused depends strongly upon the geometry used. Also, a large percent focused could still mean a small intensity if detector or oven orifice sizes are small.

V. APPARATUS*

A. General

The molecular beam apparatus (see Figs. V A.1 - V A.4) is designed to be used mainly for experiments involving rotational state selection and focusing of beams of polar molecules. The long length of the vacuum envelope[V A.1] makes it appropriate for such experiments. Much of the design is due to Dr. K. H. Kramer, who was a post doctoral research associate in the group.

A second oven ("B oven") mount is located such that a secondary beam of short path length can cross the focused beam at the center of a rotating goniometer. The detector assembly, mounted on the goniometer, can rotate a limited amount (a total of sixty degrees) around the scattering center.

An important feature of the apparatus is a sliding vacuum seal between the oven and stainless steel chambers. This is controlled by a screwdriver inserted through a "quick-coupling."[V A.2] The vacuum seal, in conjunction with a gate valve (below (f) in Fig. V A.2), allows one to open (or to pump on) the oven chamber without disturbing the vacuum inside the rest of the vacuum envelope.

The pumping system (and traps) is sufficient to lower the pressure to less than 1×10^{-7} torr provided the chamber is clean and in good condition.

- - - - -

* Parts of this section are common to the theses of R. J. Beuhler, Jr. and this writer.

V A.1 The stainless steel vacuum envelope was a gift of General Dynamics (Convair-Astronautics Division), San Diego, Calif. to the research group. It has been acknowledged in ref. V B.3.

V A.2 This quick coupling is not shown in Fig. V A.2, but it is opposite the quick-coupling at (c).

BLANK PAGE

Fig. V A.1 Photograph (overall view) of the molecular beam apparatus.

The vacuum chamber consists of two stainless steel cylinders (3/8" thick wall) and a brass oven chamber (on the right). The detector assembly is at the top left (see Figs. V C.3C and V C.4C) with the B- oven flange and the pump control panel (see Fig. V A.4, below. Two liquid nitrogen traps ("hat-shaped") fit on top of the center section (see Fig. V A.5B). A liquid nitrogen reservoir leads to the oven trap (see Fig. V A.5A) and another to a trap surrounding the detector wire and ion optics (Fig. V C.3A). One of two liquid nitrogen cooled baffles and an oil diffusion pump are visible below.

The larger steel cylinder may be heated electrically to $\sim 65^{\circ}C$ (to help in degassing it), by heating wires beneath an asbestos layer

Some of the extraneous background apparatus is not directly used in the experiments.

Further details are given in Fig. V A.2.

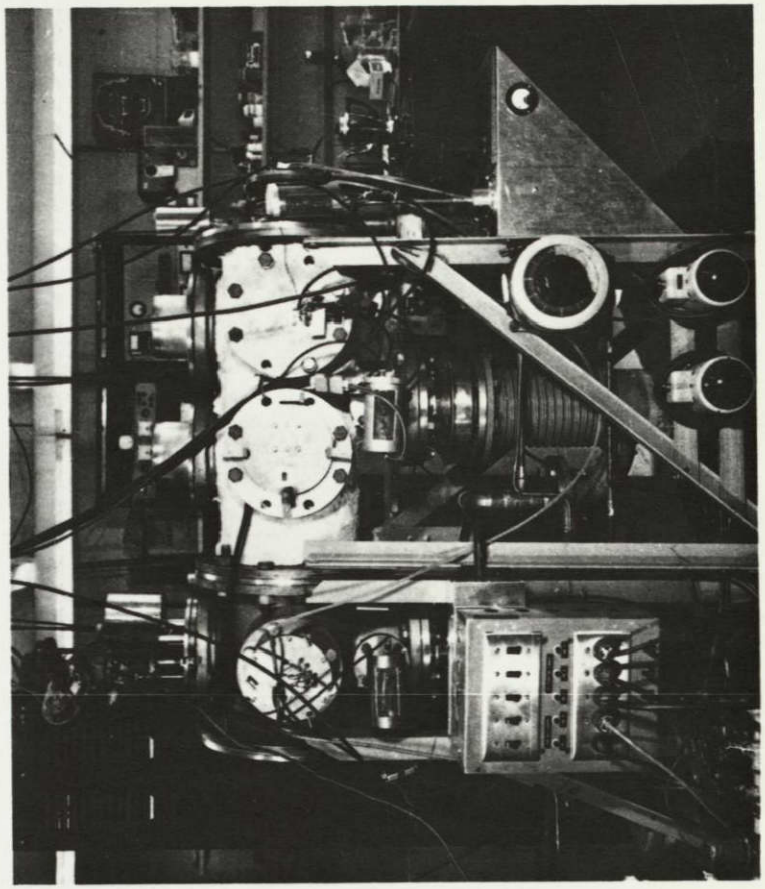

Fig. V A.1

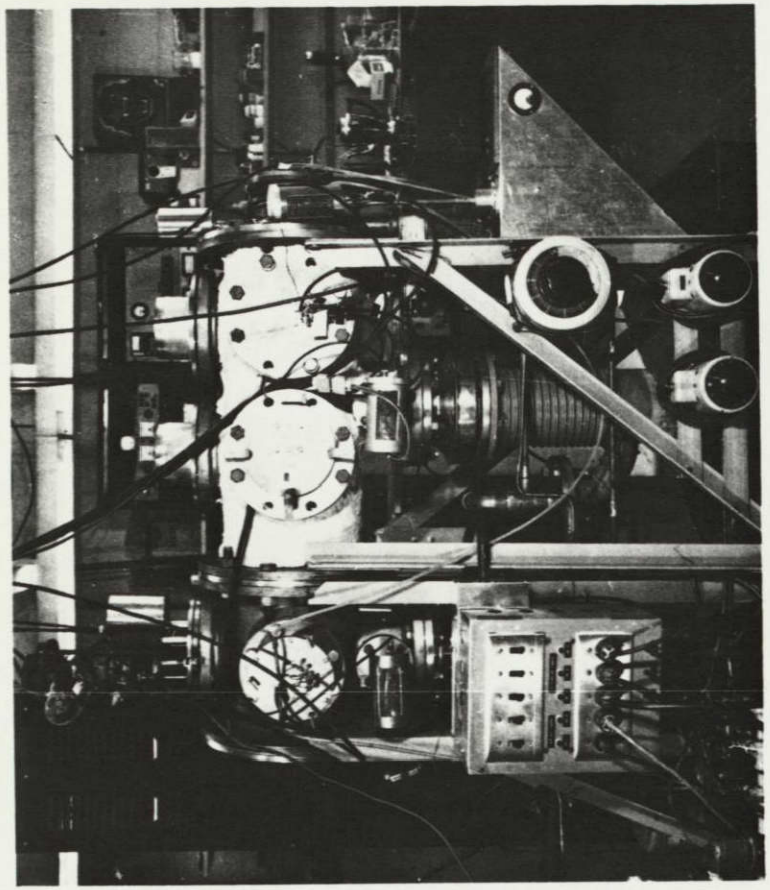

Fig. V A.1

Fig. V A.2 Diagram of vacuum envelope.

Port sizes (I.D.) and flange diameters in inches are shown.

a. A-oven, electrical feedthroughs, and water cooling attached to flange.

b. Three screws on flange to adjust oven position.

c. $^{1}/_{2}$" quick coupling for ion gauge tube.

d. Below chamber. $2\ ^{3}/_{8}$" I.D. pipe to $3\ ^{3}/_{4}$" flange. Gate valve (Consolidated Vacuum Corp. (CVC) type VCS-21) and CVC oil diffusion pump (PMC-115) attached.

e. "Quick-coupling" for liquid nitrogen trap.

f. Electrical feedthroughs.

g. Liquid nitrogen traps (top).

h. Window or waveguide feedthrough.

i. Ion gauge.

j. Cryo-baffle; National Research Corp. (NRC) model 0315-1-006. Six inch CVC oil diffusion pumps (PMC 1440) attached.

k. Goniometer (top) with detector assembly (detector filaments, ion optics, mass filter, and electron multiplier). Liquid nitrogen trap around detector filaments.

l. B-oven.

m. Window attached.

n. Ion optics and detector wire electrical feedthroughs. Also two one inch quick couplings for B-oven liquid nitrogen trap.

o. Flange may be replaced with one with a $^{7}/_{16}$" center hole to give a separate detector chamber.

p. Beam stop attached. A bellows and screws are used to adjust the beamstop position.

q. Four high voltage feedthroughs for focusing fields.

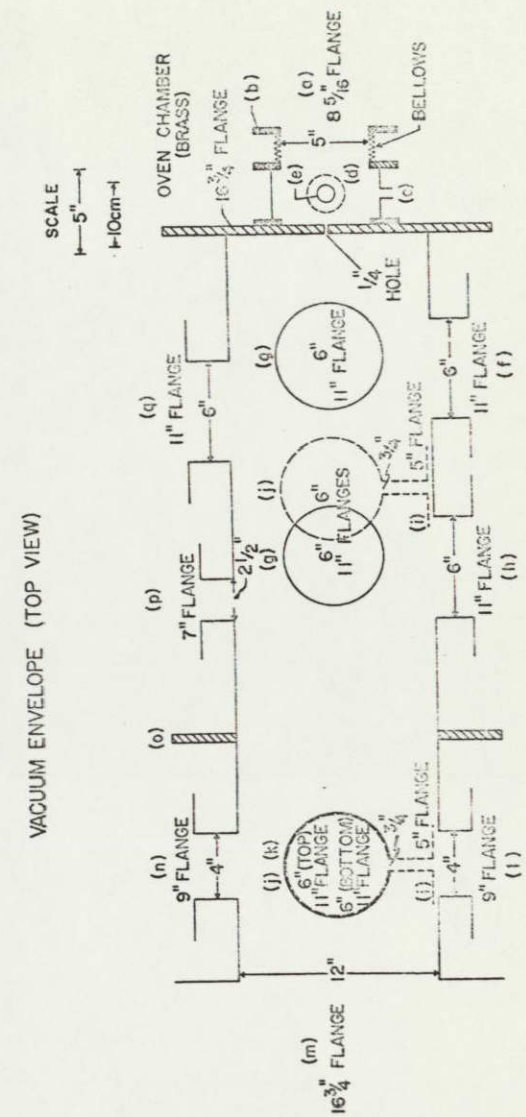

Fig. V A.2

Fig. V A.3 Apparatus views

A. A second view of the apparatus (taken from the other side). The water cooled oven chamber is seen (left). Attached to the three side flanges are (from left to right) high voltage feedthroughs (shielded) the control rod for the movable beam stop, or "obstacle" and detector system electrical feedthroughs. Quick couplings used for the B-oven liquid nitrogen trap are also on the last flange.

B. Two young (in 1965) graduate students; Robert J. Beuhler, Jr. (left) and Theodore G. Waech, who used the apparatus after the initial work of Dr. K. H. Kramer, are shown with the partially dismantled apparatus and a chart full of noise.

B

A

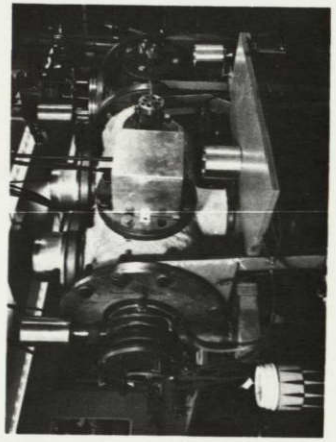

Fig. V A.3

Fig. V A.4 The vacuum pump control panel.

It is designed to protect the vacuum system from overheating or oxidizing of diffusion pump oil. A diffusion pump (DP1, DP2, or DP3) heater cannot be operated if the vacuum envelope pressure is above ~ 1 torr, if neither rotary pump (RP1 or RP2) is on, or if no water is flowing through its cooling coils (see Fig. V A.1).

S_1, S_2 DPST toggle switches (for RP1 and RP2 respectively)

S_3, S_4 S_5 SPST toggle switches (for DP1, DP2, and DP3)

CR1, CR2, CR3, CR4 control relays

F1, F2, F3, F4, F5 fuses (10A, 15A, 20A, 20A, and 3.2A respectively)

VS mercury column vacuum switch

FS1, FS2 water flow switches

(FS1 is McDonnel Model FS1;

FS2 is Penn type 605, Model 1000)

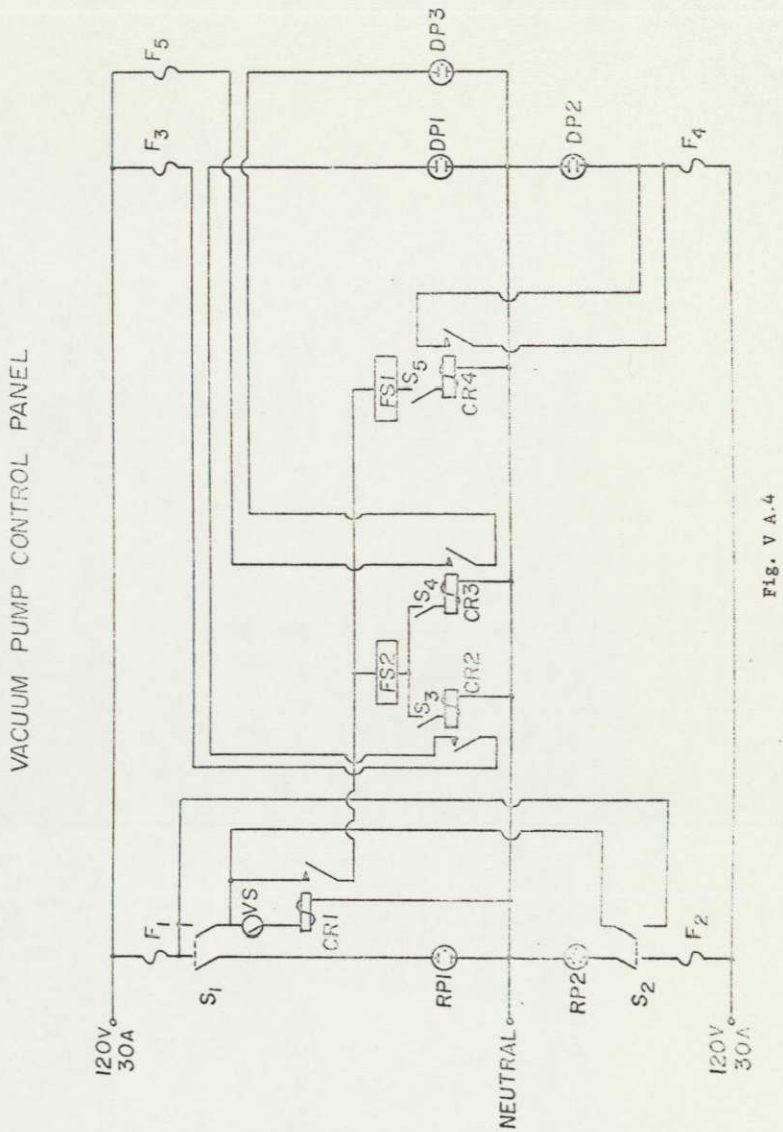

Fig. V A.4

Fig. V A.5 Liquid nitrogen traps, an oven, and a velocity selector disk.

A. Photograph of oven chamber liquid nitrogen trap. The oven "faces" this trap (copper) which condenses out A-beam material which effuses at large angles with respect to the focusing field axis.

B. Field chamber liquid nitrogen trap (inverted). This trap (and another identical trap) fits on top of the vacuum envelope (see Fig. V A.1, top center), above the focusing fields. The copper attached piece shown may be used as a cold collimator when inserted between two velocity selector disks (see Fig. V B.1). The fin design of the trap was based on the concepts of Ref. V A.1.

C. A monel oven. Various front pieces can be screwed on with say, a 0.007" circular hole, or, as shown here (left), with provision for a slit. The oven body and the front piece can be heated with coils of 0.010" diameter tungsten wire.

D. An aluminum velocity selector disk. It has sixty teeth and sixty slots (see Fig. V B.1).

- - - - -

V A.1 G. Scoles, C. J. N. Van den Meijdenberg, J. W. Bredewout, and J. J. M. Beenaker, Physica 31, 233 (1965).

A

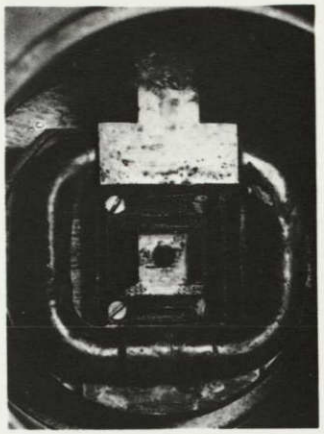

B

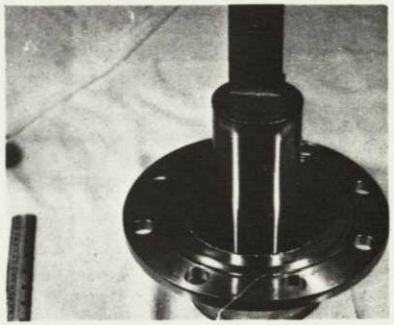

C

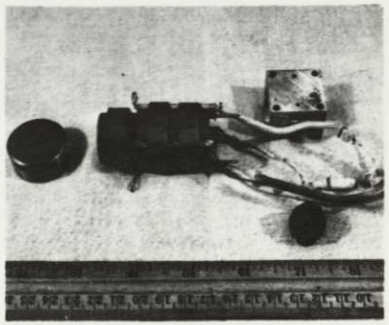

D

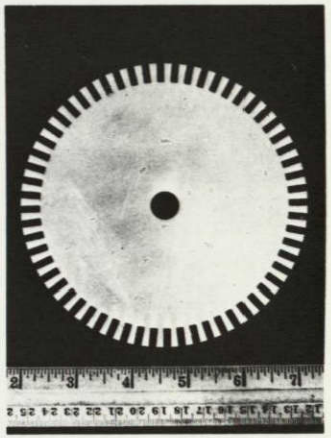

Fig. V A.5

B. Velocity selector

The velocity selector consists of disks on a rotor (see Figs. V A.5D and V B.1). The velocity of particles transmitted through "open channels" of the selector is proportional to the rate of rotation[V B.1] of the disk assembly by a motor.[V B.2] When a maxwellian beam is velocity selected at its most probable velocity, about 1/20th of the beam is transmitted.

Using the notation of ref. V B.1 and Fig. V B.2 (not to be confused with that of other sections of this thesis), the resolution and peak transmitted velocity can be found.

The nominal velocity may be correlated with f(Hz), the frequency of the oscillator which controls the motor. For the given motor,

$$\omega = \pi f$$

$$v_0 = L\,\frac{\omega}{\phi} = L\,\frac{\pi f}{\phi} = L\,\frac{60\,\ell_1 f}{r\phi}$$

$$v_0\,(m/sec) = 0.900\,f$$

- - - - -

V B.1 See H. O. Hostettler and R. B. Bernstein, Rev. Sci. Instr. 31, 872 (1960), for details.

V B.2 Barden S38H5 bearings are used for the motor and Fafnir MM20EXC2 CR bearings are used for the rotor.

BLANK PAGE

The resolution may be calculated using values given in Fig. V B.2.

$$r\phi = 6\tfrac{2}{3}\, \ell_1 = 0.840''$$

$$\beta \equiv \frac{d}{L} = 0.01626$$

$$\eta \equiv \frac{\ell_1}{\ell_1 + \ell_2} = \frac{1}{2}$$

$$\gamma = \frac{\ell_1}{r\phi} = 0.150$$

R = resolution = $\dfrac{\gamma - \beta}{1 - \gamma^2} = 0.137$

Then the selector has a resolution (FWHM) of 13.7%

$$\frac{\nu_{MAX}}{\nu_0} = \frac{1 - \beta}{1 - \gamma} = 1.157$$

$$\frac{\nu_{MIN}}{\nu_0} = \frac{1 + \beta}{1 + \gamma} = 0.884$$

Fig. V B.1 The assembled velocity selector.

The velocity selector is positioned to be used with the (four-pole) focusing field assembly shown. Its motor is beneath the field assembly. One tooth has been removed from each of five disks so that the selector can transmit a beam while not rotating. A hole is drilled opposite each broken tooth for better balancing. A bulb and photocell (right) are used to "count" the teeth as the rotor rotates.

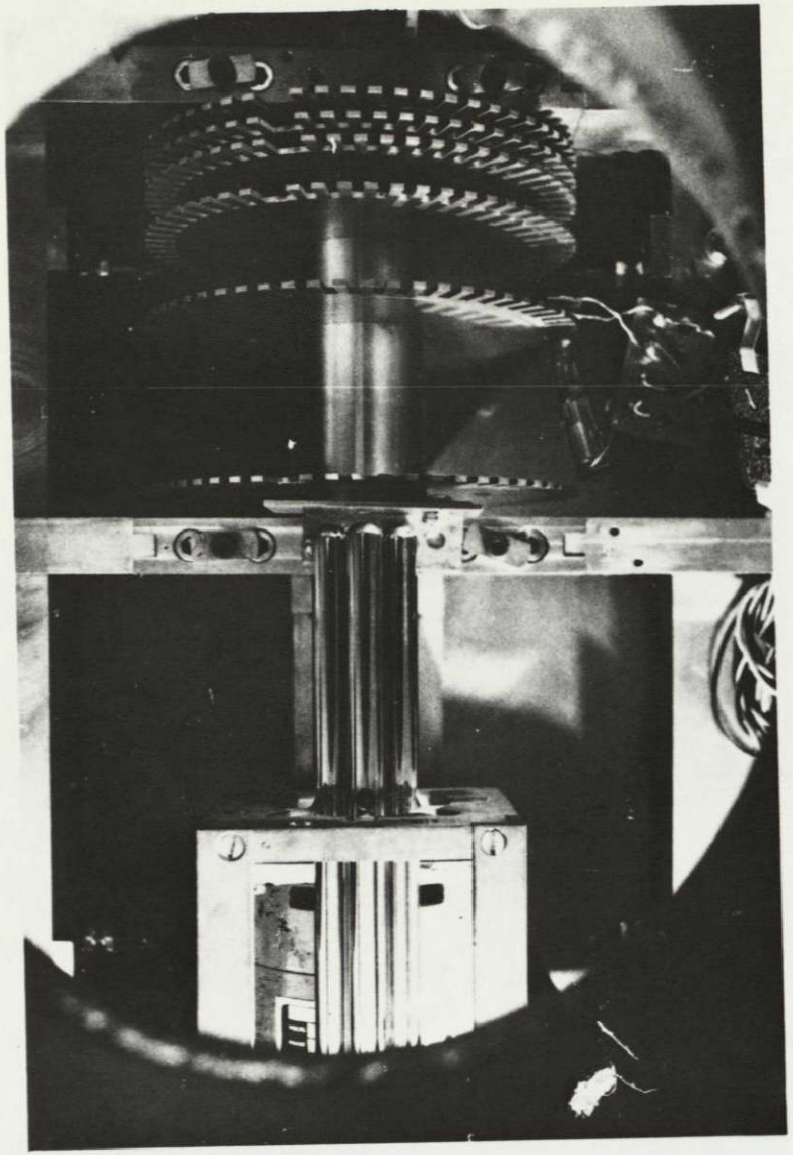

Fig. V B.1

Fig. V B.2 Velocity selector geometry.

Part of the "unrolled"[V B.1] rotor is shown with an expanded vertical dimension. One open channel is shown. The fractions indicate the amount of a tooth or space below the horizontal line.

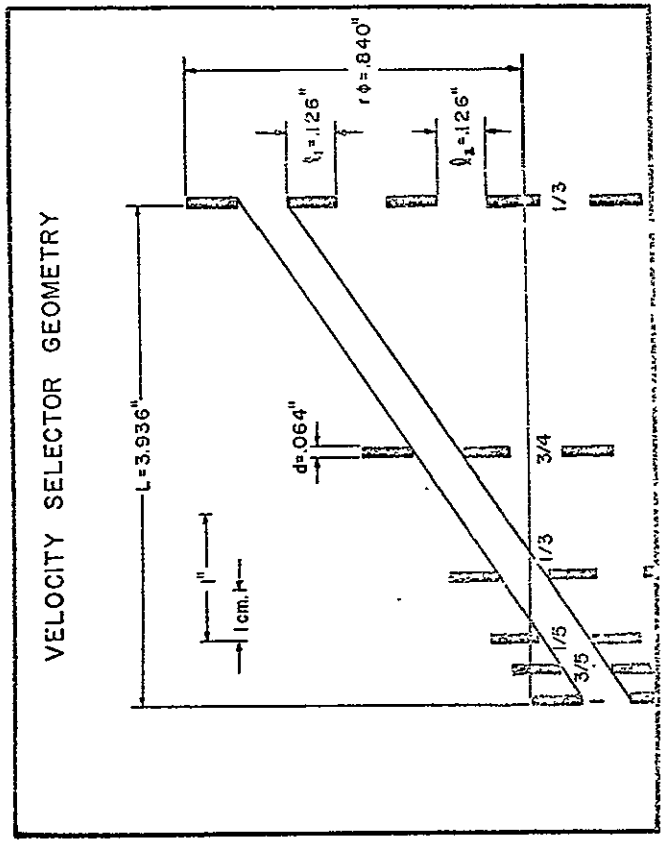

Fig. V B.2

Fig. V B.3 Velocity selector circuit.

With this circuit the velocity selector could select beams with velocities from essentially zero to about 500 m/sec, depending upon the alignment of the rotor with respect to the motor, the bearing grease (Apiezon H was used copiously), etc. The synchronous motor turns at half the audio generator frequency if it is "in sync."

VELOCITY SELECTOR CIRCUIT

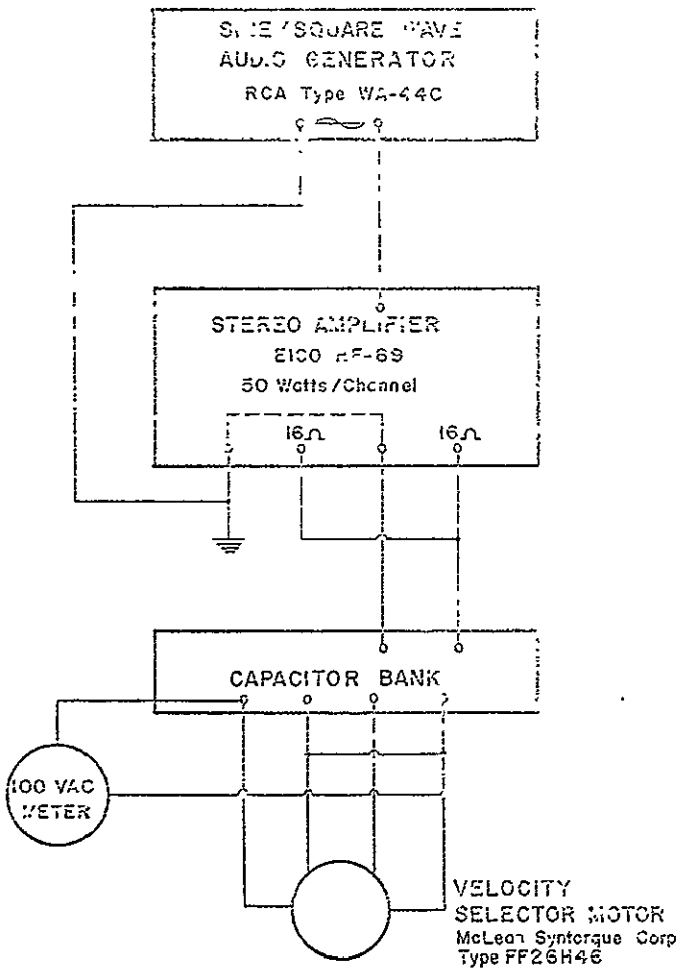

Fig. V B.3

C. Detector system

A detector system diagram is shown in Fig. V C.1. Lock-in detection is utilized with a chopped AC beam although an electrometer can be used for unchopped (DC) beams. Detection is by surface ionization, but again one has another option. A thoriated tungsten ribbon may be used as an electron bombardment source to ionize the beam molecules. Figs. V C.2 - V C.4 show parts of the detector system.

Fig. V C.1 Detector system diagram.

The molecular beam is ionized on the surface of platinum - tungsten ribbon (A) or a 0.010" diameter tungsten wire (B). The ions are guided into the mass filter by the ion optics (approximate voltages as shown). The ions are somewhat "focused" by two einzel lenses (below and above mass filter). The ions are accelerated into the electron multiplier, where they are "converted" to electrons and the current amplified. The multiplier signal goes to the cathode follower (see Fig. V C.2), and then to a phase sensitive detector, (model RJB lock-in amplifier, Electronics, Missiles and Communications, Inc., Mt. Vernon, N. Y.). The reference signal for the lock-in, from a light chopped synchrononly with the molecular beam, comes from a photocell (see Fig. V C.5A). The rectified output signal from the lock-in is displayed on a recorder (Leeds & Northrup Speedomax G, model S - 60,000 series) for easy viewing.

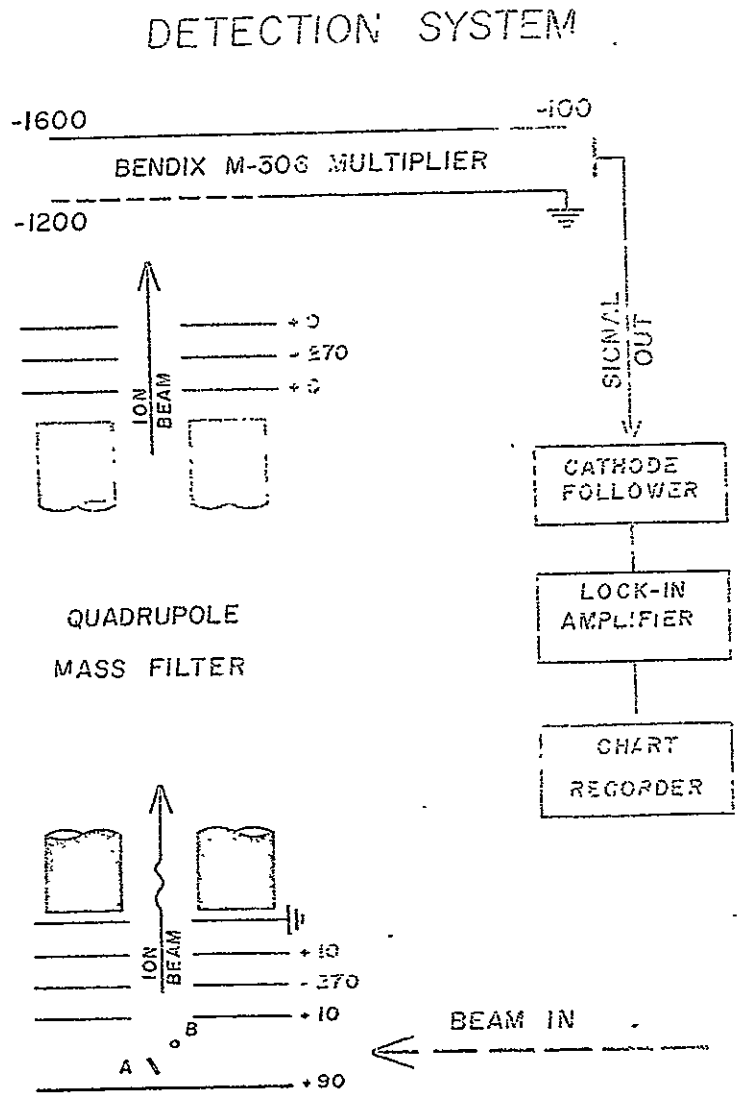

Fig. V C.1

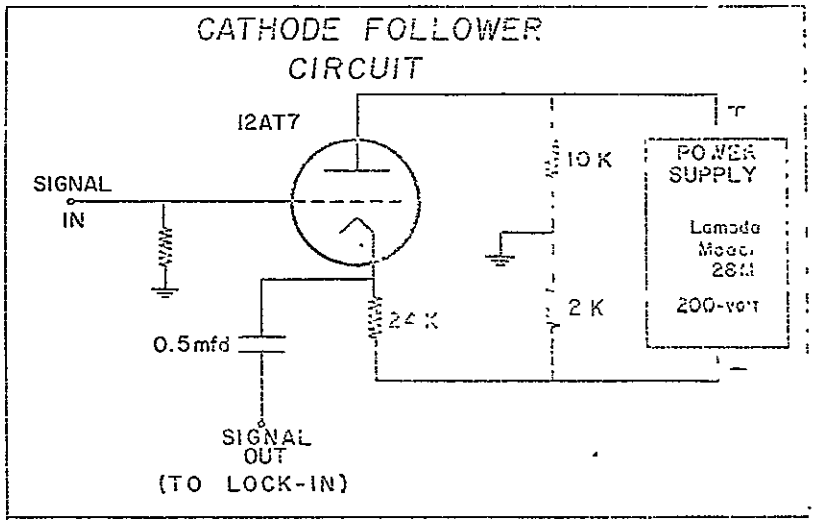

Fig. V C.2 Cathode follower circuit.

Half of a 12AT7 electron tube is used. See Fig. V C.7

Fig. V C.3 Detector assembly photographs.

A. Ion optics on end of mass filter. The ion optics of Fig. V C.1 is more recent.

B. Ion optics components. At the upper left a detector wire is spot welded to crinkled nickle foil on a stainless steel holder. A dismantled holder is at the right. An ion optics plate is placed below these.

C. Dismantled detector assembly. The quadrupole mass-filter is at right. Its height can be adjusted by the use of gears (left) on the three shafts. The voltages on the electron multiplier (in its elbow housing at the upper left) are controlled by a resistor network.

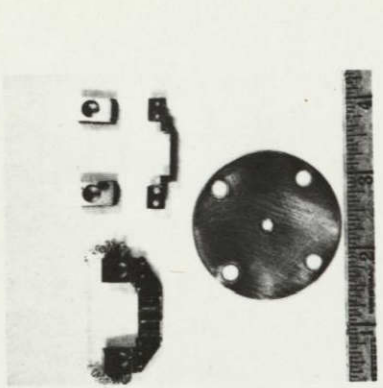

B

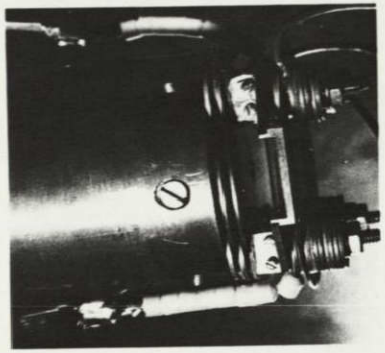

A

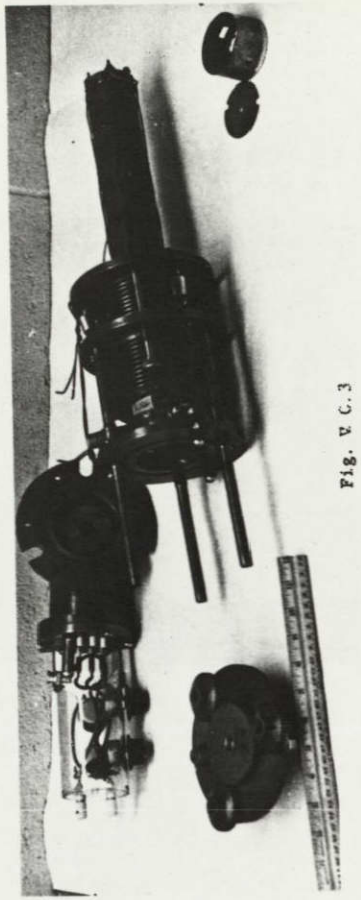

C

Fig. V C. 3

CHOPPER MOTOR CIRCUIT

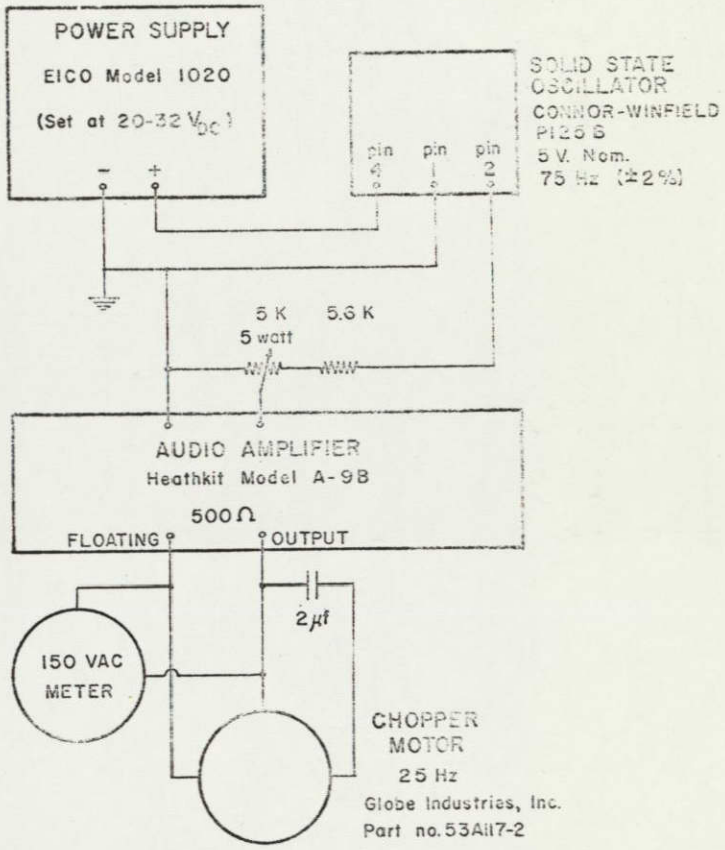

Fig. V C.4 Chopper motor circuit.

Fig. V C.5 Detector system photographs.

A. Chopper motor. The chopper motor is mounted on the stainless steel flange on which the oven chamber is attached. The V-shaped chopper blades chop the beam and, synchronously, the light from a bulb shining on a photocell, at 25 Hz. The amplified photocell output serves as the reference signal.

B. Detector assembly on goniometer (see Figs. V A.1 and V C.3). Tubes (minus reservoir) to right are for filling detector liquid nitrogen trap.

C. Glass rack. It is used for holding gases to be used in forming a beam or in activating or deactivating detector filaments.

D. View of detector end of apparatus. The liquid nitrogen trap surrounding the ion optics is clearly visible. A four-pole field assembly and microwave horn are in the background. Components such as the field assemblies and the velocity selector are attached to the angle steel as shown. See Fig. V D.1B.

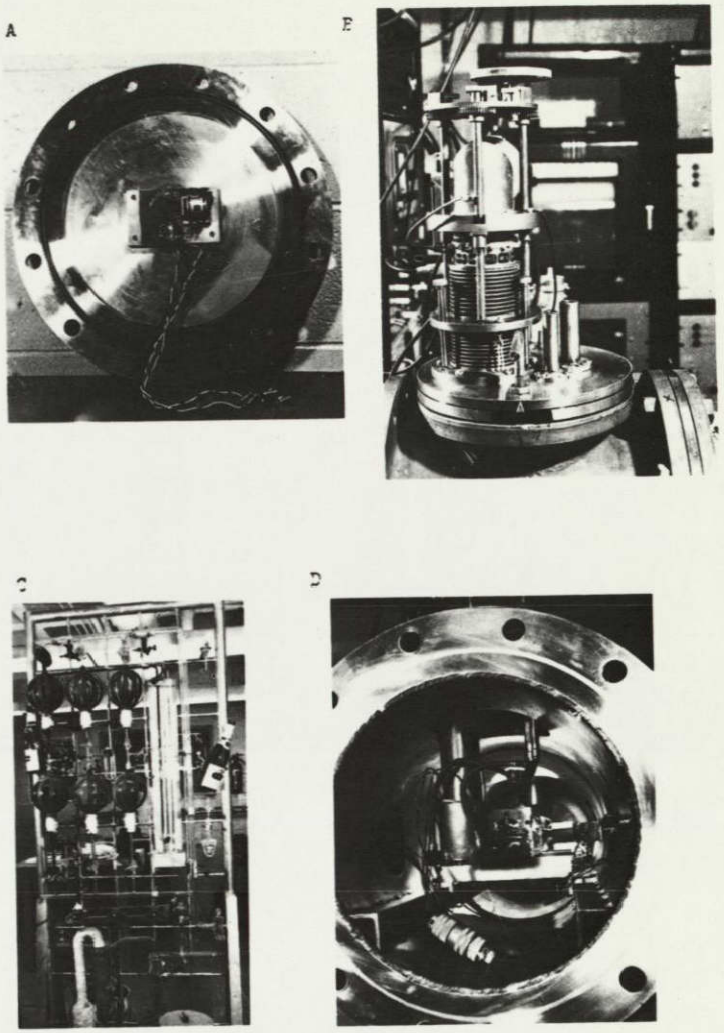

Fig. V C.5

Fig. V C.6 Liquid nitrogen trap surrounding detector assembly.

The trap is shown below a platinum-tungsten filament holder (see Fig. V C.3). The two liquid nitrogen connections (one is illustrated with a flexible copper tube) lead to a reservoir (see Fig. V A.1). The beam enters through a rectangular channel 0.200" wide. The copper tube (right) is, in use, soldered to the trap.

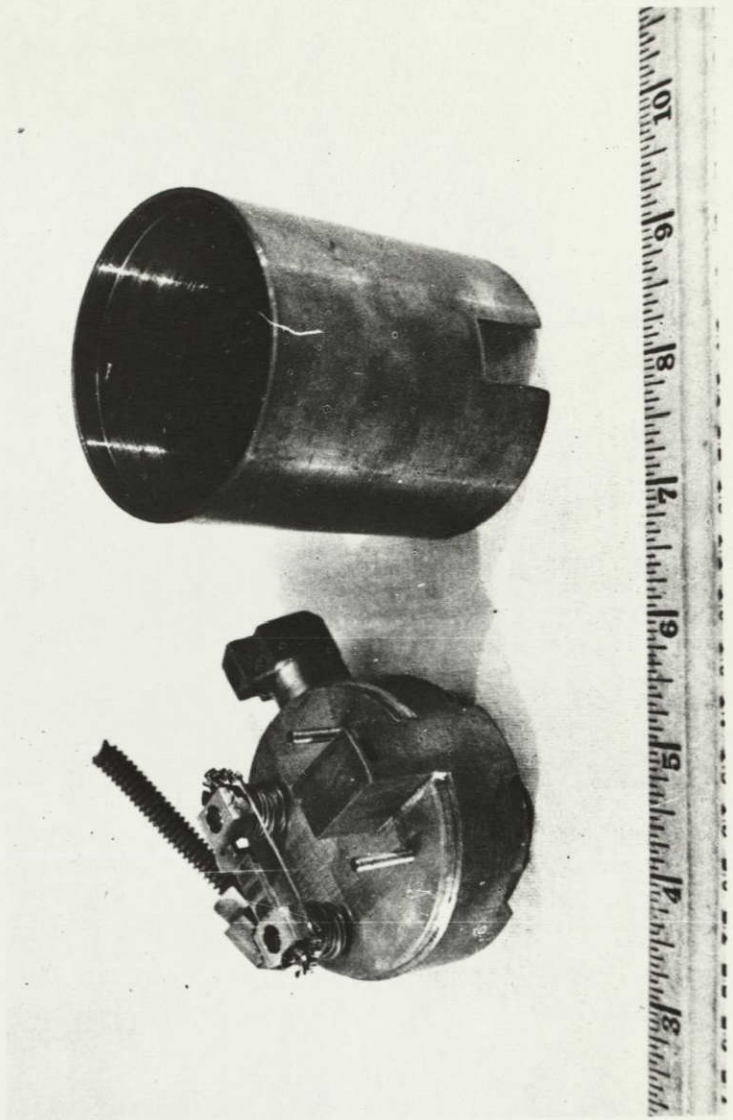

Fig. V C.6

Fig. V C.7 DC power supply.

This power supply gives $6.3V_{DC}$ to heat the electron tube filament in the cathode follower, (see Fig. V C.2). The $1.5\ V_{DC}$ and $12.6\ V_{AC}$ outputs can be used to run bulbs whose light is chopped and goes to a photocell. This is done to get a 25 Hz lock-in reference signal, and also, by "counting" selector teeth, to determine the velocity of molecules transmitted by the velocity selector.

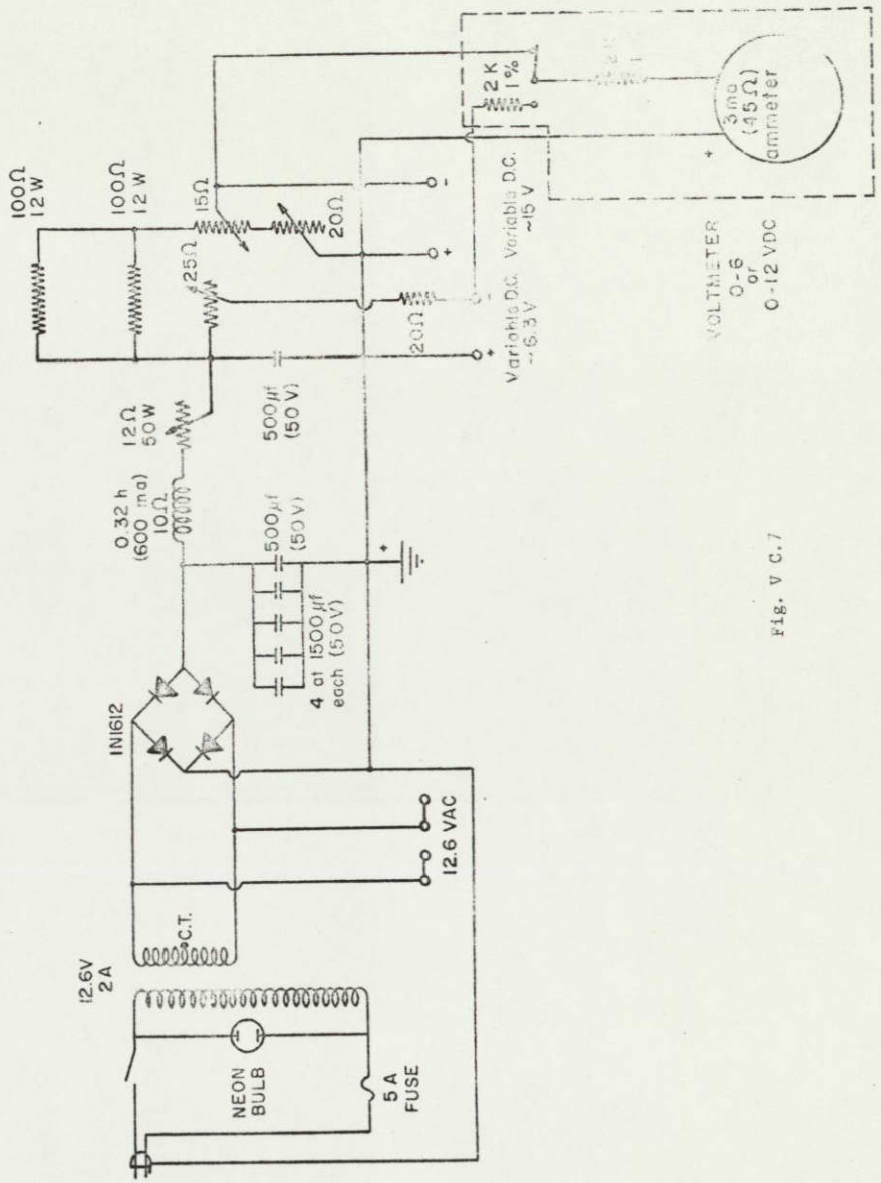

Fig. V C.7

D. Focusing Fields.

The focusing field assemblies consist of steel (usually stainless steel) rods carefully cemented with epoxy resin to ceramic end [illegible]. The rods are in turn expoxied to a brass frame. Several fields are illustrated in Fig. V D.1.

For the four-pole field, the rod radius (R_{rod}) should be (if circular rather than hyperbolic rods are used)[V D.1]

$$R_{rod} = 1.148R$$

where R is the distance from the center of the field to the [illegible] of any rod. However, at this laboratory, 1.16 was used rather than 1.148 (as others have also done).[V D.2]

For much of the work, the high voltage switch of Fig. V D.1 was used to turn the field on and off.

- - - - -

V D.1 I. E. Dayton, F. G. Shoemaker, and R. F. Mozley, Rev. Sci. Instr. 25, 485 (1954).

V D.2 H. G. Bennewitz and R. Wedemeyer, Z. Physik 172, 1 (1963).

BLANK PAGE

Fig. V D.1 Focusing fields.

A. Four-pole field assembly. The brass top-shaped piece is one of two used to space the rods while they are being cemented in place. The piece to its left can be used in aligning the field assembly in the vacuum envelope, but more often threads, weighted on their ends, were appropriately hung on the rods to form "crosshairs" on the center line of the assembly.

B. A two-pole field assembly. Note the ceramic rods used to hold the metal rods in place. The thumbscrews are used to align the field assembly.

C. End-on view of the ten-pole field assembly ($\alpha = +\frac{1}{3}$). See Fig. IV D.3.

D. Two ten-pole field assemblies. The brass pieces in the foreground are used to hold the steel rods until they are epoxied in place.

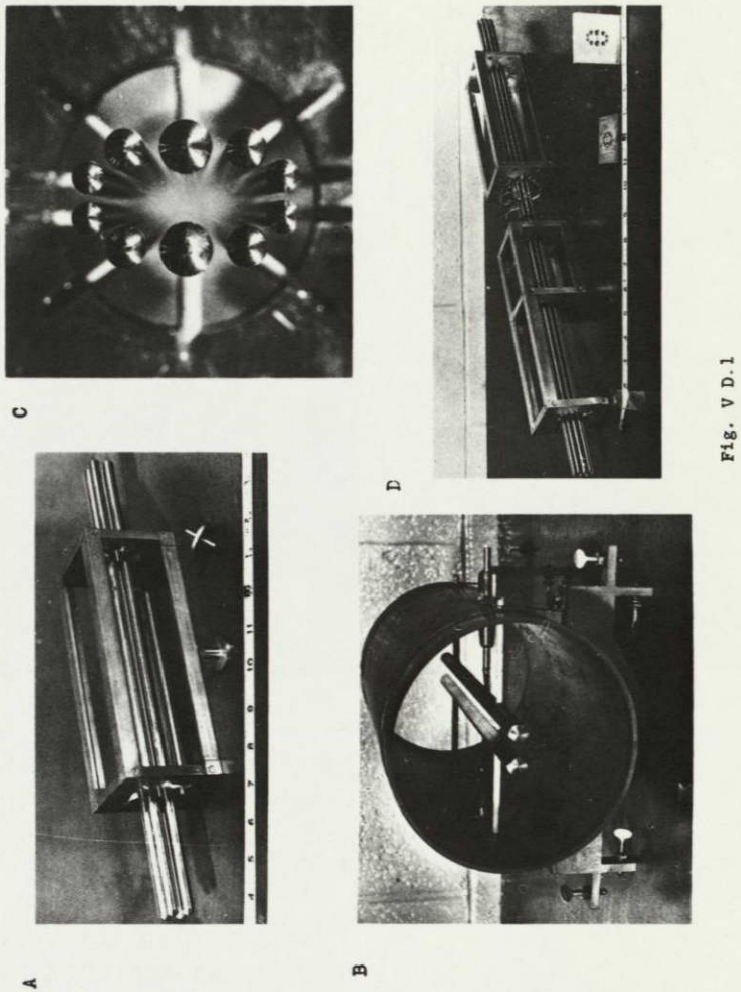

C D A B

Fig. V D.1

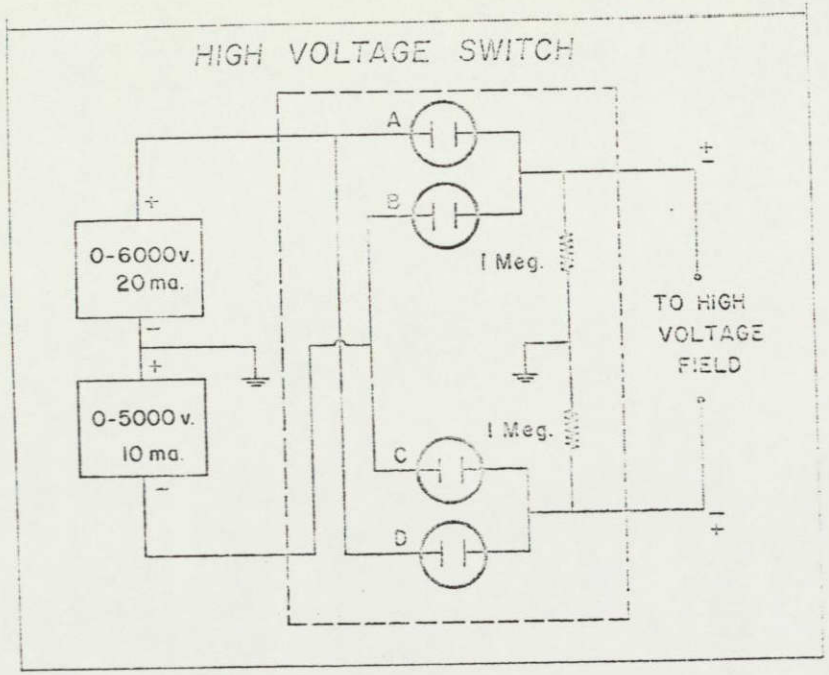

Fig. V D.2 High voltage switching circuit.

Switches A, B, C, and D are normally open vacuum switches (Jennings R5C 4052B 31001). Switches A and C or switches B and C can be made to close together, but only two can be closed at one time.

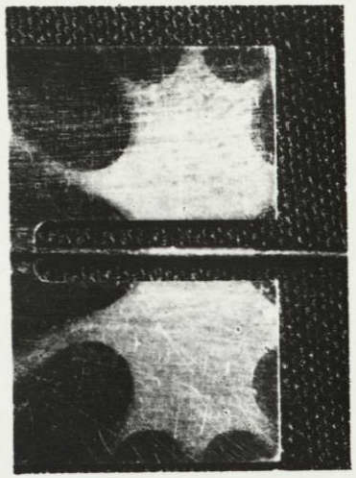

Fig. V D.3 Beam stop and collimator.

For ten-pole focusing, this beam stop and collimator was attached to the velocity selector (a similar one is in Fig. V B.1). Beam material condensed on the collimator and formed a shadow of the field rods.

E. Microwave system.

The microwave system changed throughout the work, but two systems are shown in Figs. V E.1 and V E.2. Some photographs of the systems appear in Fig. V E.3.

BLANK PAGE

Fig. V E.1 Microwave system A.

This was used for Fig. III B.2 (in the paper included), in section III B. Certain of the equipment was borrowed from Prof. R. C. Woods.

a. Heathkit (Model AG - 10) sine-square generator at 25 Hz.

b. To lock-in detector (for beam) reference.

c. Hewlett-Packard 8690A sweep oscillator.

d. Hewlett-Packard 8694A plug in (8-12.4 GHz).

e. Hewlett-Packard 175A oscilloscope.

f. Hewlett-Packard X281B adapter (coax to waveguide).

g. Microlab X157A ferrite isolator.

h. Hewlett-Packard X752C multihole directional coupler.

i. Microlab X155A variable attenuators (0-20db).

j. Polarad B126293 adapter.

k. Andrew 51747-12 flexible waveguide.

l. Andrew 55000-75 pressure window.

m. Polarad CA-Ks horn antenna.

n. Microtech flexible waveguide.

o. Hewlett-Packard 5256A frequency converter.

p. Hewlett-Packard 5245L counter.

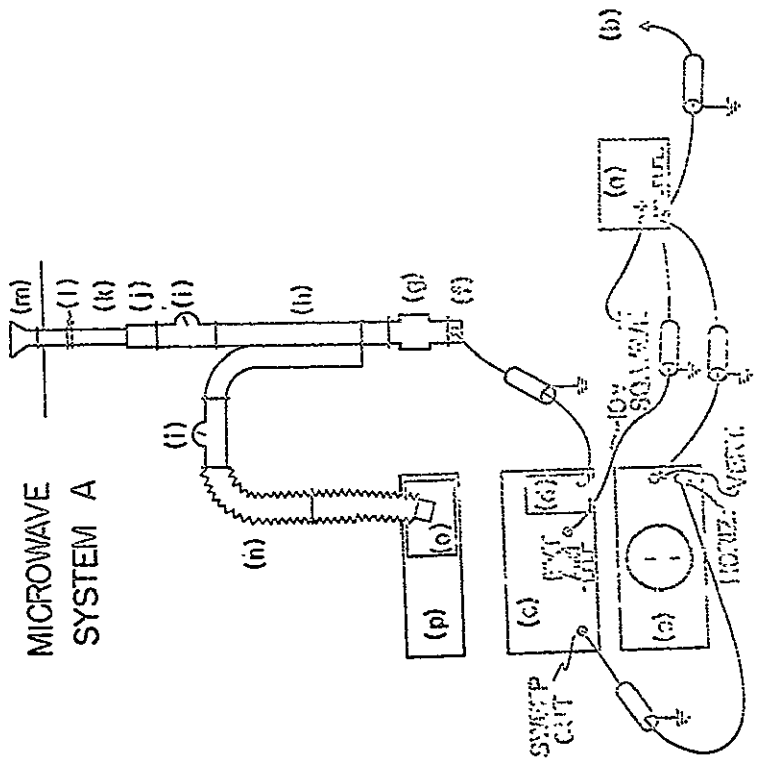

Fig. V E.1

Fig. V E.2 Microwave system B.

This microwave system was used in the earlier part of the work. It had disadvantages in that the power was inadequately stabilized in the range of interest; also it had somewhat too low power for the experiments and lacked an internal sweep necessitating manual MHz frequency scan. The parts are identified below.

a. Heathkit model AG-10 sine-square wave generator.

b. One tube amplifier. This gives an output of 40 V_{DC} for no input. A positive input (above a certain minimum) results in an output voltage of zero.

c. Polarad 1107 H microwave signal generator (3.8-8.2 GHz).

d. Polarad 1509 frequency doubler (10.0-15.0 GHz).

e. Hewlett-Packard M532A wavemeter

f. Polarad CA-K's microwave horns

g. Hewlett-Eackard M424A crystal detector.

h. Hewlett-Packard 175A oscilloscope.

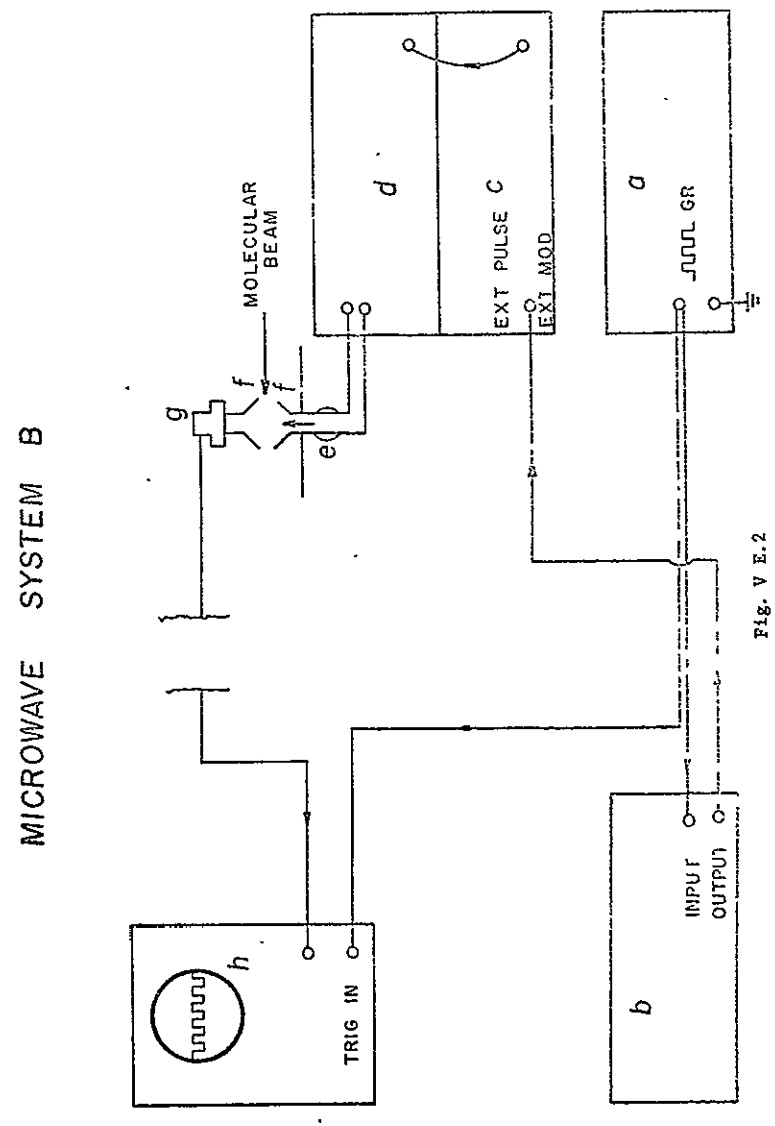

Fig. V E.2

Fig. V E.3 Microwave system photographs.

A. Microwave electronics for system B. The sine-square wave oscillator, the frequency doubler, and the microwave signal generator are shown.

B. Waveguide comporents. The wavemeter, flexible waveguide, and the microwave feed through flange are shown.

C. Some microwave components. Present are the directional coupler, a microwave horn, an adapter (for microwave flanges with different dimensions), and a crystal detector.

D. The microwave - molecular beam crossing-zone. The microwave horn and the beamstop ("obstacle") are in the center, between two four-pole field assemblies.

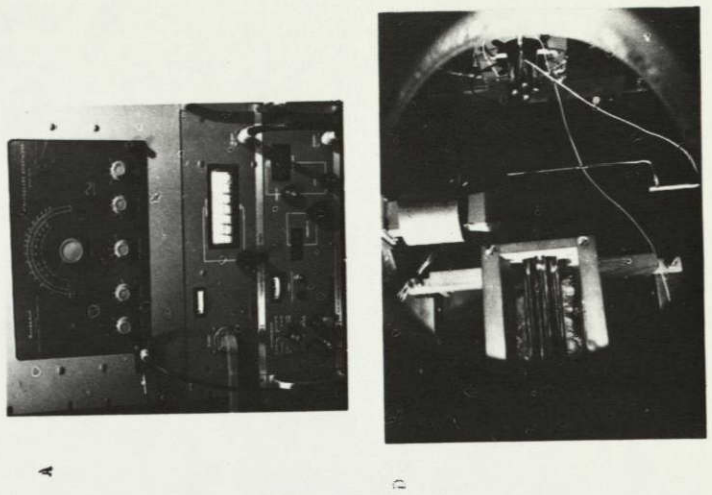

A

D

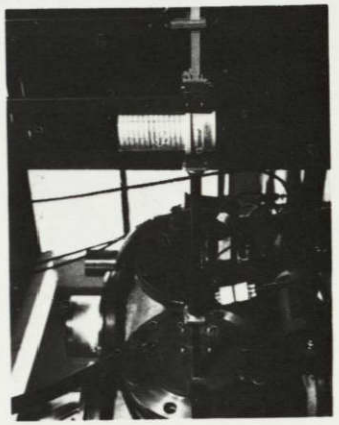

B

C

Fig. V E.3

VI. RESONANCES IN H + H SCATTERING

A. Introduction

The focusing methods in the preceding sections were developed mainly as tools to produce state-selected molecular beams, useful for studying collisions between neutral atoms or other molecules.

In the next section some calculations (already published) are presented concerning collisions of atomic hydrogen, i.e., the elastic scattering of H by H atoms. The results of proposed experiments of this type may be used to confirm knowledge of the ground state interaction potential between H atoms. Up to the present time, however, such atomic scattering experiments have been technically too difficult to carry out.

However, the results of the next section have already found application. Dr. G. Herzberg of the National Research Council of Canada has used them to help fit new spectral[VI A.1] observations on H_2. R. E. Roberts, R. B. Bernstein and C. F. Curtiss used these results as the starting point in calculations on termolecular recombination kinetics[VI A.2] for the reaction

$$H + H + M \quad H_2 + M \qquad (M = He, Ar, \text{ or } H_2)$$

R. J. LeRoy and R. B. Bernstein have discussed the inconsistencies between the theoretical and experimental ground state energies of H_2.

- - - - -

VI A.1 Private communication.

VI A.2 R. E. Roberts, R. B. Bernstein and C. F. Curtiss, Chem. Phys. Lett. 2, 0000 (1968).

They considered the influence of the so-called adiabatic, relativistic and non-adiabatic corrections to the clamped nuclei potential. In addition, they explained inconsistencies (of several cm^{-1}) between the vibrational levels of H_2 computed by several authors.[VI A.3]

VI A.3 R. J. LeRoy and R. B. Bernstein, J. Chem. Phys. 49, 0000 (1968). This writer noticed the use of nuclear masses in the reduced mass of H_2 by Wolniewicz (ref. VI B.4). LeRoy suggests that nuclear rather than atomic masses are more proper bound state calculations and that more reliable recent values of Planck's constant and the Bohr radius are available and should be used in such calculations.

B. "Calculated Spectrum of Quasibound States for H_2 ($^1\Sigma_g^+$) and Resonances in H + H Scattering," by T. G. Waech and R. B. Bernstein, J. Chem. Phys. 46, 4905 (1967).

(See journal article for this section.)

C. Computer program for potential fit

A computer program was desired to find an analytical fit to the Kolos-Wolniewicz clamped nuclei potential for a large range of R. A series (Eq.. VI B.1) was found using the method of Forsythe[VI C.1]. Although Forsythe suggested that the fitted variable (V) be expanded as a sum of polynomials, here the polynomials were used to find the coefficients (a_n) of a series in ($\frac{R-S}{2.S}$), with R in au, and also the coefficients (A_n) of a series in R - Re (Equ. VI B.2).

Attempts were made at accurately fitting the potential with a series in terms of more complicated variables, but they were unsuccessful.

The computer program (in Fortran IV language) follows.

VI C.1 See ref. VI B.10.


```
1
2
5
4
5
6
7
8
9
10
11
12
13
14
15
16
17
18
19
20
21
22
23
24
25
26
27
28
29
30
```

```
            X(J)=(R(J)-5.)/2.5
            V(J)=0.
            PM1(J)=0.
         10 P(J)=1.
      C INITIALIZE
            SIGMA2=9.
            ALPHA(1)=0.
            W=M
            BETA(1)=0.
            D=VECPRO(F,F,M)
            PRINT 4
            DO 12 I=1  ,N
            OMEGA=VECPRO(F,P,M)
            S(I)=OMEGA/W
            D=D-S(I)**2*W
            SIGMAS=SIGMA2
            SIGMA2=D/(M-I)
      C TEST SIGMA HERE
         17 DO 11 J=1  ,M
         11 P2(J)=P(J)**2
            ALPHA(I+1)=VECPRO(X,P2,M)/W
            DO 13 J=1  ,M
         13 PP1(J)=(X(J)-ALPHA(I+1))*P(J)-BETA(I)*PM1(J)
            W=W
            W=VECPRO(M,PP1,M)
            DO 14 J=1  ,M
            V(J)=V(J)+S(I)*P(J)
            PM1(J)=P(J)
         14 P(J)=PP1(J)
            BETA(I+1)=W/WM1
         12 PRINT 4, I,  SIGMA2, S(I) , ALPHA(I+1) , BETA(I)
```

IV C.3

```
            PRINT 3
            DO 15 J=1  ,M
            DIFF=V(J)-F(J)
            DIFW=2.0000.*DIFF
         15 PRINT 5, R(J),X(J),F(J),V(J),DIFF ,DIFW
      C  CALCULATE COEFFICIENTS
            DP1(2,1)=-ALPHA(2)
            DO 101 K=1,N
        101 DP1(K,K)=1.
            DO 102 K=3,N
            KM1=K-1
            KM2=K-2
            DP1(K,KM1)=DP1(KM1,KM2)-ALPHA(K)
        102 DP1(K,1)=-ALPHA(K)*DP1(KM1,1)-BETA(KM1)*DP1(KM2,1)
            DO 103 K=4,N
            KM1=K-1
            KM2=K-2
            DO 103 L=2,KM2
        103 DP1(K,L)=DP1(KM1,L-1)-ALPHA(K)*DP1(KM1,L)-BETA(KM1)*DP1(KM2,L)
            PRINT 105
            DO 106 L=1,N
            TP1(L)=0.
            DO 104 K=L,N
        104 TP1(L)=TP1(L)+S(K)*DP1(K,L)
            TP3(L)=TP1(L)
        106 PRINT 4, L, TP1(L)
            CL=1.43957360
            PRINT 122
            GAMMA(1)=1.
            GAMMA(2)=1.
            DO 117 J=2,N
```

IV C.4

```
C GAMMA(N)=(N-1)FACTORIAL
  119 GAMMA(J+1)=GAMMA(J)*J
      DO 120 K=1,N
      TP(K)=0.
      DO 121 L=K,N
      K1=L-K
      T    =GAMMA(L  )/GAMMA(K  )/GAMMA(K1-1)
  121 TP(K)=T     *GL**K1*TP1(L)+TP(K)
      TPS(K)=TP(K)
      TPT(K)=TP(K)/2.5**(K-1)
      TPU(K)=TP(K)/1.784355626**(K-1)
  120 PRINT 2, K, TPS(K), TPT(K), TPU(K)
      PRINT 111
C  CALCULATE V
      DO 109 J=8,220
      V(J)=0.
      U(J)=0.
      Q=J
      Q=Q/20.
      Z=(Q-5.)/2.5
      Z2=(Q-1.401066)/2.5
      Z3=Z
      DO 108 I1=1,N
      I2=I1-1
C  U IS CALCULATED WITH SINGLE PRECISION COEFFICIENTS AND WITH A
C  TRANSFORMED VARIABLE.
      U(J)=U(J)+TPS(I1)*Z2**I2
C  U3  IS SA  E AS U CALCULATED USING SINGLE PRECISION COEFFICIENTS
      U3(J)=U3(J) TPS(I1)*Z3     **I2
  108 V(J) V(J)-TP1(I1)*Z **I2
```



```
  109 PRINT 5, Q, V(J), U(J), U3(J)
      END
      FUNCTION VECPRO(A,B,M)
      TYPE DOUBLE A, B ,VECPRO
      DIMENSION A(90),B(90)
      VECPRO=0.
      DO 100 J=1  ,M
  100 VECPRO=VECPRO-A(J)*B(J)
      RETURN
      END
      END
         FINIS
†EXECUTE.
1.000000  1.401066         92        33
+.5797972      .4
+.4733730      .5
+.2333659      .6
+.0779739      .7
-.0200556      .8
-.0836422      .9
-.1245585       1.0
-.1500562       1.1
-.1649342       1.2
-.1720459      1.3
-.1735627      1.35
-.1744017      1.39
-.1744744      1.4
-.1744744      1.4
-.1744746     1.4010
-.1744746     1.4010
-.1744746     1.401066
```

154	-.1744746	1.401066
155	-.1744746	1.4011
156	-.1744746	1.4011
157	-.1744[illegible]	1.41
158	-.1740[illegible]	1.45
159	-.1728[illegible]	1.5
160	-.1624570	1.7
161	-.1500670	1.8
162	-.1468496	1.9
163	-.1381312	2.0
164	-.1381312	2.0
165	-.1291062	2.1
166	-.1201203	2.2
167	-.1111725	2.3
168	-.1024127	2.4
169	-.0939273	2.5
170	-.0857810	2.6
171	-.0780164	2.7
172	-.0706703	2.8
173	-.0637841	2.9
174	-.0573118	3.0
175	-.0513185	3.1
176	-.0457832	3.2
177	-.0407003	3.3
178	-.0360578	3.4
179	-.0318402	3.5
180	-.0280272	3.6
181	-.0245978	3.7
182	-.0215297	3.8
183	-.0188060	4.0

IV C.7

184	-.0142247	4.1
185	-.0123371	4.2
186	-.0106810	4.3
187	-.0092303	4.4
188	-.0079602	4.5
189	-.0068703	4.6
190	-.0059178	4.7
191	-.0050923	4.8
192	-.0043752	4.9
193	-.0037646	5.0
193	-.0032369	5.1
194	-.0027740	5.2
195	-.0023800	5.3
196	-.0020423	5.4
197	-.0017521	5.5
198	-.0015030	5.6
199	-.0012899	5.7
200	-.0011069	5.8
201	-.0009498	5.9
202	-.0008150	6.0
203	-.0007002	6.1
204	-.0006040	6.2
205	-.0005192	6.3
206	-.0004406	6.4
207	-.0003824	6.5
208	-.0003328	6.6
209	-.0002906	6.7
210	-.0002466	6.8
211	-.0002154	6.9
212	-.0001860	7.0
213	-.0001434	7.2
214	-.0001066	7.4

IV C.8

215	-0.0003868	7.6	
216	-0.0003562	7.8	
217	-0.0003525	8.0	
218	-0.0003404	8.25	
219	-0.0003314	8.5	
220	-0.0003234	8.75	
221	-0.0003185	9.0	
222	-0.0003150	9.25	
223	-0.0003139	9.35	
224	-0.0003121	9.5	
225	-0.0003116	9.60	
226	-0.0003106	9.75	
227	-0.0003102	9.80	

END

DATE FILMED

4 / 17 / 70